Optimization of Overtopping Ramps for Utilization of Wave Energy

Kofoed, Jens Peter

Publication date:
2000

Document Version
Også kaldet Forlagets PDF

Jens Peter Kofoed

Optimization of Overtopping Ramps for Utilization of Wave Energy

Hydraulics & Coastal Engineering Laboratory
Department of Civil Engineering
Aalborg University

December 2000

Hydraulics & Coastal Engineering Laboratory
Department of Civil Engineering
Aalborg University
Sohngaardsholmsvej 57
DK-9000 Aalborg, Denmark

Optimization of Overtopping Ramps for Utilization of Wave Energy

by

Jens Peter Kofoed

December 2000

Published 2000 by
Hydraulics & Coastal Engineering Laboratory
Aalborg University

Preface

The present report *Optimization of Overtopping Ramps for Utilization of Wave Energy* is the result of the project *Optimization of Overtopping Ramps for Utilization of Wave Energy for Power Production* sponsored by the Danish Wave Energy Programme under the Danish Energy Agency (J. no. 51191/98-0017), at Hydraulics & Coastal Engineering Laboratory, Aalborg University (AAU). The project is a part of the Ph.D. study *Overtopping of Marine Structures* carried out by the author. The final report (the Ph.D. thesis) is expected to be available in spring, 2002.

In addition to the present report the performed research has resulted in a number of other publications. These are Kofoed (2000a), Kofoed (2000b), Kofoed and Frigaard (2000b) and Kofoed and Burcharth (2000).

Professor H. F. Burcharth has been the manager of the project and Associate Professor Peter Frigaard is the supervisor of the Ph.D. study.

The author wishes to thank his colleagues and the technical staff within the department for their contributions to the project.

Aalborg, December 2000.

Jens Peter Kofoed.

Table of Contents

List of Symbols

a	:	Amplitude of regular wave [m]
A_c	:	Armor crest freeboard defined as vertical distance from SWL to armor crest
c	:	Wave velocity defined as $c = \frac{L}{T}$ [m/s]
c_{rc}	:	Sector of the curved part of slope, circular curved slope [°]
d	:	Water depth [m]
d_r	:	Draught [m]
E_{f,d_r}	:	Energy flux integrated from the draught up to the surface [W/m]
$E_{f,d}$	:	Energy flux integrated from the sea bottom up to the surface [W/m]
f	:	Frequency [Hz]
f_p	:	Peak frequency [Hz]
g	:	Acceleration of gravity, where set to 9.82 m/s^2
h_{hp}	:	Extension of horizontal plate at the draught of the slope [m]
H	:	Wave height [m]
H_s	:	Significant wave height [m]
H_{m0}	:	Significant wave height based on spectral estimate [m]
k	:	Wave number defined as $\frac{2\pi}{L}$ [m^{-1}]
k_p	:	Wave number based on L_p defined as $\frac{2\pi}{L_p}$ [m^{-1}]
L	:	Wave length [m]
L_0	:	Deep water wave length [m]
L_m	:	Wave length based on T_m [m]
L_{m0}	:	Deep water wave length based on $\frac{g}{2\pi}T_{m0}^2$ [m]
L_p	:	Wave length based on T_p [m]
L_{p0}	:	Deep water wave length based on $\frac{g}{2\pi}T_{p0}^2$ [m]
m_{-1}	:	The minus first spectral moment [m^{2}s]
m_0	:	The zero'th spectral moment [m^2]
N	:	Number of waves [-]
N_{window}	:	Number of subseries [-]
P	:	Power obtained as potential energy by overtopping per unit time [W] or [W/m]

P'	:	Non-dimensionalized power obtained as potential energy by overtopping per unit time defined as $P' = \frac{P}{P_{wave}}$ [-]
P_{ot}	:	Probability of overtopping [-]
P_{V_w}	:	Probability of a certain overtopping volume in a wave V_w given that overtopping occurs [-]
P_{wave}	:	The power that is passing through a vertical cross section of the water column, perpendicular to the wave direction with unit width [W] or [W/m]
p^+	:	Excess pressure caused by wave [N/m^2]
q	:	Average wave overtopping rate per width [m^3/s/m]
$q_{sim}(t)$	:	Simulated wave overtopping rate time series per width [m^3/s/m]
$q_{meas}(t)$	:	Measured wave overtopping rate time series per width [m^3/s/m]
q^i_{window}	:	Average wave overtopping rate per width within a subseries T_{window} long [m^3/s/m]
Q	:	Dimensionless average overtopping rate defined as $\frac{q}{\sqrt{gH_s^3}}$ where nothing else is stated [-]
r_{rc}	:	Radius of curved part of slope, circular curved slope [m]
R	:	Dimensionless freeboard defined as $\frac{R_c}{H_s}$ where nothing else is stated [-]
R^2	:	Square of the Pearson product moment correlation coefficient [-]
R_c	:	Crest freeboard [m]
r_l	:	Large radius in ellipse (used in description of elliptic shape of ramp top) [m]
Ru	:	Run-up level [m]
Ru_{max}	:	Maximum run-up level [m]
$Ru_{2\%}$	:	Run-up level exceeded by 2 % of irregular waves [m]
s	:	Wave steepness defined as $\frac{H}{L}$ [-]
s_{m0}	:	Deep water wave steepness defined as $\frac{H_s}{L_{m0}}$
S_η	:	Spectral density of wave elevation [m^2/s]
t	:	Time [s]
T	:	Wave period [s]
T_m	:	Average period [s]
T_{m0}	:	Deep water average period [s]
T_{window}	:	Size of subseries [s]
u	:	Horizontal particle velocity component [m/s]
T_p	:	Spectral peak period [s]
V_w	:	Overtopping volume in a wave per width [m^3/m]
w_c	:	Distance between side walls at slope crest [m]
w_{d_r}	:	Distance between side walls at slope draught [m]
x	:	Coordinate in the direction the wave is traveling [m]
α	:	Slope angle [°]
α_m	:	Optimal slope angle used in λ_α [°]
β	:	Fitting coefficient in λ_α

η : Wave elevation [m]

η_c : Wave crest elevation [m]

γ : Peak enhancement factor [-]

γ_b : Reduction coefficients taking the influence of berm into account : [-]

γ_h : Reduction coefficients taking the influence of shallow foreshore into account [-]

γ_r : Reduction coefficients taking the influence of roughness into account [-]

γ_w : Specific weight of water defined as $\gamma_w = \rho_w g = 10{,}016\ kg/(m^2 s^2)$

γ_β : Reduction coefficients taking the influence of angle of wave attack into account [-]

κ : Fitting coefficient in λ_{d_r}

λ_{d_r} : Correction factor describing the influence of limited draught on the average overtopping rate [-]

λ_m : Correction factor describing the influence of various geometry modifications on the average overtopping rate [-]

λ_s : Factor for correction of the average overtopping rate for small dimensionless crest free boards R [-]

λ_α : Correction factor describing the influence of varying slope angle on the average overtopping rate [-]

ρ_w : Density of water $\rho_w = 1{,}020\ kg/m^3$

ξ : Surf similarity parameter defined as $\xi = \frac{\tan\alpha}{\sqrt{\frac{H}{L}}}$ [-]

ξ_p : Surf similarity parameter defined as $\xi_p = \frac{\tan\alpha}{\sqrt{\frac{H_s}{L_p}}}$ [-]

ξ_{p0} : Surf similarity parameter defined as $\xi_{p0} = \frac{\tan\alpha}{\sqrt{\frac{H_s}{L_{p0}}}} = \frac{\tan\alpha}{\sqrt{2\pi\frac{H_s}{gT_p^2}}}$ [-]

List of Abbreviations

AAU	:	Aalborg University
MWL	:	Mean water level
SWL	:	Still water level
WEC	:	Wave energy converter
WD	:	Wave Dragon

CHAPTER 1

Introduction

Under the Danish Wave Energy Programme a number of wave energy converters (WEC's) have been suggested and tested. Among these WEC's are devices like the Wave Dragon (WD), Wave Plane, Sucking Sea Shaft, Power Pyramid and others. Common for these devices is that they utilize the wave energy by leading overtopping water to a level higher than the mean water level (MWL). In the literature the vast majority of the overtopping investigations have focused on structure designs that minimize the amount of overtopping and wave situations where small or moderate amounts of overtopping occur. Furthermore, a number of the proposed wave energy devices utilizing overtopping are floating structures, which means that the structure is not extending all the way to the seabed, but has a limited draught. It has been found that only very limited information is available in the literature on how to estimate overtopping of such structures.

In the light of this a generic study of wave overtopping of marine structures is carried out as a Ph.D. project at Hydraulics & Coastal Engineering Laboratory, AAU. This project has been supported by the Danish Wave Energy Programme. In this report the part of this project which focus on maximization of overtopping is described. Thus, the aim of this report is to provide a guideline for how to calculate overtopping rates for a wide variety of geometric layouts of overtopping ramps when subjected to a large range of sea states and point out overtopping ramp layouts resulting in large overtopping rates.

In the project it has been investigated how different geometric parameters as profile shape, shape of guiding walls, shape of cross section, draught (especially with regard to floating structures) and crest freeboard influence the overtopping rates. This has been done through literature studies, theoretical considerations and model tests in a wave tank. By use of the model tests the influence of the

parameters has been evaluated. The variation of the overtopping rates over time has also been evaluated, as this influence the efficiency and the demand for a reservoir of a certain wave power device.

It is expected that the findings of this project will be useful for the inventors and developers of WEC's of the overtopping type. In Denmark the WEC's of the overtopping type Wave Dragon, the Wave Plane and the Power Pyramid are obvious users of the results.

CHAPTER 2

State of the art

In this chapter a summary of the present status of knowledge concerning wave overtopping is presented. The focus in this presentation is put on performed studies on cases where large amounts of overtopping is observed and where more generic layouts of the structure are investigated (rather overtopping of linear smooth plates than site–specific rubble mound breakwaters).

In general overtopping occurs when the run-up exceeds the crest freeboard. Therefore it is considered reasonable to also look into research done on wave run-up.

These research topics are governed by empirical relationships obtained mainly from small scale model tests in laboratories.

2.1 Wave run-up

Early studies based on model tests with regular waves on smooth slopes by Hunt (1959) shows that the run-up level Ru is given by

$$\frac{Ru}{H} = \frac{2.3 \tan \alpha}{\sqrt{\frac{H}{T^2}}} \tag{2.1}$$

for breaking waves.

For non-breaking waves it is given that

$$\frac{Ru}{H} \approx 3 \tag{2.2}$$

This means that according to Hunt (1959) the run-up level Ru for non-breaking waves are not dependent on the wave period T or the slope angle α. However, Le Méhauté et al. (1968) states that run-up is increasing as the slope decrease until the point where breaking begins. Then the run-up decrease as the slope decrease further. The run-up for non-breaking waves increases with increasing wave steepness s (because of non-linear effects), while run-up of breaking waves decrease for increasing wave steepness (because of turbulent dissipation). Le Méhauté et al. (1968) also quotes Grantham (1953) for stating that maximum run-up occurs for a given incident wave for $\alpha = 30°$.

In TACPAI (1974) it is stated that a convex slope increases run-up.

Ahrens and Titus (1985) states that run-up on smooth slopes is largely controlled by three factors:

- Surf conditions (ξ).
- Slope angle (α).
- Non-linear effects ($\frac{\eta_c}{H}$).

Van der Meer and Stam (1992) carried out large-scale tests using irregular waves. From these tests with smooth slopes the following relation was found:

$$\frac{Ru_{2\%}}{H_s} = 1.5\xi_{p0} \tag{2.3}$$

valid for $0.5 < \xi_{p0} < 2.0$.

The maximum of wave run-up is found for $2.0 < \xi_{p0} < 4.0$, and then decreasing with ξ_{p0} for $\xi_{p0} > 4.0$.

Further on tests with rock slopes are discussed. For surging waves ($\xi_{p0} > 6.0$) similar results are found for smooth and rock slopes, while for lower ξ_{p0}-values significant reductions in run-up levels are found for rock slopes compared to smooth slopes.

A more comprehensive overview on wave run-up in general is available in Burcharth and Hughes (2000).

2.2 Wave overtopping

Early studies by Saville and Caldwell (1953) investigates overtopping of a vertical wall using regular waves. The results of the study is presented in graphs using various dimensionless parameters.

Josefson (1978) performed a study of a WEC utilizing overtopping. In this study a number of model tests was carried out using regular waves. From the results of the tests the following was concluded:

- For maximization of obtained power, overtopping times crest freeboard (maximum efficiency), the slope angle increases with increase of wave steepness.
- Introduction of concave edge on upper part of slope results in a reduction of the efficiency.
- Introduction of converging walls on slope results in a reduction of the efficiency.
- A combination of the two modifications results in a slight increase of the efficiency.

According to CIRIA/CUR (1991) the slope angle is getting less important as crest heights are lower and larger overtopping rates occurs.

An overview of later investigations of overtopping in general is given in Burcharth and Hughes (2000). In table 2.1 later overtopping investigations based on model tests of various coastal structures exposed to irregular waves are presented.

Detailed description the methods can be found in either Burcharth and Hughes (2000) or the original reference given in table 2.1.

In the current study the results presented by Van der Meer and Janssen (1995) is used for comparison. The study by Van der Meer and Janssen (1995) is based on a large number of both small and large scale model tests and includes a number of tests with geometries that are usable in the current study (straight impermeable slopes).

In Van der Meer and Janssen (1995) the expressions in the overtopping model depends on ξ_{p0}. However, as overtopping ramps of the type that is typically utilized in WEC's of the overtopping type almost always will result in ξ_{p0} larger than 2 the overtopping model used further on in this report is

$$\frac{q}{\sqrt{gH_s^3}} = 0.2e^{-2.6\frac{R_c}{H_s}\frac{1}{\gamma_r\gamma_b\gamma_h\gamma_\beta}} \tag{2.4}$$

Authors	Structures	Overtopping model	Dimensionless overtopping rate Q	Dimensionless freeboard R
Owen (1980), Owen (1982)	Impermeable smooth, rough, straight and bermed slopes	$Q = ae^{-bR}$	$\frac{q}{gH_s T_{m0}}$	$\frac{R_c}{H_s}(\frac{s_{m0}}{2\pi})^{0.5}\frac{1}{\gamma}$
Bradbury and Allsop (1988)	Rock armoured impermeable slopes with crown walls	$Q = aR^{-b}$	$\frac{q}{gH_s T_{m0}}$	$(\frac{R_c}{H_s})^2(\frac{s_{m0}}{2\pi})^{0.5}$
Aminti and Franco (1988)	Rock, cube and Tetrapod double layer armor on rather impermeable slopes with crown walls (single sea state)	$Q = aR^{-b}$	$\frac{q}{gH_s T_{m0}}$	$(\frac{R_c}{H_s})^2(\frac{s_{m0}}{2\pi})^{0.5}$
Ahrens and Heimbaugh (1988)	7 different seawall/revetment designs	$Q = ae^{-bR}$	$\frac{q}{\sqrt{gH_s^3}}$	$\frac{R_c}{(H_s^2 L_{p0})^{\frac{1}{3}}}$
Pedersen and Burcharth (1992)	Rock armored rather impermeable slopes with crown walls	$Q = aR$	$\frac{qT_{m0}}{L_{m0}^2}$	$\frac{H_s}{R_c}$
Van der Meer and Janssen (1995)	Impermeable, smooth, rough straight and bermed slopes	$Q = ae^{-bR}$	$\frac{q}{\sqrt{gH_s^3}}\sqrt{\frac{s_{p0}}{\tan\alpha}}$ for $\xi_{p0} < 2$ $\frac{q}{\sqrt{gH_s^3}}$ for $\xi_{p0} \geq 2$	$\frac{R_c}{H_s}\frac{\sqrt{s_{p0}}}{\tan\alpha}\frac{1}{\gamma}$ for $\xi_{p0} < 2$ $\frac{R_c}{H_s}\frac{1}{\gamma}$ for $\xi_{p0} \geq 2$
Franco et al. (1994), Franco and Franco (1997)	Vertical wall breakwater with and without perforated front	$Q = ae^{-bR}$	$\frac{q}{\sqrt{gH_s^3}}$	$\frac{R_c}{H_s}\frac{1}{\gamma}$
Pedersen (1996)	Rock armored permeable slopes with crown walls	$Q = R$	$\frac{qT_{m0}}{L_{m0}^2}$	$3.2 \cdot 10^{-5}\frac{H_s^5 \tan\alpha}{R_c^3 A_c B}$
Hedges and Reis (1997)	Impermeable smooth, rough, straight and bermed slopes (Data from Owen (1982))	$Q = a(1-R)^b$ for $0 \leq R < 1$ $Q = 0$ for $R \geq 1$	$\frac{q}{\sqrt{gRu_{max}^3}}$	$\frac{R_c}{Ru_{max}}$

Table 2.1: Models for average overtopping rate formulae, based on Table VI-5-7 in Burcharth and Hughes (2000).

that according to Van der Meer and Janssen (1995) is valid for $\xi_{p0} \geq 2$. The coefficients γ_b, γ_h, γ_r and γ_β are introduced to take the influence of a berm, shallow foreshore, roughness and angle of wave attack, respectively, into account. All these coefficients are in the range 0.5 to 1.0, meaning that when maximizing overtopping the coefficients should be 1.0 which is the case for no berm, no shallow foreshore, smooth slope (no roughness) and head-on waves. This is also the case in the current study.

The fact that overtopping ramps of the type that is typically utilized in WEC's of the overtopping type typically result in ξ_{p0} larger than 2 is reasonable as the overtopping rate according to Van der Meer and Janssen (1995) is reduced if the slope angle α is changed so ξ_{p0} is smaller than 2 for a fixed wave situation.

Oumeraci et al. (1999) did an investigation of overtopping of dikes with very low crest freeboards (R_c down to zero) caused by high water levels. This investigation showed good agreement with Van der Meer and Janssen (1995) for relative crest freeboards in the range tested by Van der Meer and Janssen (1995). However, for relative crest freeboards R ($R = \frac{R_c}{H_s}$) close to zero the tests by Oumeraci et al. (1999) shows that the expression given by Van der Meer and Janssen (1995) (eq. 2.4) overpredicts the average overtopping rate.

Kofoed and Nielsen (1997) did an investigation of overtopping in connection with an evaluation of the WEC WD. In this investigation the overtopping ramp had a limited draught ($d_r/d = 0.3$) as the WD is a floating structure. Tests were performed with different slope angles α (linear ramps, $\alpha = 35°$, $40°$, $45°$ and $50°$) and it was found that the optimal slope angle is around $40°$. However, for slope angles between $35°$ and $50\ °$ no significant variation in overtopping rates were found. The results of the tests with $\alpha = 40°$ were fitted to an overtopping model as the one use by Van der Meer and Janssen (1995) for $\xi_{p0} \geq 2$ (see table 2.1). This resulted in coefficients a and b that were different from the coefficients given by Van der Meer and Janssen (1995) and also were dependent of the peak period T_p. This is due to the fact that the tests were performed with a limited draught, which is not the case for Van der Meer and Janssen (1995).

Furthermore, a limited number of variations of the slope geometry were tested by Kofoed and Nielsen (1997), but it was concluded that non of the tested slope geometries were superior to a linear ramp in terms of maximizing the overtopping rates.

Martinelli and Frigaard (1999b) performed laboratory tests with a floating model of the WD. These tests indicated that the overtopping rate was reduced by up to 50 % because of the movements, compared to tests with a fixed model. However, the reduction of the overtopping rate due to a floating structure is highly dependent on the structure it self. The tests showed that movements should be minimized in order to make the reduction as small as possible.

Kofoed and Frigaard (2000a) did some preliminary investigations on a wave energy device utilizing wave overtopping by leading the overtopping water to reservoirs in different levels in order to capture the water at the level it reaches and thereby achieve a higher efficiency. The results of this investigation showed that the use of 3 reservoirs in different level instead of one resulted in 38 - 53 % more potential energy in the overtopping water.

CHAPTER 3

Model tests

In this chapter the conditions for the performed model tests are described. At first the purpose of the tests is given followed by an account for the used sea states and the investigated geometric parameters. At last the used used model test setup is presented.

3.1 Purpose of model study

During the model tests the influence on the amount of overtopping and the obtained potential energy of the following geometrical parameters are investigated (see figure 3.1):

- Slope angle.
- Crest freeboard.
- Draught.
- Profile shape.
- Shape of guiding walls.

All model tests are performed in a wave basin and the modeled structures are subjected to irregular 2-D waves. The model tests are performed using fixed structures and a constant water depth of 0.5 m. Although the models used in

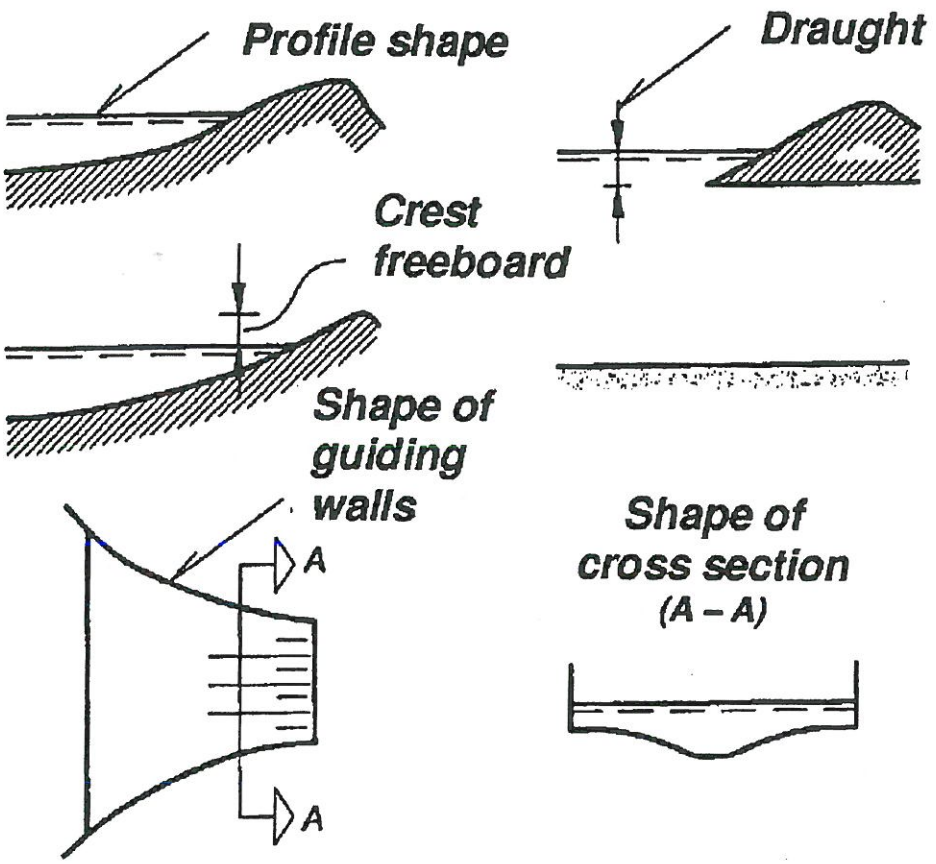

Figure 3.1: Investigated geometric parameters.

the tests do not represent any specific prototype structures, a length scale of 1:50 seems appropriate. This results in a prototype water depth of 25 m.

The amount of overtopping of the structure is dependent on wave parameters as:

- Wave type, regular/irregular.
- Wave height.
- Wave period.
- Spectral shape.
- Wave groupiness.
- Angle of wave attack.
- Directional spreading.

Furthermore, overtopping is dependent on the geometric parameters describing the structure as mentioned above and also on surface roughness and permeability of the structure. In this model study it has been chosen to focus on the influence of the geometry rather than covering a large number of different wave parameters. Thus, parameters as spectral shape, wave groupiness, angle of wave attack and directional spreading are not tested and the only wave situations consisting of irregular 2-D waves covering the wave situations typical for the North Sea west of Denmark are used.

It is commonly accepted that introduction of surface roughness and permeability decreases the amount of overtopping, and therefore only smooth and non-permeable structures are tested in this study. As point of departure tests are performed with a linear profile. For this type of structure the influence of the slope angle, the crest freeboard and the draught on the overtopping is investigated and compared to existing expressions from the literature. The motivation for testing ramp geometries with limited draught is the fact that a number of the suggested overtopping based WEC's are floating, and it is thus important to know how large a draught it is feasible to use for this type of structure. For hereby-found suitable values (in terms of obtained amount of potential energy in the overtopping water volume) of crest freeboard, angle of slope and draught, tests are performed with structures modified as follows:

- Ramp with horizontal plate added at the ramp bottom.
- Ramp with convex upper part.

- Ramp with concave upper part.
- Converging leading walls (linear).
- Converging leading walls (curved).

From the performed tests knowledge about the influence of a range of geometrical parameters, larger than what is considered for structures normally used in coastal engineering, on overtopping is obtained.

3.2 Sea states used in model tests

In all the performed model tests irregular 2-D waves have been used. The irregular waves are generated using the parameterized JONSWAP-spectrum (Hasselmann et al. (1973)):

$$S_\eta(f) = \frac{1.4}{\gamma}\frac{5}{16}H_s^2 f_p^4 f^{-5}\gamma^\delta(-\frac{5}{4}(\frac{f_p}{f})^4) \tag{3.1}$$

$$\delta = e^{(-\frac{(f-f_p)^2}{2\sigma_f^2 f_p^2})} \tag{3.2}$$

where

$\sigma_f = 0.10$ for $f \leq f_p$
$\sigma_f = 0.50$ for $f > f_p$

The spectral enhancement factor γ has been set to 3.3, corresponding to a location in the Danish part of the North Sea.

All of the tested ramp geometries have been subjected to a large variety of wave conditions - in total 37 sea states for each of the tested geometries. The sea states have been selected so the far majority of sea states that occurs over time in the Danish part of the North Sea are covered. This means that focus is put on sea states that occurs often and not as much extreme sea states as it often is the case for coastal defense structures such as breakwaters or dikes.

The selected sea states are presented in table 3.1, where the significant wave height H_s and the wave peak period T_p is given along with the resulting peak wave steepness s_p and surf similarity parameter (Iribarren number) ξ_{p0}, depending on the ramp slope.

T_p [s]		H_s [m] 0.5	1.0	2.0	3.0	4.0	5.0	6.0	7.0	8.0
	s_p [%]	2.0	4.0	6.0						
4	ξ_{p0} ($\alpha = 20$ °)	2.6	1.8	1.3						
	ξ_{p0} ($\alpha = 30$ °)	4.1	2.9	2.0						
	ξ_{p0} ($\alpha = 40$ °)	5.9	4.2	3.0						
	ξ_{p0} ($\alpha = 50$ °)	8.4	6.0	4.2						
	ξ_{p0} ($\alpha = 60$ °)	12.2	8.7	6.1						
	s_p [%]	0.9	1.8	3.6	5.4	7.2	8.9			
6	ξ_{p0} ($\alpha = 20$ °)	3.9	2.7	1.9	1.6	1.4	1.2			
	ξ_{p0} ($\alpha = 30$ °)	6.1	4.3	3.1	2.5	2.2	1.9			
	ξ_{p0} ($\alpha = 40$ °)	8.9	6.3	4.5	3.6	3.1	2.8			
	ξ_{p0} ($\alpha = 50$ °)	12.6	8.9	6.3	5.2	4.5	4.0			
	ξ_{p0} ($\alpha = 60$ °)	18.4	13.0	9.2	7.5	6.5	5.8			
	s_p [%]		1.1	2.1	3.2	4.3	5.4	6.4	7.5	8.6
8	ξ_{p0} ($\alpha = 20$ °)		3.6	2.6	2.1	1.8	1.6	1.5	1.4	1.3
	ξ_{p0} ($\alpha = 30$ °)		5.8	4.1	3.3	2.9	2.6	2.4	2.2	2.0
	ξ_{p0} ($\alpha = 40$ °)		8.4	5.9	4.8	4.2	3.8	3.4	3.2	3.0
	ξ_{p0} ($\alpha = 50$ °)		11.9	8.4	6.9	6.0	5.3	4.9	4.5	4.2
	ξ_{p0} ($\alpha = 60$ °)		17.3	12.2	10.0	8.7	7.7	7.1	6.5	6.1
	s_p [%]			1.5	2.3	3.1	3.8	4.6	5.4	6.1
10	ξ_{p0} ($\alpha = 20$ °)			3.2	2.6	2.3	2.0	1.9	1.7	1.6
	ξ_{p0} ($\alpha = 30$ °)			5.1	4.2	3.6	3.2	2.9	2.7	2.6
	ξ_{p0} ($\alpha = 40$ °)			7.4	6.1	5.2	4.7	4.3	4.0	3.7
	ξ_{p0} ($\alpha = 50$ °)			10.5	8.6	7.4	6.7	6.1	5.6	5.3
	ξ_{p0} ($\alpha = 60$ °)			15.3	12.5	10.8	9.7	8.8	8.2	7.7
	s_p [%]			1.2	1.8	2.4	3.0	3.6	4.2	4.8
12	ξ_{p0} ($\alpha = 20$ °)			3.9	3.2	2.7	2.4	2.2	2.1	1.9
	ξ_{p0} ($\alpha = 30$ °)			6.1	5.0	4.3	3.9	3.5	3.3	3.1
	ξ_{p0} ($\alpha = 40$ °)			8.9	7.3	6.3	5.6	5.1	4.8	4.5
	ξ_{p0} ($\alpha = 50$ °)			12.6	10.3	8.9	8.0	7.3	6.8	6.3
	ξ_{p0} ($\alpha = 60$ °)			18.4	15.0	13.0	11.6	10.6	9.8	9.2
	s_p [%]				1.5	2.0	2.5	3.0	3.5	4.0
14	ξ_{p0} ($\alpha = 20$ °)				3.7	3.2	2.8	2.6	2.4	2.3
	ξ_{p0} ($\alpha = 30$ °)				5.8	5.1	4.5	4.1	3.8	3.6
	ξ_{p0} ($\alpha = 40$ °)				8.5	7.3	6.6	6.0	5.6	5.2
	ξ_{p0} ($\alpha = 50$ °)				12.0	10.4	9.3	8.5	7.9	7.4
	ξ_{p0} ($\alpha = 60$ °)				17.5	15.2	13.6	12.4	11.5	10.7

Table 3.1: Sea states used in the model tests.

The duration of each of the sea states has been 30 minutes in model scale, corresponding to approx. 3.5 hours in full scale - or 1,100 to 3,600 waves depending on the peak period. This means that each of the tested ramp geometry has been subjected to in the order of 70,000 waves.

3.3 Investigated geometric parameters

In this section the geometries tested in the current study are described. The geometries have been put into 3 categories. At first a number of linear ramps have been tested. Secondly, tests with a number of modifications of the ramp profile were carried out and at last modifications of the side walls of the ramp were applied.

3.3.1 Linear ramps

The tests with linear ramps have been done with the ramp geometries given by table 3.2.

Geometry	α [°]	$\frac{R_c}{d}$ [-]	$\frac{d_r}{d}$ [-]
AA01	**20** (1:2.8)	0.16	0.32
AA02	**30** (1:1.7)	0.16	0.32
AA03	**40** (1:1.2)	0.16	0.32
AA04	**50** (1:0.8)	0.16	0.32
AA05	**60** (1:0.6)	0.16	0.32
AB01	40 (1:1.2)	**0.04**	0.32
AB02	40 (1:1.2)	**0.10**	0.32
AB03	40 (1:1.2)	**0.22**	0.32
AB04	40 (1:1.2)	**0.30**	0.32
AC01	40 (1:1.2)	0.16	**0.20**
AC02	40 (1:1.2)	0.16	**0.50**
AC03	40 (1:1.2)	0.16	**0.72**
AC04	40 (1:1.2)	0.16	**1.00**

Table 3.2: Geometrical parameters describing the model setup in the tests with a linear ramp.

These geometries have been selected so the influence of slope angle α, crest freeboard R_c and draught d_r can be evaluated.

In the tests were the influence of the slope angle is investigated the crest freeboard and draught have been fixed to values that is considered reasonable for a ramp in

a WEC of the overtopping type - and likewise for the tests were the influence of crest freeboard and draught, respectively, is investigated. Especially, the choice of $\alpha = 40°$ for tests with varying crest freeboard and draught is based on results from Kofoed and Nielsen (1997).

3.3.2 Modifications of the ramp profile

The tests with modifications of the ramp profile have been done with the ramp geometries given by table 3.3.

In the modifications of the ramp profile a linear ramp with specifications given for geometry BA04 in table 3.3 is used as reference. The choice of this linear ramp layout (BA04) as a reference, has been based on the results of the tests with the linear ramp layouts given in table 3.2 that indicated that a slope angle $\alpha = 30°$ is optimal, see section 4.1.1. Furthermore, for all these geometries $\frac{d_r}{d}$ is set to 0.4 and $\frac{R_c}{d}$ is set to 0.1, which is also based on the results given in section 4.1.1

Geometry	Description	α [°]	$\frac{h_{hp}}{d_r}$ [-]	$\frac{r_{rc}}{d_r}$ [-]	c_{rc} [°]
BA01	Horizontal plate	30	0.500		
BA02	Horizontal plate	30	0.250		
BA03	Horizontal plate	30	0.125		
BA04	Reference setup	30			
CA01	Convex slope	30		1.875	28
CA02	Convex slope	30		3.755	28
CA03	Convex slope	30		5.630	28
CB01	Convex slope, diff. angle	35		2.795	31
CC01	Convex slope, elliptic	45			
DA01	Concave ramp	30		1.365	30

Table 3.3: Geometrical parameters describing the model setup in tests of modifications of the ramp profile. For all these geometries $\frac{d_r}{d} = 0.4$ and $\frac{R_c}{d} = 0.1$.

A series of tests with a horizontal plate added at the draught of the ramp (geometries BA01 to BA03) have been carried out to investigate whether the overtopping rate can be improved by trying to prevent excess pressure at the draught of the ramp to "escape" under the ramp. The layouts of these ramps are given in figure B.16 to B.20 in appendix B.2.2.

A series of tests with a convex deflection of the top of the ramp (geometries CA01 to CC01) have been motivated by some of the results of the studies referenced in chapter 2. Furthermore, the idea of deflecting the ramp at the top where

up-rush velocity is lower than near the MWL, in order to extract as much of the kinetic energy as possible, seems reasonable. The layouts of these ramps are given in figure B.22 to B.30 in appendix B.2.3. Ramp geometry CC01 is a layout suggested by the inventor of the WEC WD, Erik Friis-Madsen, Löwenmark.

A concave deflection of the top of the ramp (geometry DA01) has also been tested. The layout of this ramp is given in figure B.32 in appendix B.2.4.

3.3.3 Modifications of the side walls of the ramp

A series of tests with modifications of the side walls of the ramp have been done with the ramp geometries given by table 3.4.

Geometry	Description	$\frac{w_c}{w_{dr}}$ [-]	$\frac{r_l}{d_r}$ [-]
EA01	Linear converging walls	0.848	
EA02	Linear converging walls	0.696	
EA03	Linear converging walls	0.536	
EA04	Linear converging walls	0.368	
FA02	Curved converging walls	0.696	0.475

Table 3.4: Geometrical parameters describing the model setup in tests of modifications of the side walls of the ramp.

In the series of tests with modifications of the side walls the linear ramp denoted geometry BA04 in table 3.3 is again used as reference.

The series of tests with linear converging walls (geometries EA01 to EA04) have been carried out to investigate whether the overtopping rate can be improved by "compressing" the overtopping water as is comes up the ramp in order to make it reach a higher level than it would without the converging walls. The layouts of these guiding walls are given in figure B.34 in appendix B.3.1. In the tests with curved converging walls (geometry FA02) the idea is the same as for the linear converging walls. The layout of the guiding walls is given in figure B.39 in appendix B.3.2.

3.4 Model test setup

The model tests have been carried out in the deep water 3-D wave tank at the Hydraulics & Coastal Engineering Laboratory, AAU using a length scale of 1:50. This wave tank is approximately 8 x 16 m and is equipped with a 3-D wavemaker with 10 segments of the piston type. In the current setup a 0.5 m wide flume has

been built in the wave tank as shown in figure 3.2 and in the photos in figure 3.3. Performing the model tests in the wave tank and the especially for the purpose built flume has some advantages compared to performing the model tests in a regular wave flume. The fact that the majority of the tested geometries are with limited draught means that the reservoir in which the overtopping water is collected has to be placed at the side of the tested model. This takes up quite some space and therefore it is easier to fit in the wave tank than in a regular flume. Furthermore, in the wave tank there is plenty of space for passive wave absorption (gravel beaches are used) and the risk of re-reflection of waves reflected from the tested structure minimal as these waves diffracts when they exit the flume and is absorbed by the gravel beaches. This means that even though no active wave absorption system is applied there is very good control of the waves to which the tested models are exposed.

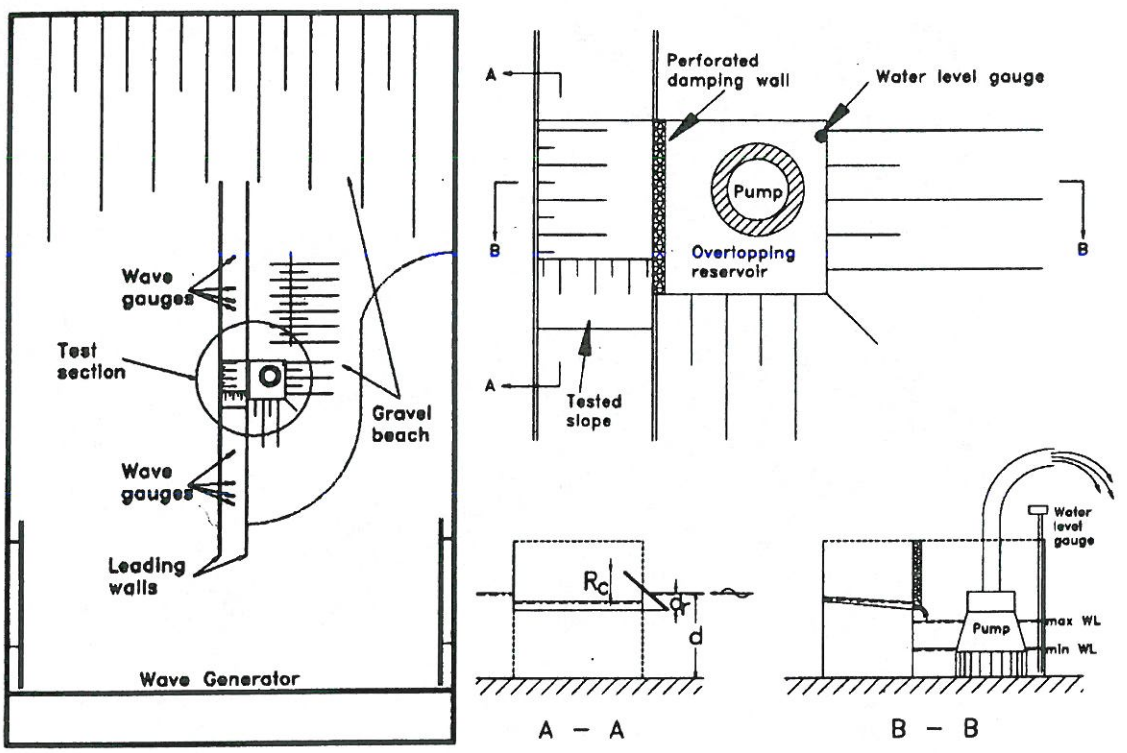

Figure 3.2: Sketch of the model test setup.

In the model test setup two measuring system have been deployed - a wave measuring system and an overtopping system.

Figure 3.3: Photos from the model test setup.

3.4.1 Wave measurements

The measuring system consist of two arrays of wave gauges - one in front of the tested structure and one behind it. Each of the arrays consists of 4 wave gauges of the resistance type placed on the center line of the flume. The gauges are placed with a distance of 0.15 m between 1. and 2. gauge, 0.25 m between 2. and 3. gauges, and 0.60 m between 3. and 4. gauge.

Placing 4 gauges with the chosen distances enables the use of SIRW method by Frigaard and Brorsen (1995) for separation of incident and reflected irregular waves. The SIRW method has the advantages compared to other separation method that it enables a separation of incident and reflected waves in the time domain. In order to achieve good output from SIRW method wave records from two wave gauges with a distance in the range of 5 to 45 % of length of the recorded waves. Thus, by deploying 4 wave gauges with different distances it is for each of the 37 wave situations possible to use a suitable pair of wave gauges for the SIRW analysis. (By combining the wave gauges within an array the following distances are available: 0.15, 0.25, 0.40, 0.60 0.85 and 1.00 m. These distances covers the tested wave situations.)

The incident wave time series calculated using the SIRW method is then used in the further wave analysis. For all the performed model tests both a time and frequency domain analysis is performed of the incident wave in front of the tested structure. In the time domain analysis the statistical distribution of the wave heights are found by zero down crossing and parameters as significant wave height H_s are calculated on this basis. In the frequency domain analysis the wave spectrum is calculated and parameters as the wave peak period T_p and the spectral estimate of the significant wave height H_{m0}.

In the further analysis of the overtopping the spectral estimate of the significant wave height H_{m0} is used rather than the H_s found from the time domain analysis.

3.4.2 Overtopping measurements

In the performed model tests the range of the overtopping discharge have been very large due to the large range of tested wave conditions and geometries. Therefore, the design of the overtopping measuring system is a compromise between being able to measure very large and very small amounts of overtopping.

The chosen measuring system is shown in figure 3.2. The system consists of a reservoir, a pump and a water level gauge. The reservoir is placed beside the overtopping ramp in order to allow free passage under the ramp, as this in most cases is not extending to the bottom. Between the ramp and the reservoir a per-

forated damping wall is placed in order to decrease the amount of disturbance on the water surface in th reservoir, as this causes noise in the water level measurements and thereby also on the overtopping rate time series. The water level gauge and the pump are connected to a PC that monitor and record the water level in reservoir. Once a preset maximum water level is reached the pump is activated for a fixed time period (3 s in the used setup) and the pumped volume of water is then known from a calibration of the pump (approx. 100 l in the used setup).

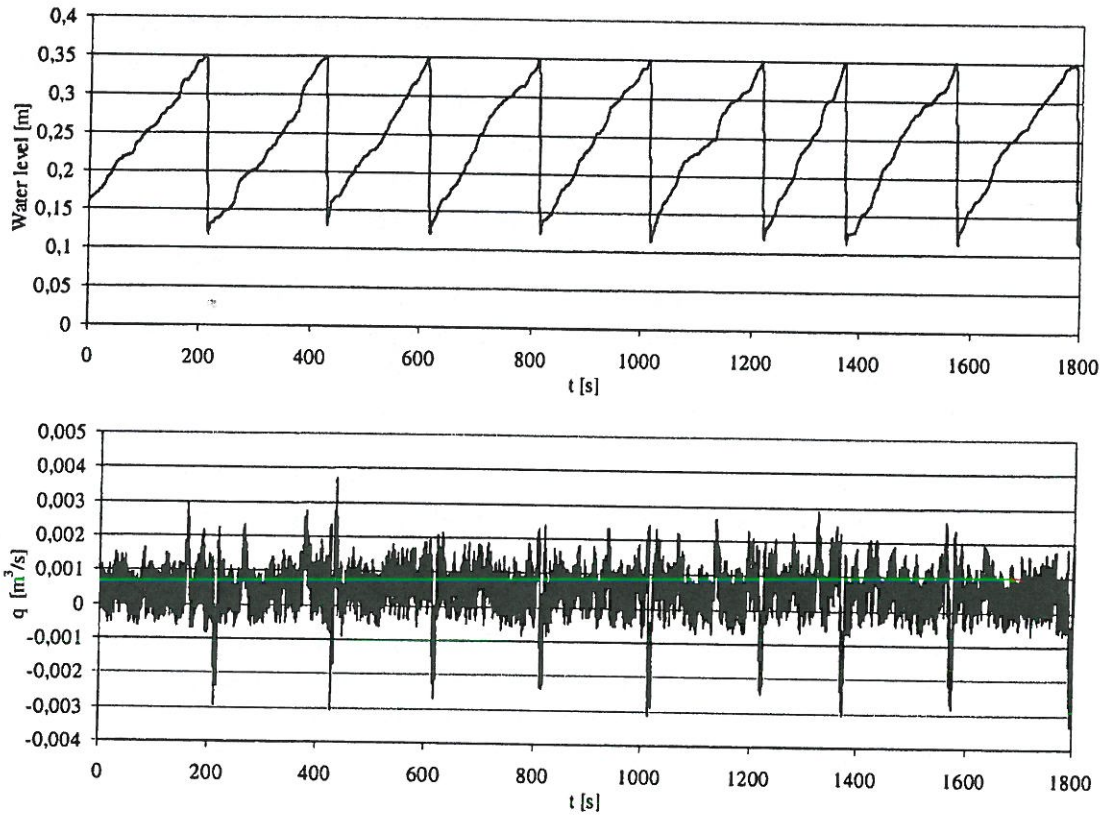

Figure 3.4: An example of a measured water level time series measured in the reservoir (top) and the corresponding time series of the derived overtopping rate.

Based on the measured water level in the reservoir the overtopping volume, and thereby also the discharge, during a test can be found. Furthermore, as the water level in the reservoir is measured continuously, the overtopping discharge time series during each test can be calculated by differentiation, see figure 3.4. When performing the differentiation in order to calculate the overtopping rate time series, the signal from the water level gauge is corrected by adding a piece of water level time series measured during the calibration of the pump at the time where the pump is emptying the reservoir. (The piece of time series is 12 s long in order to compensate for the disturbances created by the pumping.)

This is done in order to ensure that a continuous overtopping discharge time series is obtained. Though, in spite all efforts it has not been possible to make a perfect correction, which means that the time series of the overtopping rate is not completely correct at the time of the pumping. This can also be seen from figure 3.4. It is seen that the overtopping discharge sometimes is negative. A negative discharge can of course not occur, but this is an effect of the problems at the time of pumping (the large negative peaks) and the fact that disturbances in the water level measurements occurs due to small waves in the reservoir. However, if the average overtopping discharge is calculated even for very small time windows (down to the order of 10 s) these will be correct also although if pumping occurs within the time window. Another reason for not using window sizes smaller than in the order of 10 waves is the fact that the measured water level in the reservoir is delayed and smoothed by distance from the ramp and the basin, and the perforated damping wall.

The majority of the performed analyses in the current study concerns average overtopping rates. In these analyses the average overtopping rates q are typically non-dimensionalized by division by the factor $\sqrt{gH_{m0}^3}$. The dimensionless average overtopping rate is denominated Q and also a dimensionless crest freeboard R is defined as $R = \frac{R_c}{H_{m0}}$ (in both cases H_{m0} is calculated for the incident waves). Thus the non-dimensionalization is performed as specified by Van der Meer and Janssen (1995) except H_{m0} is used as the significant wave height H_s.

CHAPTER 4

Results of model tests

In the present chapter the results of the performed model tests are presented.

In appendix B the results of each of the performed tests are given in terms of average overtopping rates. In the figures in the appendix the dimensionless average overtopping rate Q (defined as $Q = \frac{q}{\sqrt{gH_{m0}^3}}$) is plotted as a function of the dimensionless crest freeboard R (defined as R_c/H_{m0}) for each of the tested geometries. It is on these results the following analyses are based.

4.1 Linear ramps

In this section the results of the model tests with linear ramps are presented and analyzed. In appendix B.1 the basic results are shown in figure B.2 to B.14.

4.1.1 Varying ramp angle

The test series with varying slope angle α shows that the average overtopping rate is slightly dependent of α, cf. figure 4.1.

A correction factor λ_α is introduced to take this dependency of the slope angle into account. By fitting a number of expressions is has been found that eq. 4.1 describes the dependency well. In figure 4.2 the effect of introducing λ_α is shown. It can be seen that the R^2 (square of the Pearson product moment correlation coefficient) is thereby increased from 0.84 to 0.89.

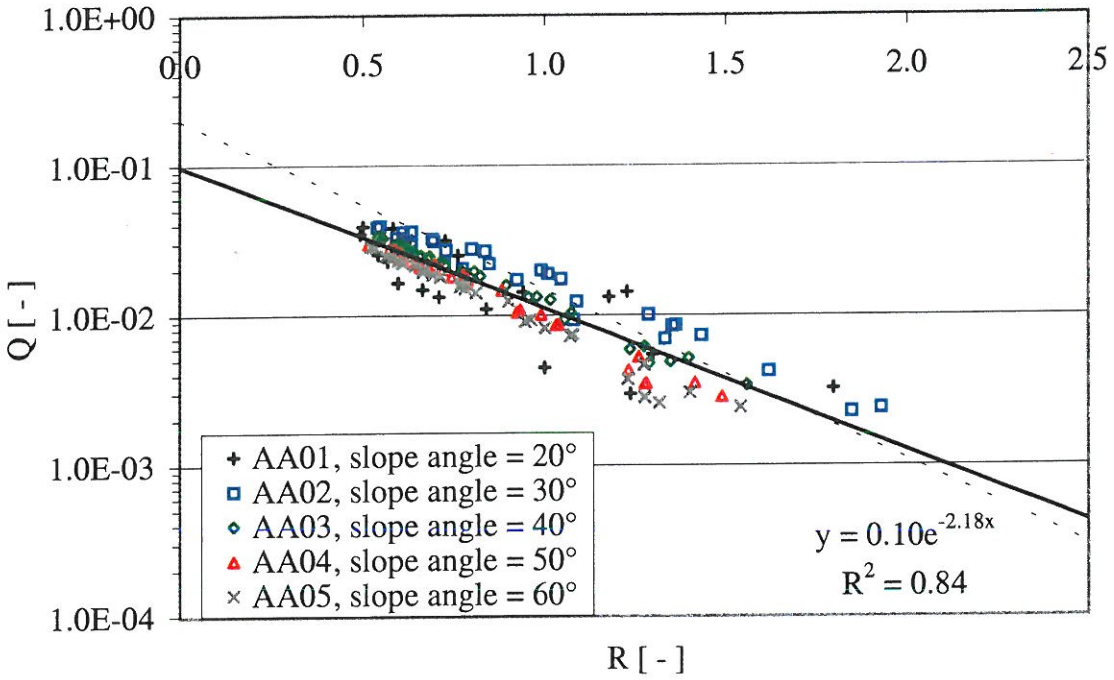

Figure 4.1: Results of tests with test geometries with varying α (test series AA). The dimensionless average overtopping rate Q is plotted as a function of the dimensionless crest freeboard R. The dotted line represents eq. 2.4 and the solid line is an exponential fit to all the showed data points.

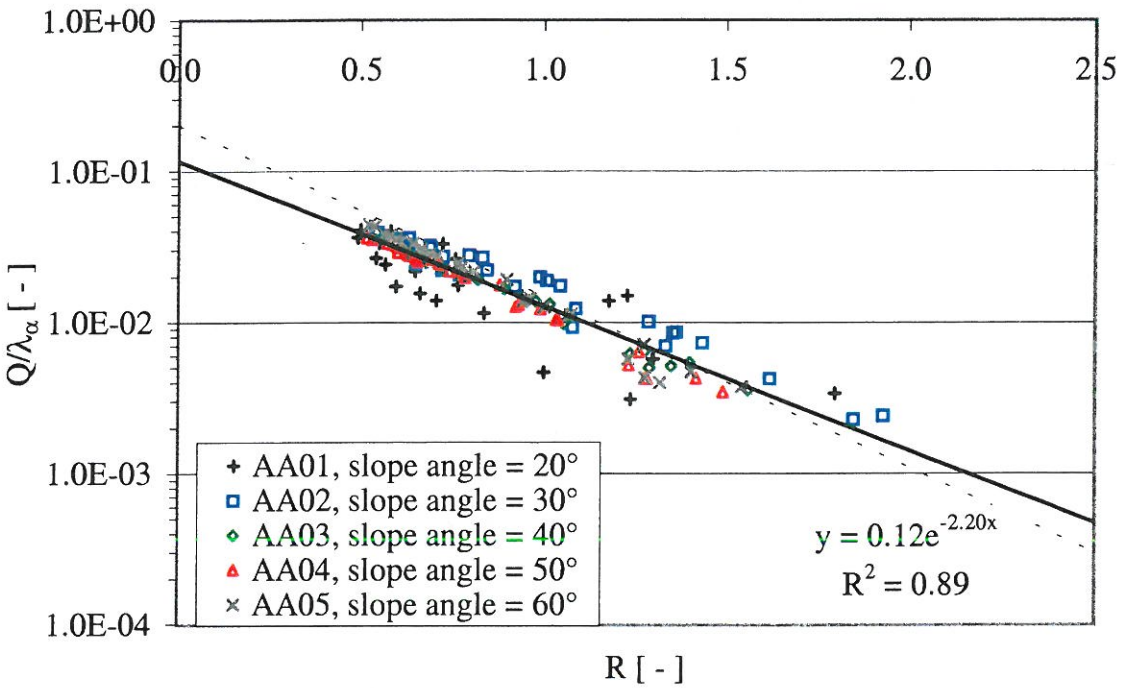

Figure 4.2: Results of tests with test geometries with varying α (test series AA). The dimensionless average overtopping rate Q divided by the correction factor λ_α is plotted as a function of the dimensionless crest freeboard R. The dotted line represents eq. 2.4 and the solid line is an exponential fit to all the showed data points.

$$\lambda_\alpha = \cos^\beta(\alpha - \alpha_m) \tag{4.1}$$

where $\alpha_m = 30°$ is the optimal slope angle and $\beta = 3$ is a coefficient, both found by best fit. The expression for λ_α in eq. 4.1 is formulated so it is 1 for the optimal (in terms of maximum overtopping) slope angle and decreases when the difference between the optimal and actual slope angle increases.

4.1.2 Varying crest freeboard

The test series with varying crest freeboard R_c shows that the average overtopping rate is very well described by an exponential expression as the one suggested by Van der Meer and Janssen (1995) (see table 2.1), cf. figure 4.3.

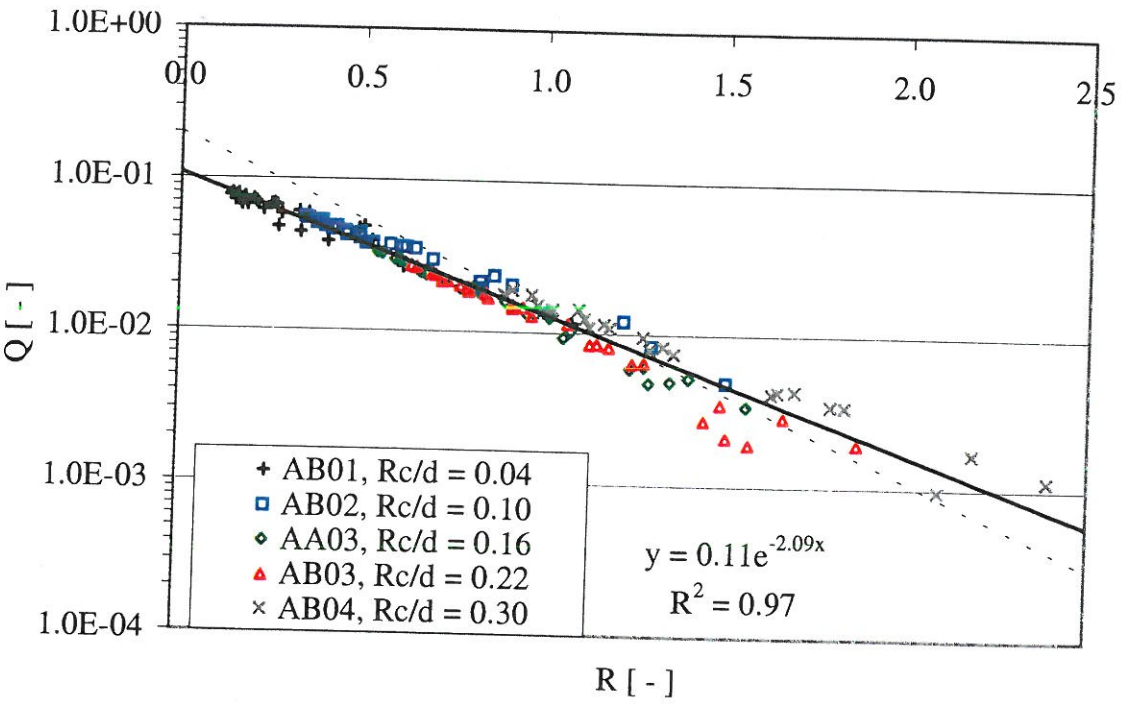

Figure 4.3: Results of tests with test geometries with varying R_c (test series AB). The dimensionless average overtopping rate Q is plotted as a function of the dimensionless crest freeboard R. The dotted line represents eq. 2.4 and the solid line is an exponential fit to all the showed data points.

From figure 4.3 it can be seen that the correlation coefficient R^2 is as high as 0.97 which indicates a very good fit.

4.1.3 Varying draught

The test series with varying draught d_r shows that the average overtopping rate is dependent of d_r, cf. figure 4.4.

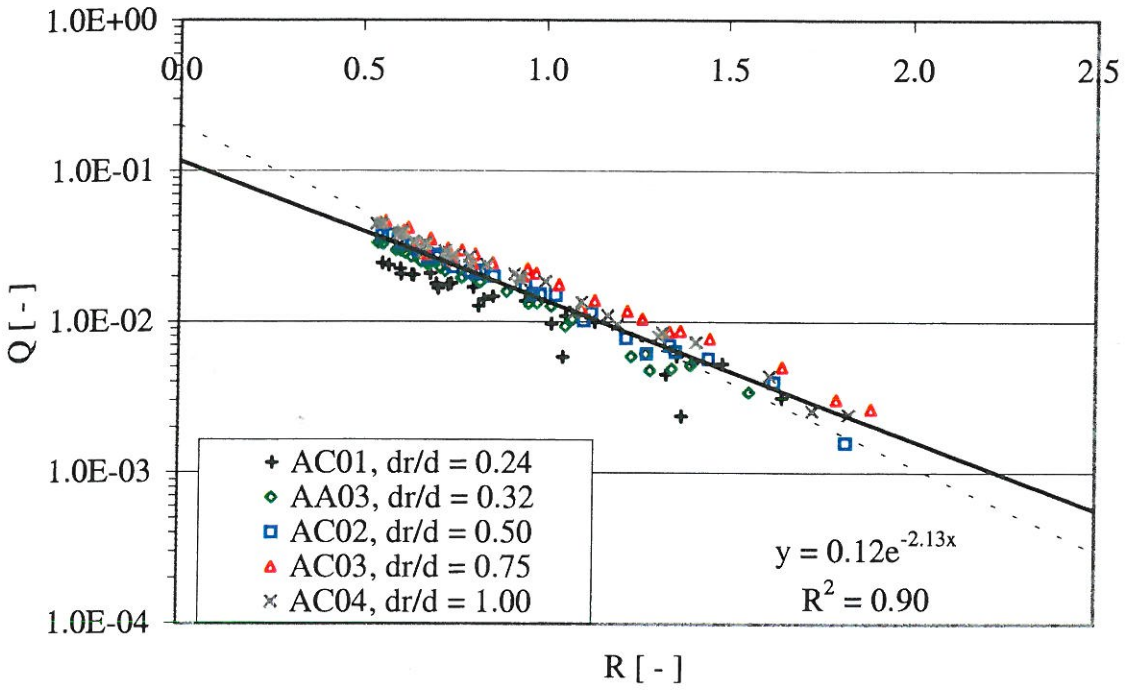

Figure 4.4: Results of tests with test geometries with varying d_r (test series AC). The dimensionless average overtopping rate Q is plotted as a function of the dimensionless crest freeboard R. The dotted line represents eq. 2.4 and the solid line is an exponential fit to all the showed data points.

It is seen that the overtopping increases with increasing draught. This is not surprising as the amount of energy passing under the ramp is decreasing with increasing draught. In order to take this effect into account a correction parameter λ_{d_r} is introduced:

$$\lambda_{d_r} = 1 - \kappa \frac{\sinh(2k_p d(1 - \frac{d_r}{d})) + 2k_p d(1 - \frac{d_r}{d})}{\sinh(2k_p d) + 2k_p d} \tag{4.2}$$

where k_p is the wave number based on L_p and κ is a coefficient controlling the degree of influence of the limited draught, found by best fit to be 0.4.

The dependency of the draught introduced by λ_{d_r} is based on the time averaged ratio between the amount of energy flux integrated from the draught up to the

surface E_{f,d_r} and the energy flux integrated from the seabed up to the surface $E_{f,d}$.

$$\begin{aligned} \frac{E_{f,d_r}}{E_{f,d}} &= \frac{\int_{-d_r}^{0} p^+ u \, dz}{\int_{-d}^{0} p^+ u \, dz} \\ &= 1 - \frac{\sinh(2kd(1-\frac{d_r}{d})) + 2kd(1-\frac{d_r}{d})}{\sinh(2kd) + 2kd} \end{aligned} \tag{4.3}$$

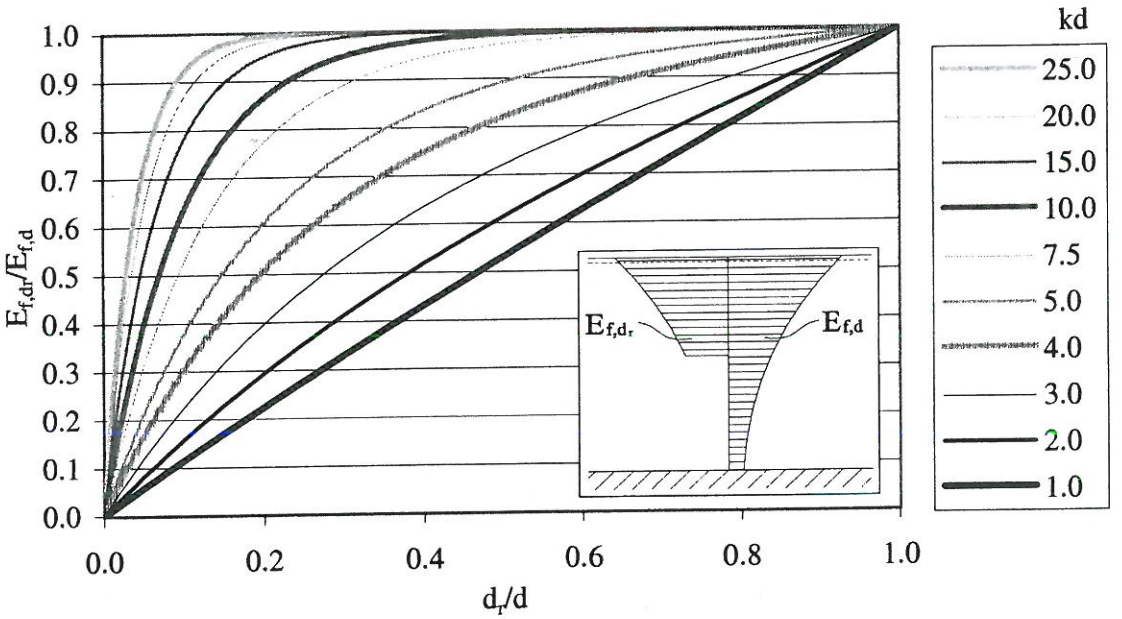

Figure 4.5: The ratio given in eq. 4.3 as a function of the relative draught $\frac{d_r}{d}$ for various values of kd.

In figure 4.5 eq. 4.3 is plotted as a function of the relative draught $\frac{d_r}{d}$ for various values of kd.

In the derivation of eq. 4.3 linear wave theory is used. Because of the limitations in the linear wave theory eq. 4.3 cannot completely describe the effect of limited draught on overtopping. Using λ_{d_r} equal to eq. 4.3 would lead to an estimation of zero overtopping for $d_r = 0$, which obviously is not the case for all combinations of H_s and R_c. Therefore, the coefficient $\kappa = 0.4$ is introduced and the expression for λ_{d_r} given by eq. 4.2 is obtained.

The result of applying λ_{d_r} is shown in figure 4.6.

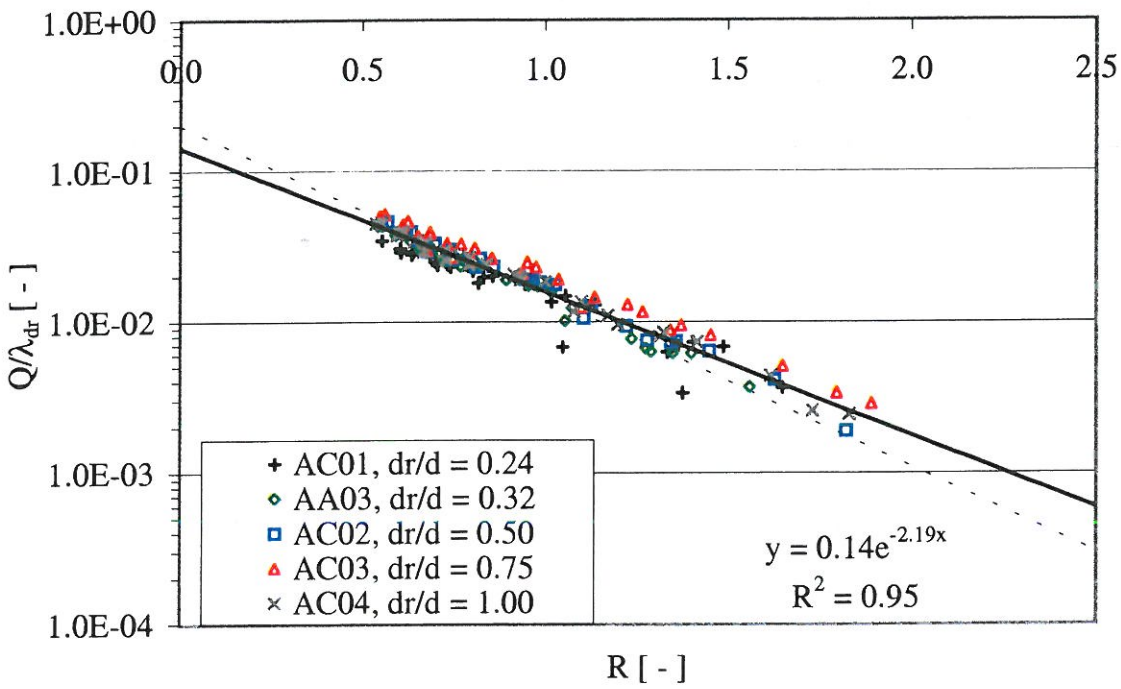

Figure 4.6: Results of tests with test geometries with varying d_r (test series AC). The dimensionless average overtopping rate Q divided by the correction factor λ_{d_r} is plotted as a function of the dimensionless crest freeboard R. The dotted line represents eq. 2.4 and the solid line is an exponential fit to all the showed data points.

As seen in figure 4.6 the correlation coefficient R^2 is hereby increased from 0.90 to 0.95.

4.1.4 Comparison with Van der Meer and Janssen (1995)

In figure 4.7 the results from the tests with linear ramps are plotted together with results given by Van der Meer and Janssen (1995) and Oumeraci et al. (1999). The data from Van der Meer and Janssen (1995) includes both data from tests with straight slopes and data from tests with slopes with a berm, foreshore, rough surface, short-crested and oblique waves. In the later case the data has been normalized using the appropriate reduction factors given by Van der Meer and Janssen (1995). The data from Oumeraci et al. (1999) includes data from 1:3, 1:4 and 1:6 slopes subjected to both 2D and 3D waves. Again the reduction factors given by Van der Meer and Janssen (1995) have been applied when appropriate. For the data from Van der Meer and Janssen (1995) and Oumeraci et al. (1999) the correction factors λ_α and λ_{d_r} are 1.

Figure 4.7 shows that for R larger than approx. 0.75 the expression given by Van der Meer and Janssen (1995) (eq. 2.4) fits the data very well. However, when R decreases from 0.75 towards 0 discrepancies increases. Motivated by these observations it is proposed that expression by Van der Meer and Janssen (1995) is modified by a correction factor λ_s in addition to the factors λ_α and λ_{d_r} introduced in the previous sections:

$$\lambda_s = \begin{cases} 0.4\sin(\frac{2\pi}{3}R) + 0.6 & \text{for } R < 0.75 \\ 1 & \text{for } R \geq 0.75 \end{cases} \tag{4.4}$$

Introduction of λ_s results in very good fit of all the data (indicated by a correlation coefficient $R^2 = 0.97$), also for R all the way down to 0, as shown in figure 4.8.

Thus on this background a new overtopping expression for non-breaking waves is formulated:

$$Q = \frac{q}{\lambda_\alpha \lambda_{d_r} \lambda_s \sqrt{g H_s^3}} = 0.2 e^{-2.6 \frac{R_c}{H_s} \frac{1}{\gamma_r \gamma_b \gamma_h \gamma_\beta}} \tag{4.5}$$

where λ_α, λ_{d_r} and λ_s are define by eq. 4.1, 4.2 and 4.4, respectively, and γ_r, γ_b, γ_h and γ_β, are defined as given in Van der Meer and Janssen (1995).

In the following analyses the definition of Q given in eq. 4.5 is used.

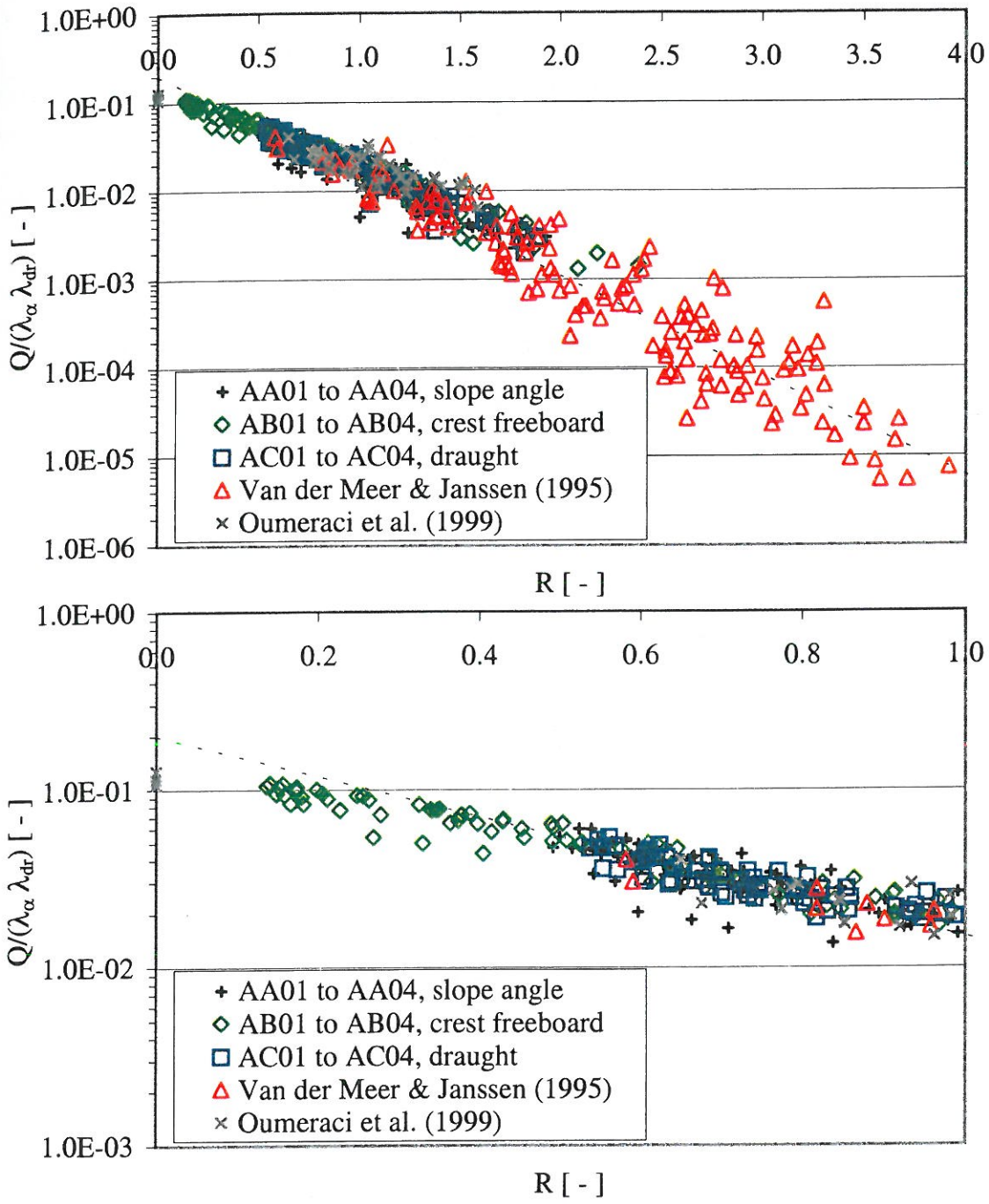

Figure 4.7: The experimental data from the tests with linear ramps plotted together with the overtopping data given in Van der Meer and Janssen 1995 for $\xi_p > 2$, and data reported by Oumeraci et al. (1999). The dotted line represents eq. 2.4. The lower graph is a zoom of the upper graph.

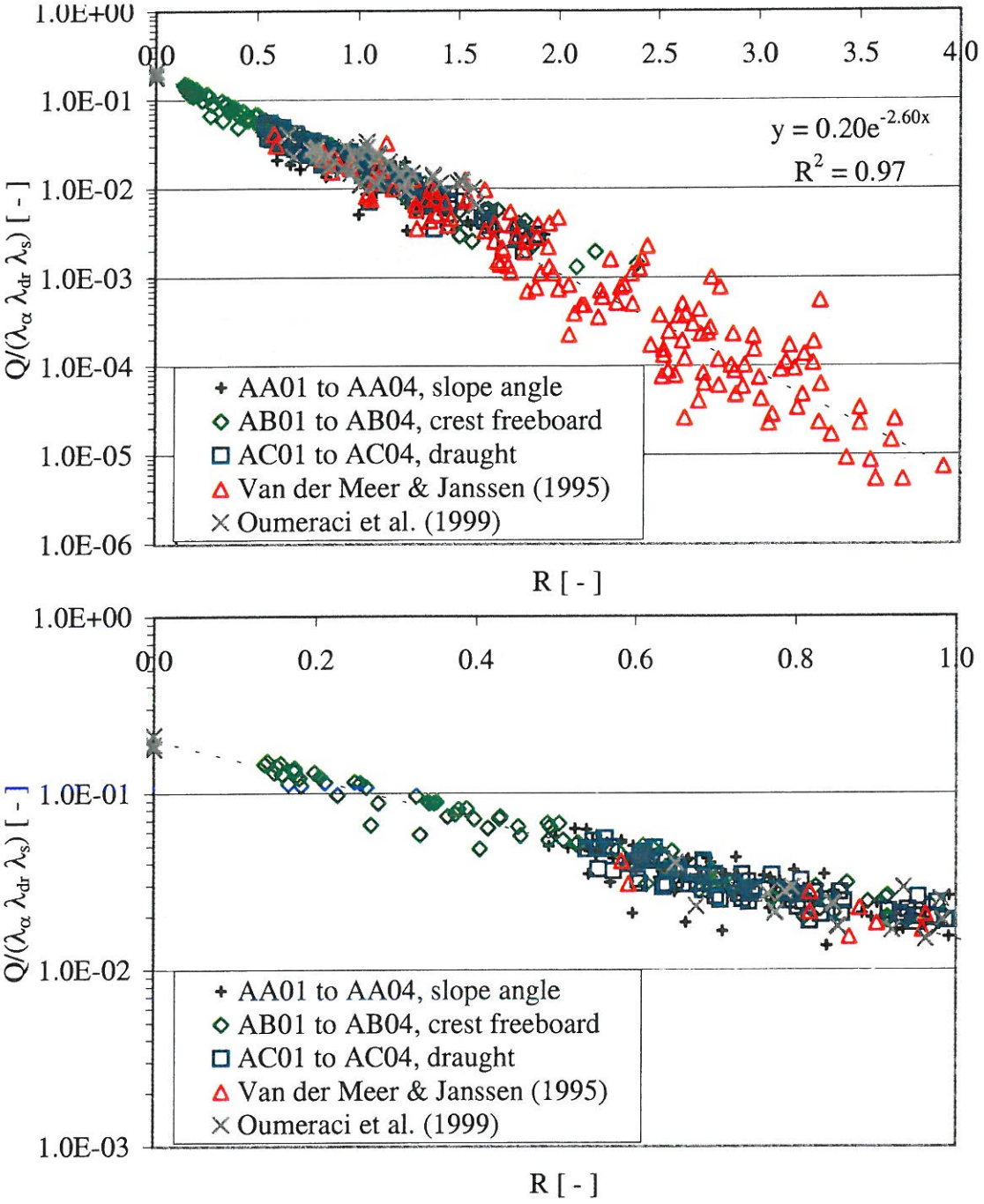

Figure 4.8: The experimental data from the tests with linear ramps plotted together with the overtopping data given in Van der Meer and Janssen 1995 for $\xi_p > 2$, and data reported by Oumeraci (1999). λ_s has been introduced. The dotted line represents eq. 2.4. The lower graph is a zoom of the upper graph.

4.1.5 Choice of setup for further tests

In order to choose the basic geometrical parameters to use in the following model tests of modifications of the ramp, an investigation of average efficiency of different tests ramp layouts. This has been done by calculating how much potential energy is obtained for each of the tested linear ramps over a year and compare this do the amount of energy present in the waves.

In this investigation five wave situations are used. These wave situations are typical for the Danish part of the North Sea and describes the conditions there in 85 % of the time. The wave situations are given by Bølgekraftudvalgets Sekretariat (1999) and are shown in table 4.1.

H_s [m]	T_p [s]	Prob. [%]	P_{wave} [kW/m]
1.0	5.6	47.6	2.5
2.0	7.0	21.4	13.6
3.0	8.4	9.6	35.0
4.0	9.8	4.1	69.3
5.0	11.2	1.7	123.7

Table 4.1: Wave situations typical for the Danish part of the North Sea. The probability and power flux for each of the wave situations are given. The given wave situations cover 85 % of the time.

In table 4.1 the wave power flux is based on wave energy transport per m wavefront P_{wave} [W/m] calculated by

$$P_{wave} = \frac{\rho g^2}{64\pi} \frac{m_{-1}}{m_0} H_s^2 \tag{4.6}$$

where m_{-1} and m_0 is the minus first and zero spectral moment, Falnes (1993).

The power obtained in terms of potential energy in the overtopping water is calculated as

$$\begin{aligned} P &= qR_c g \rho_w b \\ &= \sqrt{gH_{m0}^3} A e^{-B\frac{R_c}{H_{m0}}} R_c g \rho_w b \end{aligned} \tag{4.7}$$

The power P is calculated for each of the wave situations by use of the coefficients A and B fitted to the results of the tests of each of the geometries. The used

coefficients are given in the graphs in appendix B.1, figure B.2 to B.14. The average power P over a year is found weighing the power for each wave situation with the probability of occurrence of the wave situation. Thus the average ratio $\frac{P}{P_{wave}}$ (also called efficiency) can be calculated for each of the tested linear ramp. These ratios are plotted in figure 4.9 as functions of slope angle, relative crest freeboard and relative draught.

From the first graph in figure 4.9 the choice of slope angle $\alpha = 30°$ is obvious. The choice of crest freeboard not a obvious but keeping in mind that turbines have better performance for larger head than lower (at least in the low head range in which all overtopping devices are operating) results in a choice of a relative crest freeboard $\frac{R_c}{d} = 0.10$. When choosing the draught a consideration of getting as much overtopping as possible of course would lead to extending the ramp all the way to the bottom. However, from a cost-benefit point of view this is not considered optimal. Therefore a relative draught $\frac{d_r}{d} = 0.4$ is chosen as the benefit of going deeper in terms of obtained power is smaller the loss of power by going less deep.

In conclusion the reference and starting point of the models tested in the following is a linear ramp with a slope angle $\alpha = 30$ °, a relative crest freeboard $\frac{R_c}{d} = 0.10$ and a relative draught $\frac{d_r}{d} = 0.4$.

Comments on calculated efficiencies

From figure 4.9 it can be seen that the ratio between the amount of potential energy in the water overtopping a structure as the tested ones (with a limited draught) and the energy present in the waves averaged over time ($\frac{P}{P_{wave}}$) can be as high as 20 - 25 % for a placement of the structure in the Danish part of the North Sea. This is obtained for geometry AB01 and AB02 where $\alpha = 40°$, $\frac{d_r}{d} = 0.32$ and $\frac{R_c}{d} = 0.04$ and 0.10, respectively. For the selected reference linear ramp it is likely that an even higher $\frac{P}{P_{wave}}$-value is obtained.

In order to put these results into perspective theoretical considerations concerning regular wave overtopping of string are presented in appendix A. From this it is seen that if only the potential energy present in the regular wave is considered (this is what is meant by overtopping of a string) the maximum efficiency $\frac{P}{P_{wave}}$ is 11.5 % for shallow water and 23.1 % for deep water. Compared to the results above these are rather small values, considering that the values stated above are overall efficiencies for a number of irregular wave situations. However, by placing a ramp in the waves a part of the kinetic energy that is present in the waves are converted into potential energy in the overtopping waves which add significantly to the efficiencies.

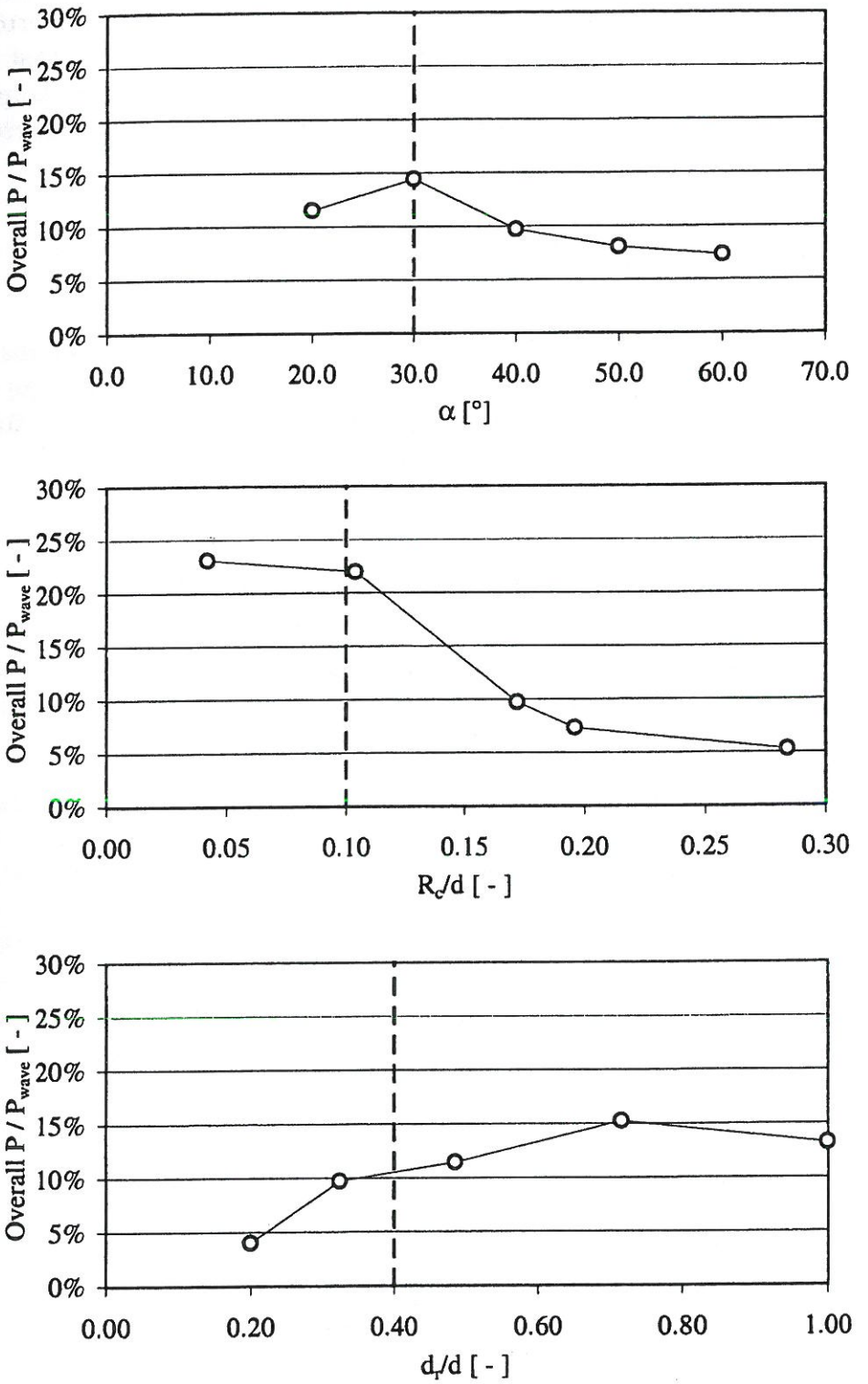

Figure 4.9: The efficiency ($\frac{P}{P_{wave}}$) of the tested linear ramps plotted as functions of slope angle, relative crest freeboard and relative draught. The vertical broken line indicates the choices for the further model tests.

It should be noted that the potential energy that is used when calculating the efficiency $\frac{P}{P_{wave}}$ is the amount of potential energy present in the overtopping water at the time it passes over the crest of the ramp. This means that unless the water level behind the ramp is not kept right to the crest of the ramp at all time some of the potential energy is lost and the efficiency thus also decreased.

4.2 Modifications of the ramp profile

In this section the results of the model tests with modifications of the ramp profile are presented and analyzed. In appendix B.2 the basic results are shown in figure B.15 to B.40. In the following the dimensionless overtopping rate Q is defined as $\frac{q}{\lambda_\alpha \lambda_{d_r} \lambda_s \sqrt{g H_s^3}}$ as it was found in section 4.1.4, eq. 4.5.

4.2.1 Horizontal plate at ramp bottom

In the test series BA horizontal plates with different lengths has been place at the ramp bottom. The effect of these horizontal plates on the overtopping rate can be seen in figure 4.10.

From figure 4.10 it is seen that the effect of adding a horizontal plate at the ramp bottom depends highly on the length of it. The longest horizontal plate (BA01) results in almost exactly the same overtopping rates as without (BA04), while a plate with half the length (BA02) results in an increase of 7 %, while a plate with a quarter of the length (BA03) results in a decrease of the overtopping rate of 9 %. This indicates that it is favorable to use a plate with a length of 25 % of the ramp draught, but it seems appropriate to perform additional tests with horizontal plates with lengths in this range in order to find the optimal length.

4.2.2 Convex top of ramp

In the test series CA the upper part of the ramp have been given a convex deflection and with an unchanged slope angle below the deflection. The effect of these deflections on the overtopping rate can be seen in figure 4.11.

From figure 4.11 it is seen that no increase in the overall overtopping rate is obtained by introducing a convex deflection with an unchanged slope angle below the deflection. In fact in the case where the largest radius of the convex part was used (CA03) an overall reduction of almost 11 % was found, while the two smaller convex deflections had no effect (less than 2 %).

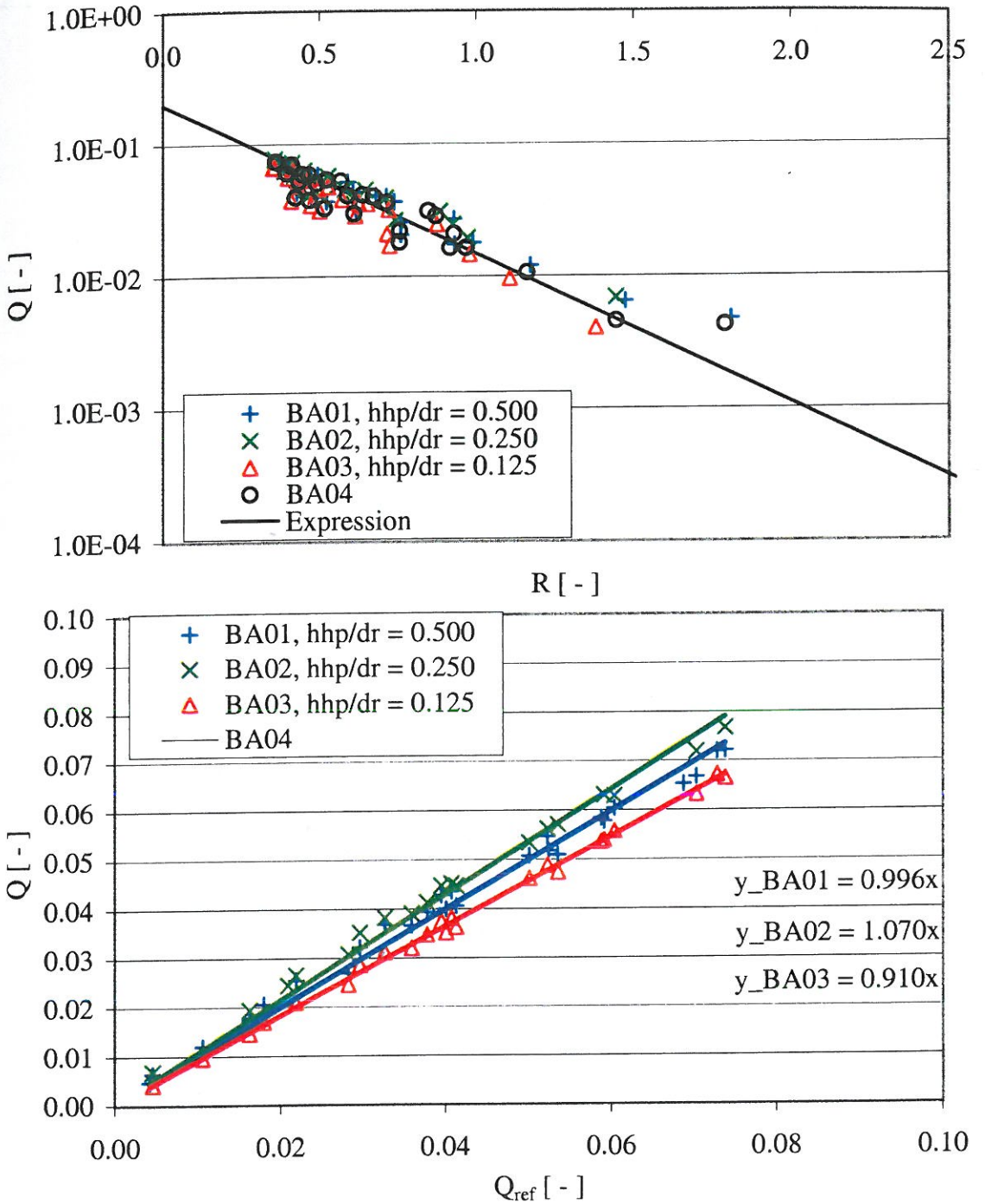

Figure 4.10: Results of tests with horizontal plate at ramp bottom (test series BA). In the upper graph the dimensionless average overtopping rate Q is plotted as a function of the dimensionless crest freeboard R. The line represents eq. 4.5. In the lower graph the results of the tests with horizontal plate at ramp bottom (Q) are compared to the corresponding results of reference test BA04 (Q_{ref}).

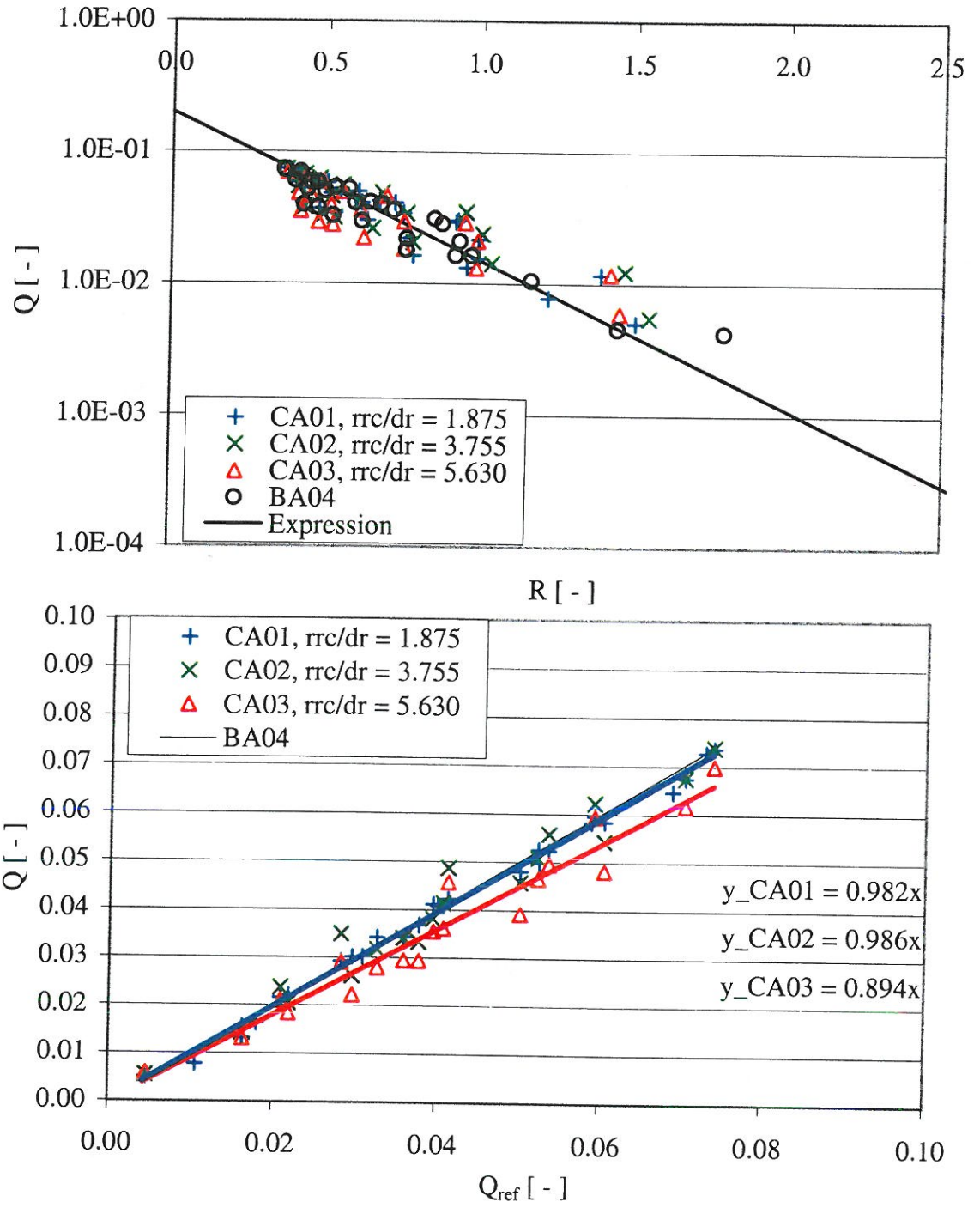

Figure 4.11: Results of tests with convex top of the ramp (test series CA). In the upper graph the dimensionless average overtopping rate Q is plotted as a function of the dimensionless crest freeboard R. The line represents eq. 4.5. In the lower graph the results of the tests with convex top of the ramp (Q) are compared to the corresponding results of reference test BA04 (Q_{ref}).

Then a series of tests also with a convex deflection but now with a changed slope angle of 35° (CB01). The effect of this can be seen in figure 4.12.

From figure 4.12 it is seen that this modification results in an overall increase of the overtopping rate of 4 %.

A test series has also been perform on a ramp with a convex top of the ramp with an elliptic shape (test series CC). This ramp geometry has been suggested by the inventor of WD, Erik Friis-Madsen, and the cross section of the ramp on WD has been modified to shape similar to the one tested in test CC01. The results of the tests are shown in figure 4.13.

From figure 4.13 it is seen that this modification results in an overall increase of the overtopping rate of 18 %. On this background it seems reasonable to do more tests of ramps with an elliptic ramp shape in order to disclose if this is the optimal shape or an even better can be found.

4.2.3 Concave top of ramp

A test series with a concave top of the ramp (test series DA) have been performed. The results of these tests are shown in figure 4.14.

From figure 4.14 it can be seen that introducing the concave top of the ramp reduces the overall overtopping rates with more than 11 %. This result is in agreement with the results reported by Josefson (1978) referred in section 2.2.

4.3 Modifications of the side walls of the ramp

In this section the results of the model tests with modifications of the ramp profile are presented and analyzed. In appendix B.3 the basic results are shown in figure B.35 to B.40.

4.3.1 Linear converging guiding walls

A series of tests have been performed with four different layouts of linear converging walls (test series EA). The results of these tests are given in figure 4.15.

From figure 4.15 it can be seen that a positive effect is obtained by using linear converging walls with an opening ratios relatively close to one (opening ratio 0.848 and 0.696 results in an increase in the overall overtopping of 15 and 4 %, respectively) while for smaller opening ratios results in reductions in the overall

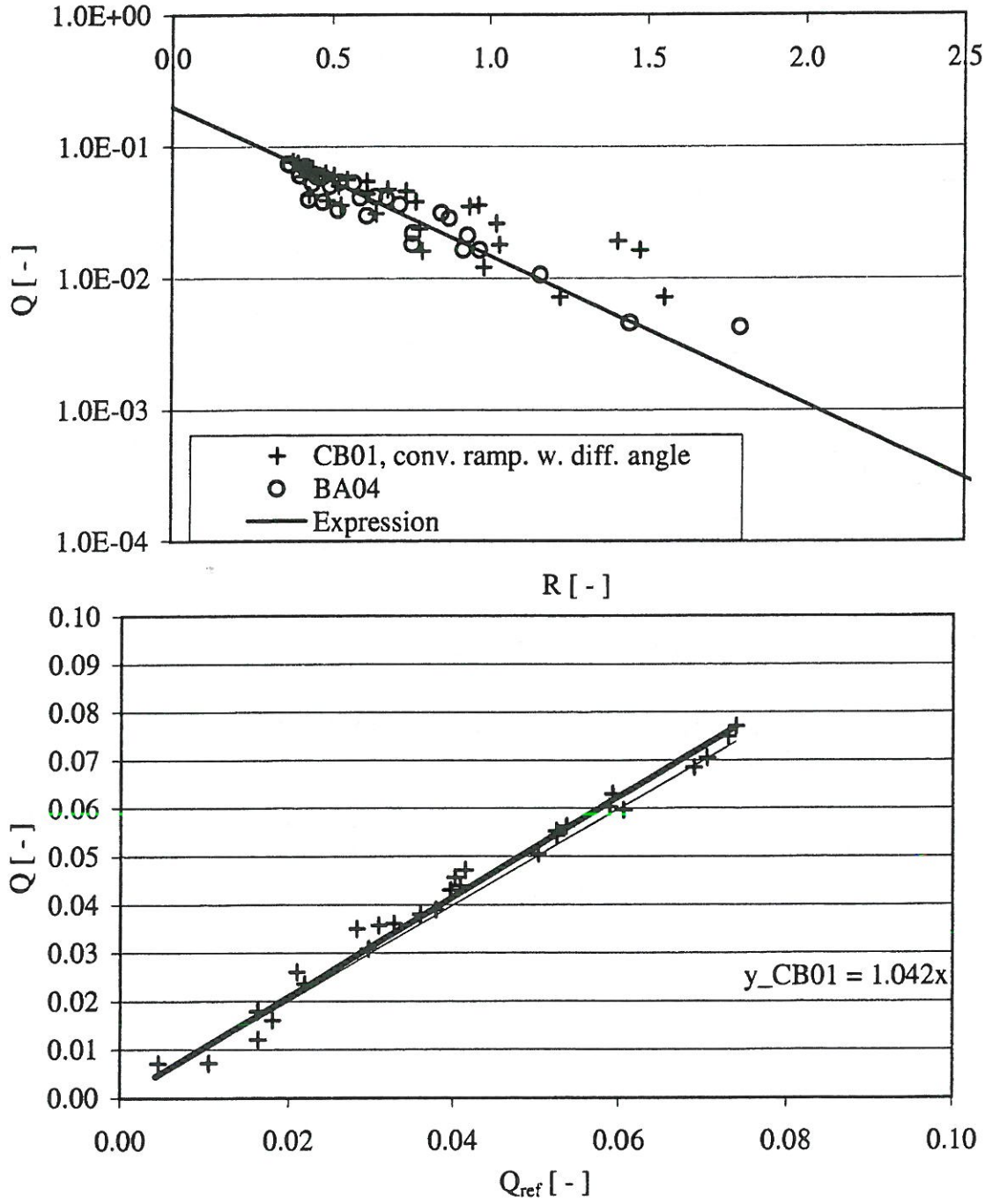

Figure 4.12: Results of tests with convex top of the ramp with a slope angle α = 35° (test series CB). In the upper graph the dimensionless average overtopping rate Q is plotted as a function of the dimensionless crest freeboard R. The line represents eq. 4.5. In the lower graph the results of the tests with convex top of the ramp with a slope angle α = 35 °(Q) are compared to the corresponding results of reference test BA04 (Q_{ref}).

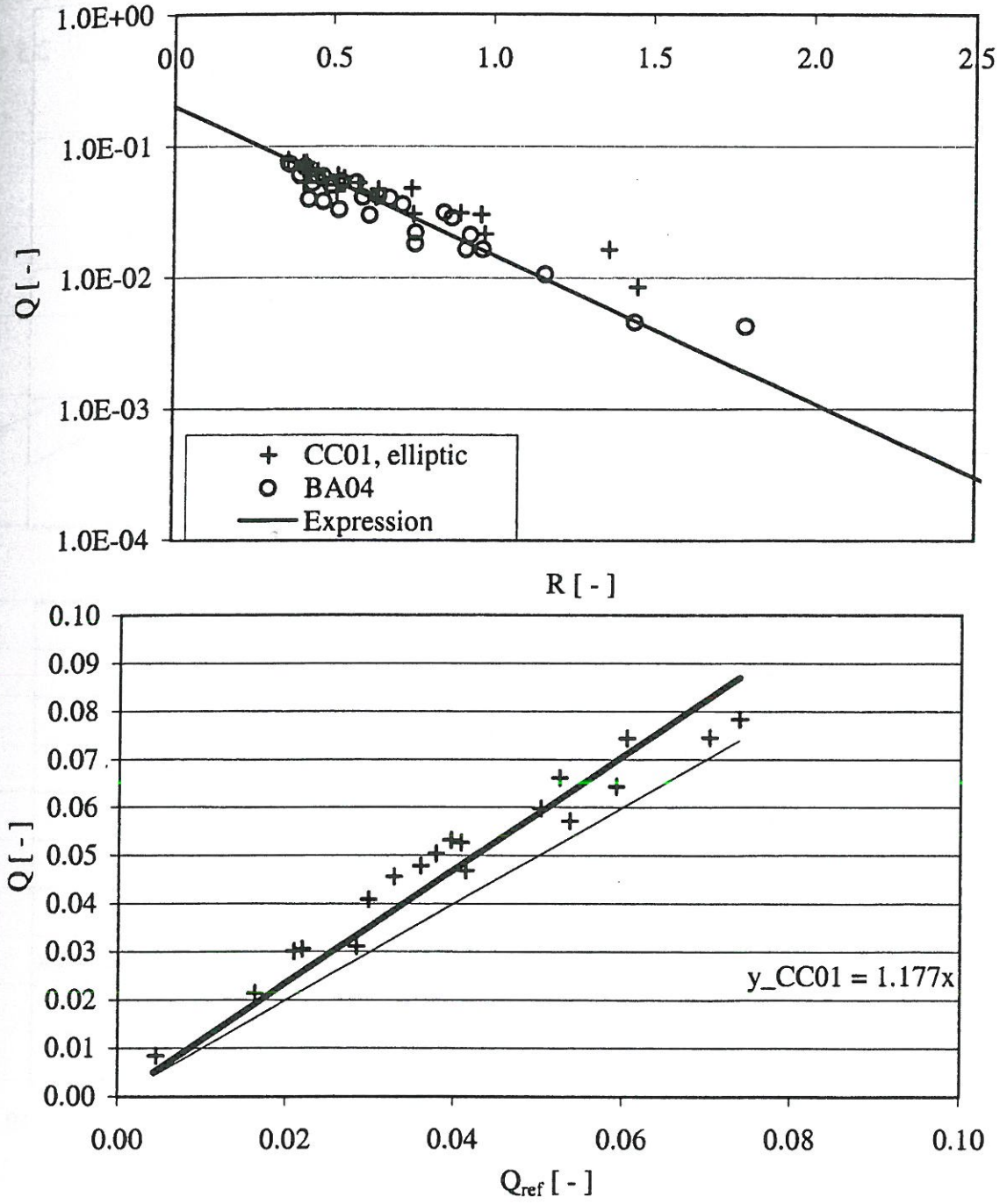

Figure 4.13: Results of tests with convex top of the ramp with an elliptic shape (test series CC). In the upper graph the dimensionless average overtopping rate Q is plotted as a function of the dimensionless crest freeboard R. The line represents eq. 4.5. In the lower graph the results of the tests with convex top of the ramp with an elliptic shape (Q) are compared to the corresponding results of reference test BA04 (Q_{ref}).

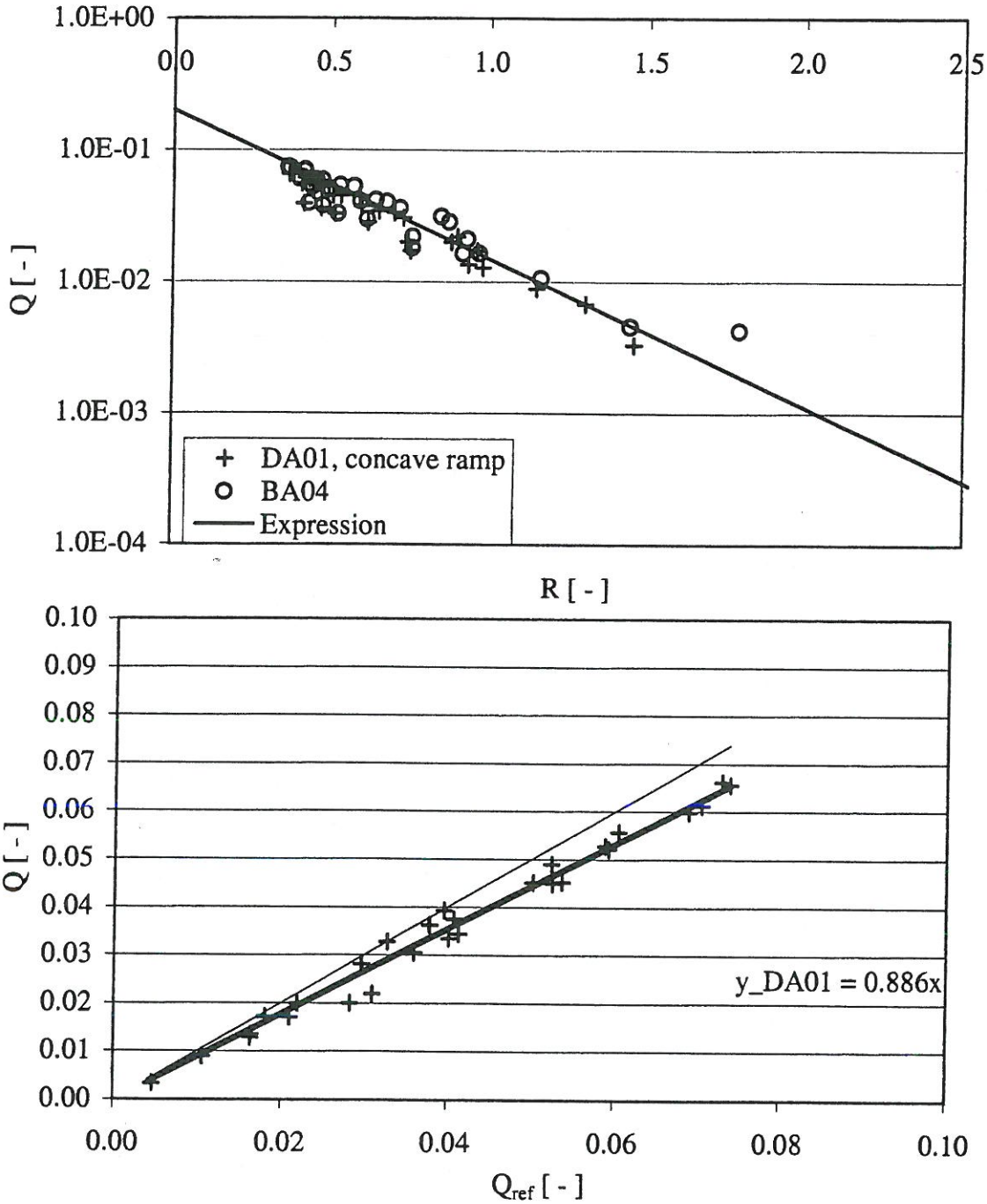

Figure 4.14: Results of tests with concave top of the ramp (test series DA). In the upper graph the dimensionless average overtopping rate Q is plotted as a function of the dimensionless crest freeboard R. The line represents eq. 4.5. In the lower graph the results of the tests with concave top of the ramp (Q) are compared to the corresponding results of reference test BA04 (Q_{ref}).

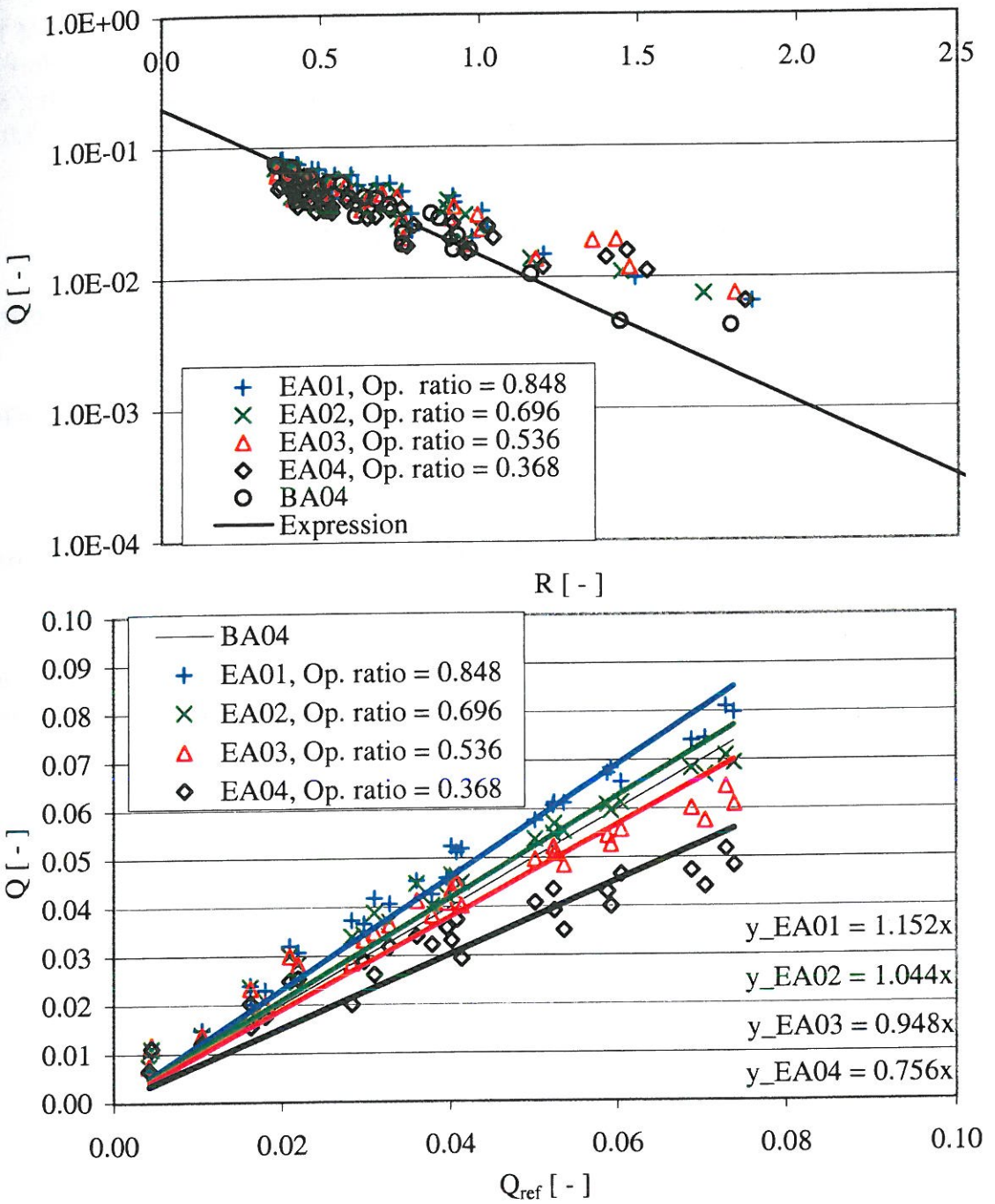

Figure 4.15: Results of tests with linear guiding walls (test series EA). In the upper graph the dimensionless average overtopping rate Q is plotted as a function of the dimensionless crest freeboard R. The line represents eq. 4.5. In the lower graph the results of the tests with linear guiding walls (Q) are compared to the corresponding results of reference test BA04 (Q_{ref}).

overtopping rate (opening ratios of 0.536 and 0.368 results in reductions of 5 and 24 %, respectively). However, for obvious reasons for an opening ratio of 1 no increase or decrease is present, and it therefore seems reasonable to perform additional tests in order to find the optimal opening ratio by testing testing a ramp with linear guiding walls with opening ratios in the range from 0.7 to 1.0.

4.3.2 Curved converging guiding walls

A test series have been performed with curved converging walls (test series FA). The results are given in figure 4.16.

From figure 4.16 it is seen that there is no effect of using curved guiding walls instead of linear.

4.3.3 Summary of the results from tests with modifications of the ramp profile

In order to provide a mean to calculate the average overtopping rates for the tested modified ramp profiles a new correction factor λ_m is introduced in the overtopping expression eq. 4.5 so it becomes:

$$\frac{q}{\lambda_m \lambda_\alpha \lambda_{d_r} \lambda_s \sqrt{g H_s^3}} = 0.2e^{-2.6 \frac{R_c}{H_s} \frac{1}{\gamma_r \gamma_b \gamma_h \gamma_\beta}} \tag{4.8}$$

The λ_m values for the tested modifications are given in table 4.2.

In appendix B.3, figure 4.10 to B.39, the layouts of the geometries listed table 4.2 is given.

4.4 Time dependency of overtopping rates

In this section an empirical model for time variation of overtopping discharge is verified through a comparison with two of the performed tests. The motivation for this is that little or no knowledge is presently available regarding the time variation of overtopping discharge for ramp layouts typical for wave energy converters of the overtopping type. In order to optimize the reservoir size and the control strategy for the turbines utilizing the overtopping water, so the loss of energy in reservoir and turbines are minimized, it is important to know how

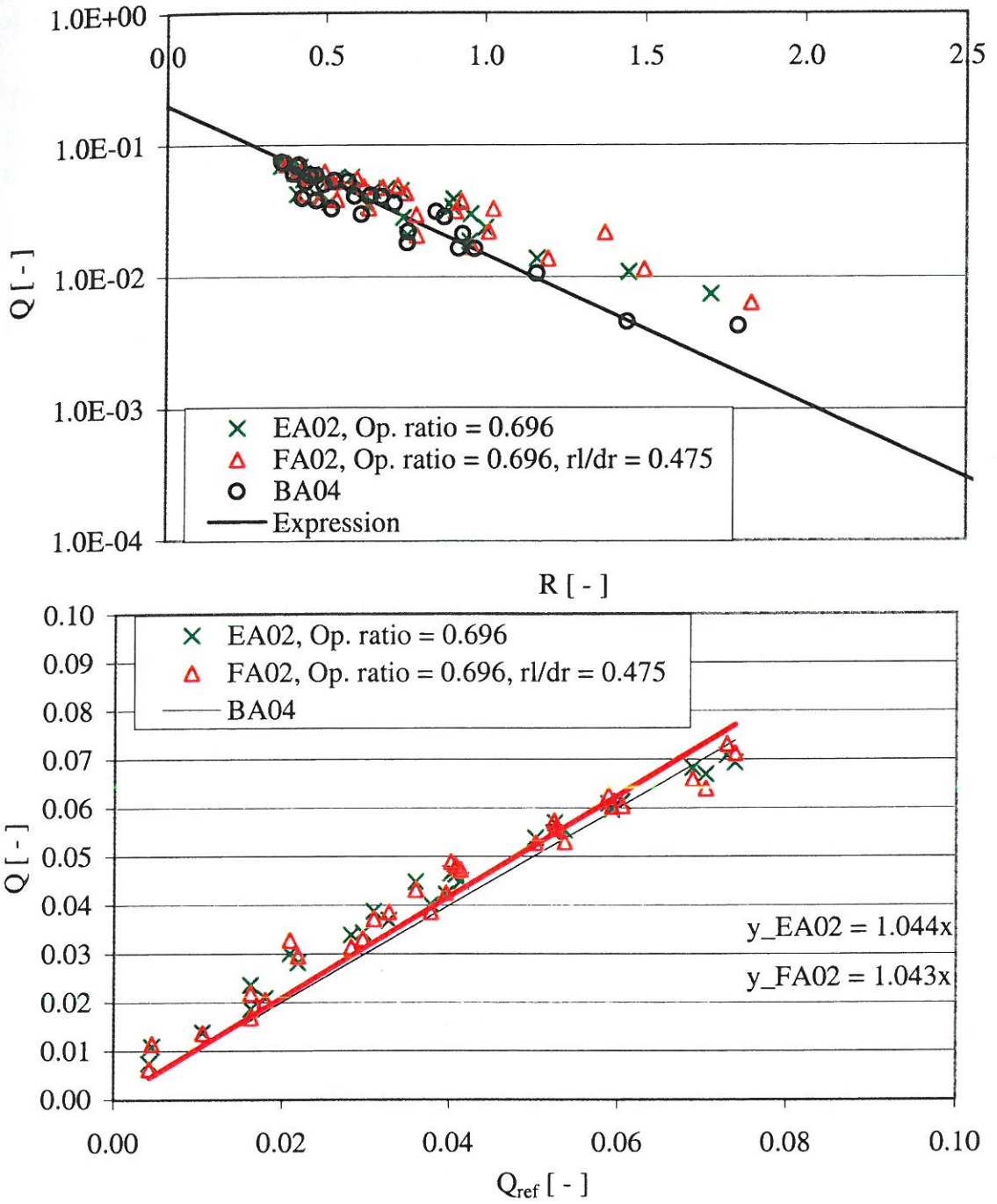

Figure 4.16: Results of tests with curved guiding walls (test series FA). In the upper graph the dimensionless average overtopping rate Q is plotted as a function of the dimensionless crest freeboard R. The line represents eq. 4.5. In the lower graph the results of the tests with curved guiding walls (Q) are compared to the corresponding results of reference test BA04 (Q_{ref}).

Session name	Description	λ_m [-]
BA01	Horizontal plate	1.00
BA02	Horizontal plate	1.07
BA03	Horizontal plate	0.91
BA04	Reference setup	1.00
CA01	Convex slope	0.98
CA02	Convex slope	0.99
CA03	Convex slope	0.89
CB01	Convex slope, diff. angle	1.04
CC01	Convex slope, elliptic	1.18
DA01	Concave ramp	0.87
EA01	Linear converging walls	1.15
EA02	Linear converging walls	1.04
EA03	Linear converging walls	0.95
EA04	Linear converging walls	0.76
FA02	Curved converging walls	1.04

Table 4.2: Correction factors λ_m to be used in eq. 4.8.

the irregular nature of ocean waves influence the variation of the overtopping discharge.

As seen in chapter 2 the main focus in literature has so far been on mean overtopping discharge for sea defense structures like seawalls, breakwaters and dikes. In some cases also the probability of an overtopping event, as well as the distribution of the largest overtopping volumes (e.g. the mean overtopping volume from the 1/250 largest overtopping events) have been investigated. However, as the objective of these studies mainly have been to investigate extreme overtopping events for sea defense structures, designed to avoid or at least limit the amount of overtopping, they cannot in general be expected to cover the parameter ranges that are of interest for wave energy devices, where generally maximum potential energy of overtopping volumes is wanted. Thus, in the present study the attention is specially directed to situations with small values of the relative crest freeboard R (smaller than, say, 0.75). The equations given by Van der Meer and Janssen (1995) have been developed for breakwaters and dikes that typically have larger values of R (see also section 4.1.4). Martinelli and Frigaard (1999a) presented an empirical model for prediction of time variation of overtopping. This model is based on formulae by Van der Meer and Janssen (1995).

4.4.1 Empirically based model

The empirical model by Martinelli and Frigaard (1999a) for calculating the overtopping discharge is based on the expression for probability of overtopping P_{ot} given by Van der Meer and Janssen (1995):

$$P_{ot} = e^{-(\frac{1}{1.21}\frac{H_s}{R_c})^{-2}} \tag{4.9}$$

Furthermore, the following expression (also given by Van der Meer and Janssen (1995)) for the probability P_{V_w} of a certain overtopping volume in a wave V_w given that overtopping occurs, is used to calculate the volume of an overtopping wave:

$$\begin{aligned} P_{V_w} &= 1 - e^{-(\frac{V_w}{a})^{\frac{3}{4}}} \;,\; a = 0.84\frac{qT_m}{P_{ot}} \\ V_w &= 0.84\frac{qT_m}{P_{ot}}(-ln(1-P_{V_w}))^{\frac{3}{4}} \end{aligned} \tag{4.10}$$

In order to calculate a time series of overtopping volumes the following procedure is used:

- P_{ot} is calculated using eq. 4.9.
- q is calculated using an overtopping formula or as in this investigation simply taken from a model test.
- For a chosen number of waves N (each assumed to be T_m long) the following is done:

  A random number p between 0 and 1 is drawn.

  If $p > P_{ot}$ then V_w^i is set to 0, else V_w^i is calculated using eq. 4.10.
- The obtained series of V_w^i 's (V_w^1 to V_w^N) is then converted into a discharge time series $q_{sim}(t)$ in order to enable a comparison with a measured discharge time series from the model tests $q_{meas}(t)$.

Figure 4.17 shows an example of the results of a simulation using the empirical(implemented in the PC program WDpower utilized in the development of WD by Jakobsen and Frigaard (1999)). Based on such simulations it is possible to test turbine configurations and control strategies, see Madsen and Frigaard (2000).

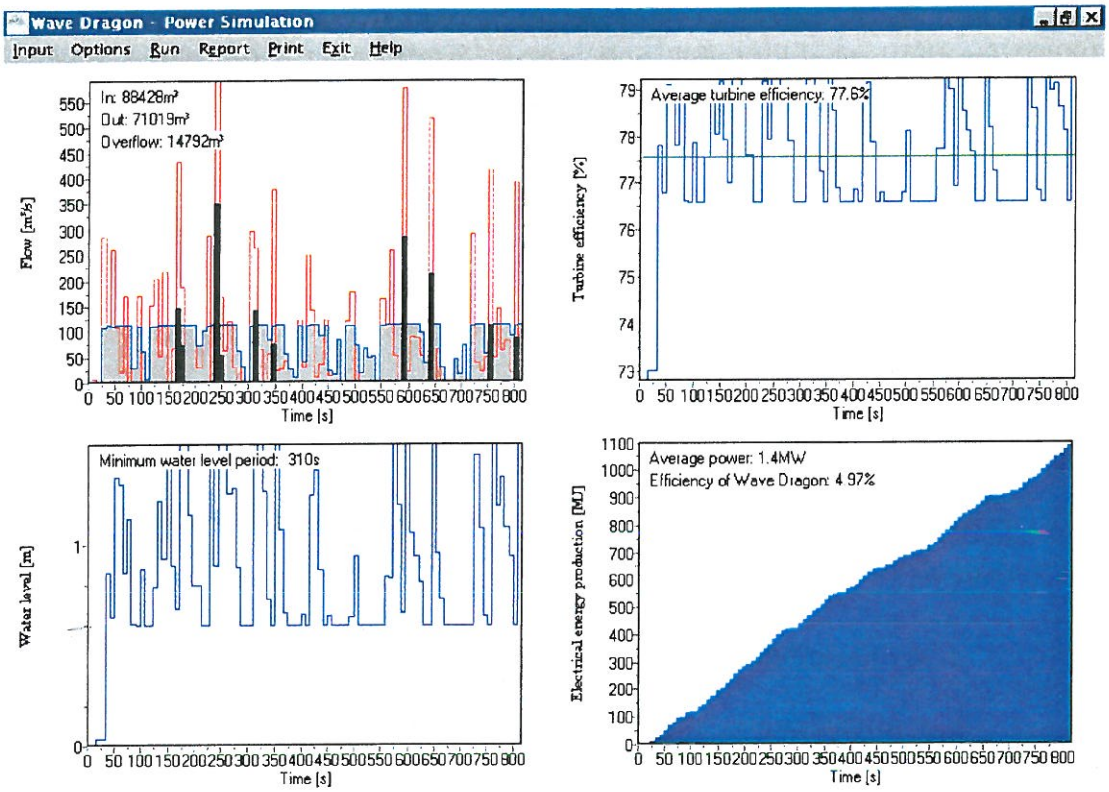

Figure 4.17: An example of a simulation performed using the empirical model WDpower.

4.4.2 Test results and comparison with empirical model

The comparison of $q_{sim}(t)$ and $q_{meas}(t)$ is performed by comparing the results of an analysis done in the following way for each of the discharge time series:

- The discharge time series is divided into N_{window} sub-series each T_{window} long.
- For each of the sub-series the average discharge values q^i_{window} (for $i = 1$ .. N_{window}) are obtained.
- Each of the values q^i_{window} are normalized by the average discharge of the whole time series q ($\frac{q^i_{window}}{q}$), and the average (which should be 1) and the standard deviation of these values are calculated.

If the probability distribution of $\frac{q^i_{window}}{q}$ of the two time series are the same it can be concluded that the simulation method is able to predict overtopping time series for ramps with low freeboards.

Two model tests have been selected for the evaluation of the simulation method. The geometry BA04 is used and the wave situations are characterized by H_s = 4.0 and 8.0 m, respectively, both with a T_p = 8.0 s. This results in relative crest freeboards R = 0.61 and 0.37, respectively.

For each of the 2 tests chosen for this analysis the comparison is done using a window size corresponding to $\frac{T_{window}}{T_m} = 60$ (assuming $\frac{T_p}{T_m} = 1.13$). The results of this are shown in figure 4.18.

Furthermore, the analysis have been done using different values for T_{window} for the test with R = 0.61. The results of this are given in figure 4.19 and 4.20.

R	$\frac{T_{window}}{T_m}$	St. dev. ($\frac{q^i_{window}}{q}$) for $q_{meas}(t)$	St. dev. ($\frac{q^i_{window}}{q}$) for $q_{sim}(t)$	Ratio
0.61	300	0.12	0.10	1.20
0.61	120	0.17	0.16	1.06
0.61	60	0.26	0.20	1.30
0.61	30	0.39	0.28	1.39
0.61	10	0.57	0.50	1.14
0.37	60	0.17	0.19	0.89

Table 4.3: Standard deviations of $\frac{q^i_{window}}{q}$ (i = 1 .. N_{window}) for $q_{meas}(t)$ and $q_{sim}(t)$ and the ratios between these.

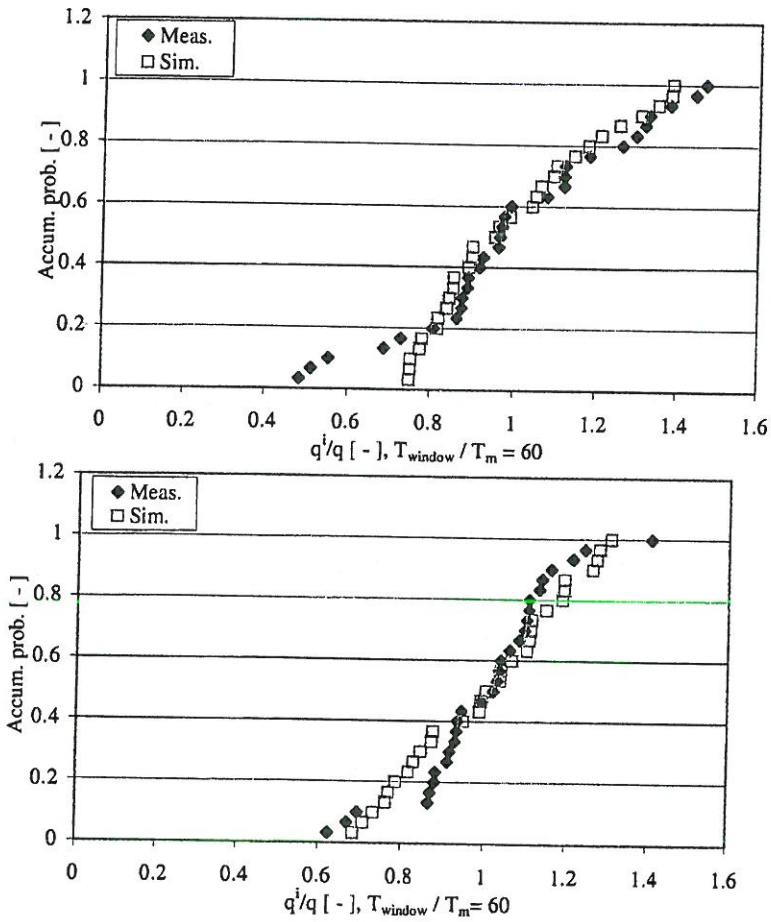

Figure 4.18: Results for the two tests with $R = 0.61$ (top) and 0.37 (bottom). The accumulated probability density for $\frac{q^i_{window}}{q}$ is plotted for $q_{meas}(t)$ and $q_{sim}(t)$, respectively.

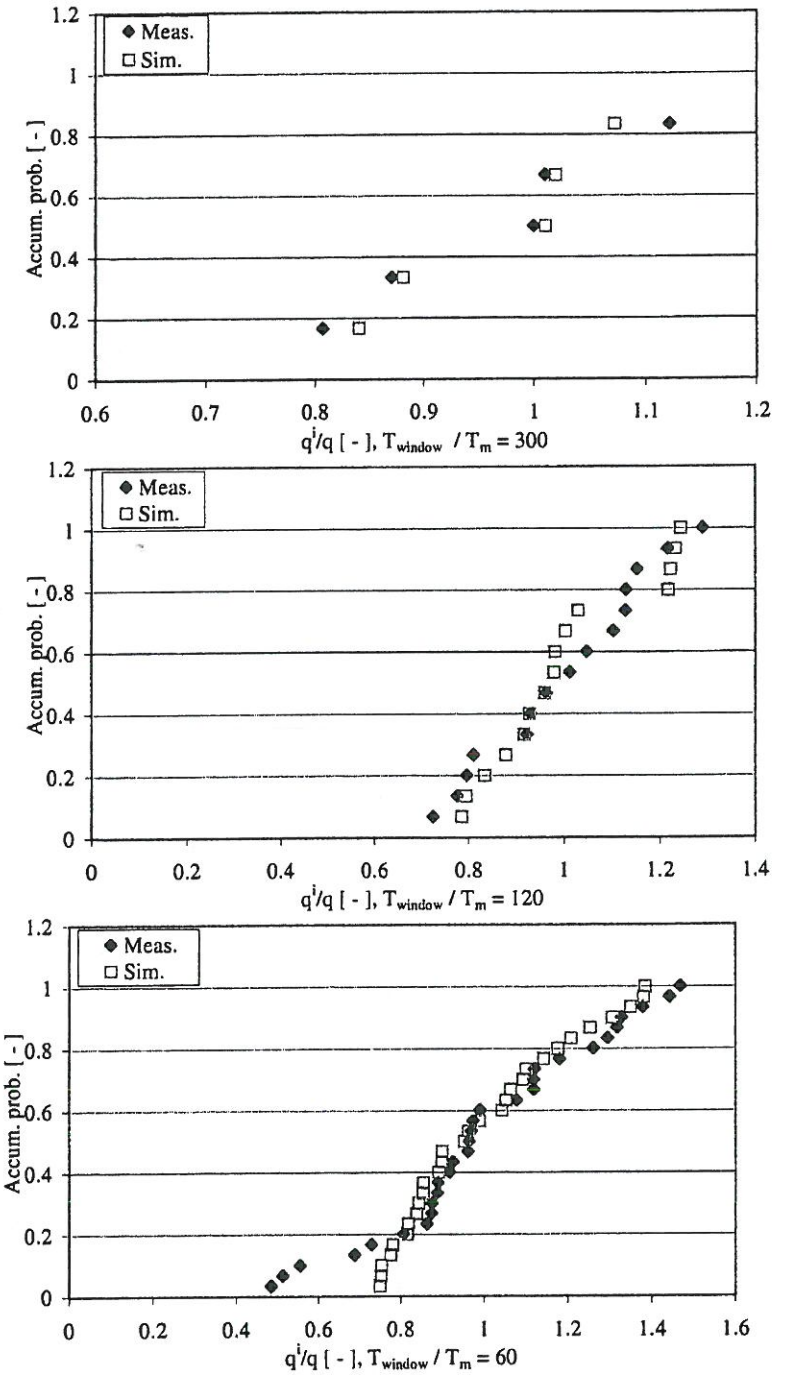

Figure 4.19: Results for the $R = 0.61$ where different T_{window} have been applied ($\frac{T_{window}}{T_m} = 300$ (top), $\frac{T_{window}}{T_m} = 120$ (middle) and $\frac{T_{window}}{T_m} = 60$ (bottom)). The accumulated probability density for $\frac{q^i_{window}}{q}$ is plotted for $q_{meas}(t)$ and $q_{sim}(t)$, respectively.

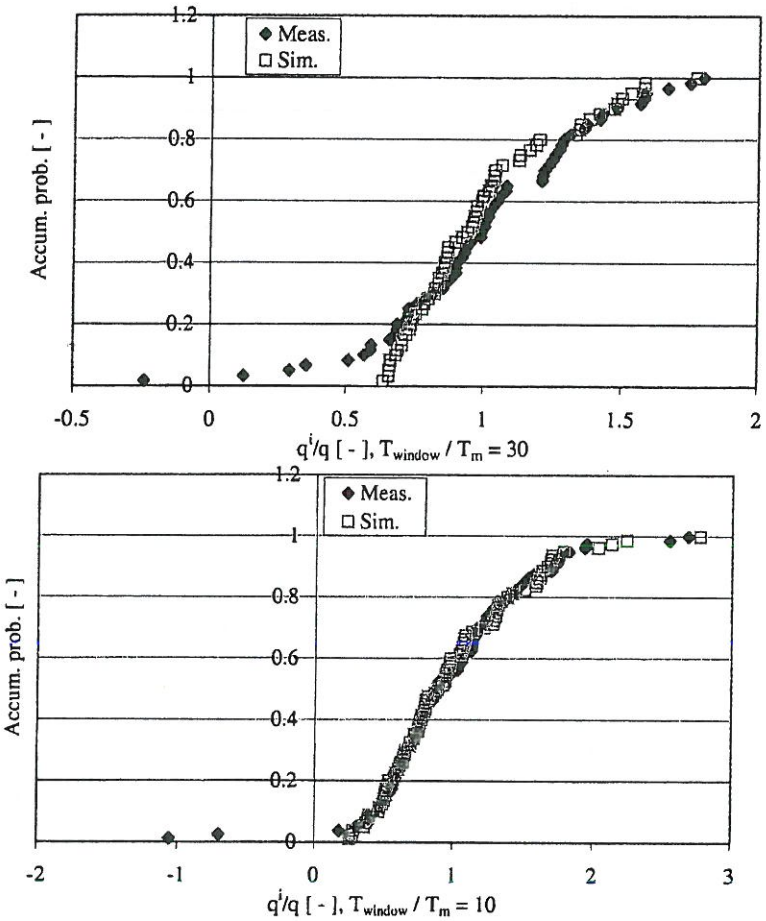

Figure 4.20: Results for the $R = 0.61$ where different T_{window} have been applied ($\frac{T_{window}}{T_m} = 30$ (top) and $\frac{T_{window}}{T_m} = 10$ (bottom)). The accumulated probability density for $\frac{q^i_{window}}{q}$ is plotted for $q_{meas}(t)$ and $q_{sim}(t)$, respectively.

In table 4.3 the standard deviations of $\frac{q^i_{window}}{q}$ (i = 1 .. N_{window}) for $q_{meas}(t)$ and $q_{sim}(t)$ is given along with the ratio between these. From the presented results the following can be observed:

- For the tests with $R = 0.61$ and 0.37 with $\frac{T_{window}}{T_m} = 60$ (figure 4.18) it is seen that good agreement is found between the analysis of $q_{meas}(t)$ and $q_{sim}(t)$. However, from table 4.3 it is see that for the test with $R = 0.61$ the standard deviation for $q_{meas}(t)$ is 30 % larger than for $q_{sim}(t)$, while for the test with $R = 0.37$ the standard deviation for $q_{meas}(t)$ is 11 % smaller than for $q_{sim}(t)$. For the simulation of overtopping for the evaluation of turbine configuration etc. in a wave energy converter these deviations are considered acceptable. From results for the test with $R = 0.61$ and varying T_{window} (figure 4.19 and 4.20) it is seen that the standard deviation for $q_{meas}(t)$ is larger (6 - 39 %) than for $q_{sim}(t)$ for all values of T_{window}. Thus the tendency is in general the same as seen for $\frac{T_{window}}{T_m} = 60$.

- For the test with $R = 0.61$ and $\frac{T_{window}}{T_m} = 30$ and 10 (figure 4.20) is is seen that q^i_{window} for a few subseries is negative. This supports that the limit of how small a value of T_{window} for which the analysis is reasonable is approx. 10 waves.

- For both $q_{meas}(t)$ and $q_{sim}(t)$ it is seen from table 4.3 that the standard deviation of $\frac{q^i_{window}}{q}$ decrease for increasing T_{window}.

CHAPTER 5

Conclusion

In this chapter conclusions from the performed study are drawn.

5.1 Overtopping of linear ramps

By use of model tests wave overtopping of non-breaking waves on a linear ramp have been investigated. The effect of limited draught and the angle (in combination with a limited draught) of the ramp on the overtopping rate have been investigated. An expression taking into account these effects have been presented. Furthermore, the results of the performed model tests have been compared to existing overtopping investigations. The model tests have "closed a gap" between existing investigations for low crest freeboards, and an overtopping expression for non-breaking waves have been proposed. This expression enables prediction average overtopping rates for relative crest freeboards down to 0. The proposed expression also includes effect of limited draught and the angle (in combination with a limited draught) of the ramp.

5.2 Overtopping of ramps with modified designs

A number of modifications of the ramp shape and shape of the side walls have also been tested. It has been found that in terms of maximizing overtopping it is favorable to apply a horizontal plate at the ramp bottom with a length of 25 % of the ramp draught (geometry BA02 results in a 7 % increase of the

overall overtopping compared to the linear reference ramp BA04), a convex top of the ramp with an elliptic shape (geometry CC01 results in a 18% increase of the overall overtopping compared to the linear reference ramp BA04) and linear guiding walls with an opening ratio of 0.848 (geometry EA01 results in a 15% increase of the overall overtopping compared to the linear reference ramp BA04). The tests with the convex top of the ramp indicates that slope angle needs to be increased as the convexity of the top of the ramp is increased (geometry CC01 that resulted in the largest increase of the overall overtopping rate has a slope angle of 45° and a large part of the ramp is convex with an elliptic shape).

The estimations given in 4.1.5 regarding the tests with linear ramps and the results of the tests with the modified ramps indicates that the ratio between the amount of potential energy in the water overtopping a structure as the tested ones (with a limited draught) and the energy present in the waves averaged over time ($\frac{P}{P_{wave}}$) is 20 - 35 % (depending on the geometry of the ramp and the side walls) if the structure is placed in the Danish part of the North Sea.

5.3 Time dependency of overtopping rates

The performed investigation of time dependency of overtopping rates has indicated that the existing empirical model given by Martinelli and Frigaard (1999a) produces reasonable results. However, the simulated overtopping discharge time series results in standard deviations of $\frac{q^i_{window}}{q}$ $(i = 1 \,..\, N_{window})$ that for one case is smaller than the measured, and in another case it is larger. This, combined with the fact that only two model tests have been used, indicates that the simulation method probably can be improved by including more model tests in the investigation.

5.4 Further research

Although a large number of model tests have already been performed within this project it seems that even more testing could be feasible. Especially the tests of modified ramp shapes have disclosed areas where additional testing is necessary in order to investigate the found positive effects on the overtopping (in terms of maximizing the overall overtopping rates) in to more details. It seems that additional tests with horizontal plates at the ramp bottom, with convex top of the ramp with an elliptic shape and with linear guiding walls with an opening ratio in the range from 0.7 to 1.0 could lead to even larger increases in the overall overtopping rates.

Furthermore, a more extensive investigation of the time dependency of overtopping rates seems to be appropriate in order to improve the simulation method.

The work carried out in this project is continued in the ongoing Ph.D. study by the author. In this work the areas mentioned above are expected to be dealt with and the results of this will be available in the Ph.D. thesis expected to be submitted in spring 2002.

References

Ahrens, J. P. and M. S. Heimbaugh (1988). *Approximate Upper Limit of Irregular Wave Runup on Riprap.* Tech. Report CERC-88-5, Coastal Engineering Research Center, Waterways Experience Station, Vicksburg, Miss.

Ahrens, J. P. and M. F. Titus (1985). Wave Run-Up formulas for smooth slopes. *Journal of waterway, port, coastal and ocean engineering Vol. 111*(No. 1), pp. 128 – 133.

Aminti, P. and L. Franco (1988). Wave overtopping on rubble mound breakwaters. *Proc. 21st. International Conference on Coastal Engineering, Malaga, Spain.*

Bølgekraftudvalgets Sekretariat (1999, December). *Bølgekraftprogram, Status 2000 - Forslag Til Systematik I Forbindelse Med Sammenligning Af Bølgekraftanlæg.*

Bradbury, A. P. and N. W. H. Allsop (1988). Hydraulic effects of breakwater crown walls. *In Proc. Conf. on Design of Breakwaters, Institution of Civil Engineers, London*, pp. 385 – 396.

Burcharth, H. F. and S. Hughes (2000). *Coastal Engineering Manual, Fundamentals of Design. Chapter 5, Part VI.* To be published by Coastal Engineering Research Center, Waterways Experiment Station, US Army Corps of Engineers,Vicksburg, USA.

CIRIA/CUR (1991). *Manual on the Use of Rock in Coastal and Shoreline Engineering.* Special pub. 83, Constriction Industry Research and Information ass., London.

Dodd, N. (1998). Numerical model of wave Run-Up, overtopping, and regeneration. *Journal of Waterway, Port, Coastal and Ocean Engineering Vol. 124*(No. 2), pp. 73 – 81.

Douglass, S. L. (1986). *Review and Comparison of Methods for Estimating Irregular Wave Overtopping Rates.* Rep. CERC-86-12, U. S. Army Corps of Engineers.

Falnes, J. (1993). *Theory for Extraction of Ocean Wave Energy.* Division of Physics, Norwegian Institute of Technology, University of Trondheim, Norway.

Franco, C. and L. Franco (1997). Wave overtopping over caisson brakwaters: New prediction formulae based on 2d and 3d model tests. *Manus submitted to the ASCE Journal of Waterway, Port, Coastal and Ocean Engineering.*

Franco, C., L. Franco, C. Restano, and J. W. Van der Meer (1995a). The effect of obliquity and Short-Crestedness on the overtopping rate and volume distribution on caisson breakwaters. *Final proceedings MCS-project, Monolithic (vertical) breakwaters.*

Franco, L., M. de Gerloni, and J. W. Van der Meer (1994). Wave overtopping on vertical and composite breakwaters. *ASCE, proc. 24th ICCE, Kobe, Japan, pp. 1030 - 1045..*

Franco, L., M. De Gerloni, and J. W. Van der Meer (1995). Wave overtopping on vertical and composite breakwaters. *Final proceedings MCS-project, Monolithic (vertical) coastal structures, Alderney Island, UK..*

Frigaard, P. and M. Brorsen (1995). A Time-Domain method for separating incident and reflected irregular waves. *Int. Journal of Coastal Engineering Vol. 24.*

Friis-Madsen, E. (1996). Offshore Wind-/Wave-Energy-Converter, international publication number WO 96/00848.

Funke, E. R. and E. P. Mansard (1979). *On the Synthesis of Realistic Sea States in a Laboratory Flume.* Hydraulics Laboratory Technical Report LTR-HY-66, National Research Council Canada, Ottawa, Canada.

Grantham, K. N. (1953). Wave Run-Up on sloping structures. *Transactions, American Geophysical Union Vol. 34*(No. 5), pp. 720 – 724.

Hasselmann, K., T. P. Barnett, E. Bouws, H. Carlson, D. E. Cartwright, K. Enke, J. A. Ewing, H. Gienapp, D. E. Hasselmann, P. Kruseman, A. Meerburg, P. Müller, D. J. Olbers, K. Richter, W. Sell, and H. Walden (1973). Measurements of Wind-Wave growth and swell decay during the joint north sea wave project (JONSWAP). *Deutsches Hydr. Zeit. A12*, pp. 1 – 95.

Hedges, T. S. and M. T. Reis (1997, January). *Random Wave Overtopping of Simple Seawalls: A New Regression Model.* Report no. CE/1/97, Dep. of Civil Engineering, University of Liverpool.

Hu, S. J. and J. L. McCauley (1997). Estimation of wave overtopping rates for irregular waves. *Journal of Waterway, Port, Coastal and Ocean Engineering Vol. 123*(No. 5), pp. 266 – 273.

Hughes, S. A. (1993). *Physical Models and Laboratory Techniques in Coastal Engineering.* Volume 7, Advanced Series on Ocean Engineering. World Scientific Publishing Co. Pte. Ltd. ISBN 981-02-1541-X (pbk).

Hunt, I. A. (1959, Sept.). Design of seawalls and breakwaters. *ASCE Vol. 85*(No. WW3, proc. paper 2172), pp. 123 – 152.

IAHR (1989). List of sea state parameters. *Journal of Waterway, Port, Coastal and Ocean Engineering, American Society of Civil Engineers Vol. 115*(No. 6), pp. 792 – 808.

Jakobsen, K. P. and P. Frigaard (1999). User's manual for the program wave dragon - power simulation. Technical report, CRAFT program Low-Pressure Turbine and Control Equipment for Wave Energy Converters (Wave Dragon), Hydraulics & Coastal Engineering Laboratory, Aalborg University.

Johnsgard, H. and G. Pedersen (1997). A numerical model for Three-Dimensional Run-Up. *Int. journal for numerical methods in fluids Vol. 24*, pp. 913 – 931.

Josefson, U. (1978). Utvärdering av en idé till vågkraftverk. Master's thesis, Chalmers University of Technology, Gøteborg, Sweden.

Kamphuis, J. W. and N. Mohamed (1978, May). Run-Up of irregular waves on plane smooth slope. *Journal of the waterway, port, coastal and ocean division Vol. 104*(WW2).

Kobayashi, N. (1998). *Wave Run-Up and Overtopping on Beaches and Coastal Structures*, Volume 5 of *Advances in Coastal and Ocean Engineering*, pp. 95 – 154.

Kofoed, J. P. (2000a, July). Model study of overtopping of marine structures for a wide range of geometric parameters. *Poster presented at 27th In. Conf. on Coastal Eng. (ICCE-2000), Sidney, Australia.*

Kofoed, J. P. (2000b). Time variation of overtopping rates applied to WD. Technical report, Non-nuclear Energy RTD Programme (CRAFT), "Low-pressure Turbine and Control Equipment for Wave Energy Converters (Wave Dragon), Hydraulic & Coastal Engineering Laboratory, Aalborg University.

Kofoed, J. P. and H. F. Burcharth (2000, Dec.). Experimental verification of an empirical model for time variation of overtopping discharge. *4th European Wave Energy Conference (EWEC 2000), Aalborg, Denmark.*

Kofoed, J. P. and P. Frigaard (2000a). Indledende hydrauliske undersøgelser af bølgeenergianlægget power pyramid (report in danish. english title: Preliminary hydraulic investigation of the wave energy device power pyramid). Technical report, Hydraulics & Coastal Engineering Laboratory, Aalborg University.

Kofoed, J. P. and P. Frigaard (2000b, Nov.). Marine structures with heavy overtopping. *4th Int. Conf. on Coasts, Ports and Marine Structures (ICOPMAS"2000"), Bandar Abbass, Iran.*

Kofoed, J. P., P. Frigaard, H. C. Sørensen, and E. Friis-Madsen (1998). Wave dragon - a slack moored wave energy converter. *Proc. of the Third European Wave Energy Conference in Patras, Greece.*

Kofoed, J. P. and A. Nielsen (1997, September). The wave dragon - evaluation of a wave energy converter. Master's thesis, Aalborg University. Graduate report in Civil Engineering.

Le Méhauté, B., R. C. Y. Koh, and L. Hwang (1968, Feb.). A synthesis of wave Run-Up. *Journal of the waterways and coastal engineering division, ASCE Vol. 94*(No. WW1, proc. paper 5807), pp. 77 – 92.

Madsen, J. B. and P. Frigaard (2000). Wave dragon: Operation strategy of the turbines. Technical report, CRAFT program Low-Pressure Turbine and Control Equipment for Wave Energy Converters (Wave Dragon), Hydraulics & Coastal Engineering Laboratory, Aalborg University.

Martinelli, L. and P. Frigaard (1999a). Example of overtopping time series. Technical report, CRAFT program Low Pressure Turbine and Control Equipment for Wave Energy Converters (Wave Dragon),Hydraulics & Coastal Engineering Laboratory, Aalborg University.

Martinelli, L. and P. Frigaard (1999b). The wave dragon: Tests on a modified model. Technical report, CRAFT-project, Department of Civil Engineering, Aalborg University.

Massel, S. R. (1996). *Ocean Surface Waves: Their Physics and Prediction.* Volume 11, Advanced Series on Ocean Engineering. World Scientific Publishing Co. Pte. Ltd. ISBN 981-02-2109-6(pbk).

Oumeraci, H., H. Schüttrumpf, and M. Bleck (1999, October). *OPTICREST Task 3.5 and 5 - Wave Overtopping at Seadikes, Comparison of Physical Model Tests and Numerical Computations.* MAS3-CT97-0116, Dept. of Hydromechanics and Coastal Engineering, Technical University of Braunschweig, Germany.

Owen, M. W. (1980). *Design of Sea Walls Allowing for Wave Overtopping.* Rep. EX 924, HR Wallingford.

Owen, M. W. (1982). The hydraulic design of seawall profiles. *Proc. Conf. on Shoreline Protection, ICE, London*, pp. 129 – 136.

Pedersen, J. (1996). *Wave Forces and Overtopping on Crown Walls of Rubble Mound Breakwaters.* Ph. D. thesis, Hydraulics & Coastal Engineering Laboratory, Department of Civil Engineering, Aalborg University, Denmark.

Pedersen, J. and H. F. Burcharth (1992). Wave forces on crown walls. *Proc. 23rd International Conference on Coastal Engineering, Venice, Italy.*

Roos, A. and J. A. Battjes (1976). Characteristics of flow in Run-Up of periodic waves. *Proc. 15th ICCE, Honolulu*, pp. 781–795.

Sakakiyama, T., R. Kajima, S. Imai, H. Katayama, and T. Shimizu (1997). Field measurements of wave overtopping on seawall covered with armor units. *Proc. 3rd Int. Symp. Waves97, Virginia, USA Vol. II.*

Saville, T. (1956, April). Wave Run-Up on shore structures. *ASCE Vol. 82*(No. WW2, proc. paper 925).

Saville, T. and J. M. Caldwell (1953). Experimental study of wave overtopping on shore structures. *Proc. Minnesota Int. Hydraulics Conv., IAHR, ASCE, Minneapolis, Minnesota, USA.*

Sørensen, H. C. and E. Friis-Madsen (1999). Wave dragon. forsøg til belysning af hydraulisk respons. rapport fase a.

SPM (1984). *Shore Protection Manual* (4th edition ed.). Department of The Army, Waterways Experiment Station, Corps of Engineers, Coastal Engineering Research Center.

TACPAI (1974). *Wave Run-Up and Overtopping.* Technical Advisory Committee on Protection Against Inundation, Government Publishing Office, The Hague.

Van der Meer, J. W. (1993). *Conceptual Design of Rubble Mound Breakwaters.* Delft Hydraulics, Publ. No. 483.

Van der Meer, J. W. (1998a). Applications and stability criteria for rock and artificial units. *Chapter 11 in "Seawalls, dikes and revetments". Edited by K. W. Pilarczyk, Balkema, Rotterdam..*

Van der Meer, J. W. (1998b). Geometrical design of coastal structures. *Chapter 9 in "Seawalls, dikes and revetments". Edited by K. W. Pilarczyk, Balkema, Rotterdam..*

Van der Meer, J. W. (1998c). Wave Run-Up and overtopping. *Chapter 8 in "Seawalls , dikes and revetments". Edited by K. W. Pilarczyk, Balkema, Rotterdam..*

Van der Meer, J. W. and L. Franco (1995). Vertical breakwaters. *Delft Hydraulics, Publ. No. 487..*

Van der Meer, J. W. and J. P. F. M. Janssen (1994). Wave Run-Up and wave overtopping of dikes. *Wave forces on inclined and vertical wall structures, ed. N. Kobayashi and Z. Demirbilek, pp. 1 - 27, ASCE. Also Delft Hydraulics, Publ. No. 485..*

Van der Meer, J. W. and J. P. F. M. Janssen (1995). Wave run-up and wave overtopping at dikes. Technical report, Task Committee Reports, ASCE.

Van der Meer, J. W. and K. W. Pilarczyk (1995). Lowcrested rubble mound structures. *In " River, coastal and shoreline protections; Erosion control using riptap and armourstone". John Wiley & Sons, England. Edited by C. R. Thorne et al., proc. Riprap workshop, Fort Collins, Colorado, USA, pp. 233 - 250..*

Van der Meer, J. W. and C. J. Stam (1992). Wave Run-Up on smooth and rock slopes of coastal structures. *Journal of Waterway, Port, Coastal and Ocean Engineering Vol. 118*(No. 5), pp. 534 – 550.

Van Oorschot, J. H. and K. D'Angremond (1968). The effect of wave energy spectra on wave Run-Up. *Proc. 11th. conf. on coastal engineering, London Vol. II*, pp. 888 – 900.

Verdonck, R., P. Troch, J. D. Rouck, and H. F. Burcharth (1998, June). *OPTICREST Task 1 - Review of Available Information.* MAST III, MAS3-CT97-0116, Ghent University, Aalborg University.

APPENDIX A

Regular wave overtopping a string

The purpose of this appendix is to determine the maximum overtopping volume of water passing over a string placed in regular wave at some level between the still water level and the amplitude of the wave. Furthermore, the power present in this overtopping volume of water is calculated and compared to the total amount of power in the wave.

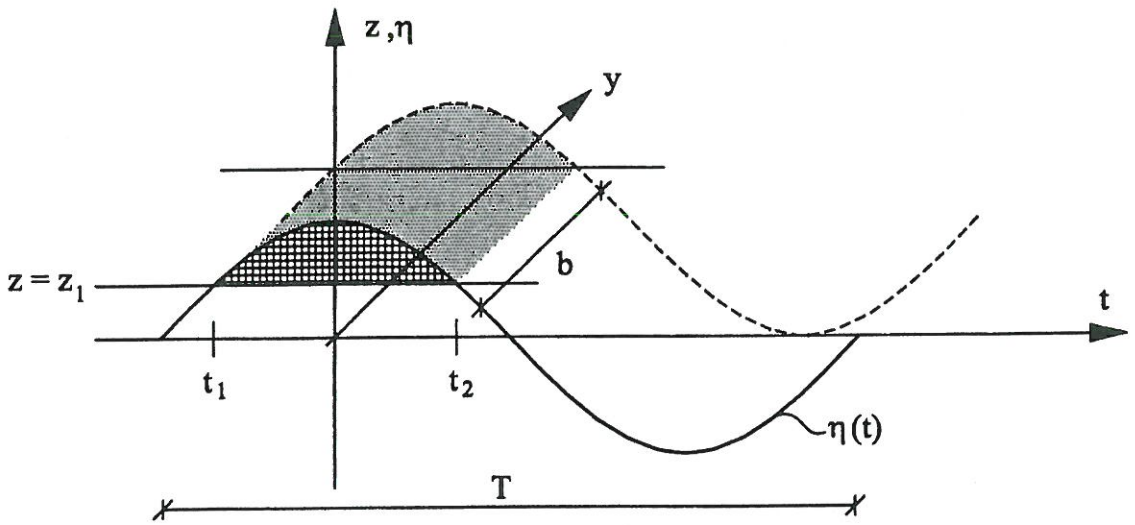

Figure A.1: Definition sketch.

A regular wave is given by

$$\eta(x,t) = a\cos(kx - \omega t) \tag{A.1}$$

where $\eta(x,t)$ is the water elevation, a the wave amplitude, $\omega = \frac{2\pi}{T}$ the cyclic frequency, T the wave period, t the time, $k = \frac{2\pi}{L}$, L the wave lengt and x the horizontal coordinat in the direction of the wave.

A string is imagined placed at $z = z_1$ as shown in figure A.1. Now the flow of water that is passing above this string at a fixed location, $x = 0$, (in average over one wave periode T), $Q(z_1)$ [m^3/s], is calculated for a section with the width b in the direction perpendicular to the wave direction.

$$\begin{aligned}
Q(z_1) &= \frac{1}{T}\int_{t_1}^{t_2} bc(\eta(t) - z_1)dt \\
&= \frac{bL}{T^2}\int_{x_1}^{x_2} (a\cos(-\frac{2\pi}{T}t) - z_1)dt \\
&= \frac{bL}{T^2}(\int_{-\frac{T}{2\pi}\cos^{-1}(\frac{z_1}{a})}^{\frac{T}{2\pi}\cos^{-1}(\frac{z_1}{a})} \cos(\frac{2\pi}{T}t)dt - z_1\frac{T}{\pi}\cos^{-1}(\frac{z_1}{a})) \\
&= \frac{bL}{\pi T}(a\sin(\cos^{-1}(\frac{z_1}{a})) - z_1\cos^{-1}(\frac{z_1}{a})) \\
&= \frac{bL}{\pi T}(a\sqrt{1-(\frac{z_1}{a})^2} - z_1\cos^{-1}(\frac{z_1}{a})) \qquad \text{(A.2)}
\end{aligned}$$

where $c = \frac{L}{T}$ is the wave velocity.

From this overtopping discharge, the power obtained if the water is captured in the height of the string (as potential energy), $P(z_1)$ [W], can be calculated as:

$$\begin{aligned}
P(z_1) &= \gamma_w Q_{mean}(z_1)z_1 \\
&= \frac{bL\gamma_w}{\pi T}(az_1\sqrt{1-(\frac{z_1}{a})^2} - z_1^2\cos^{-1}(\frac{z_1}{a})) \\
&= \frac{bL\gamma_w}{\pi T}az_1(\sqrt{1-(\frac{z_1}{a})^2} - \frac{z_1}{a}\cos^{-1}(\frac{z_1}{a})) \qquad \text{(A.3)}
\end{aligned}$$

where $\gamma_w = \rho_w g$ is the specific weight of water, ρ_w is the density of water and g is the gravity acceleration.

A plot of equation (A.2) and (A.3) (for the following values of parameters: $a = 1$ m, $T = 7.7$ s, $L = 83.9$ m, $d = 20$ m, $b = 1$ m and $\gamma_w = 10,016$ kg/(m^{2}s^2)) is shown in figure A.2.

Now the optimal choice of z_1, z_1^{max}, in terms of max. power that can be obtain is determined:

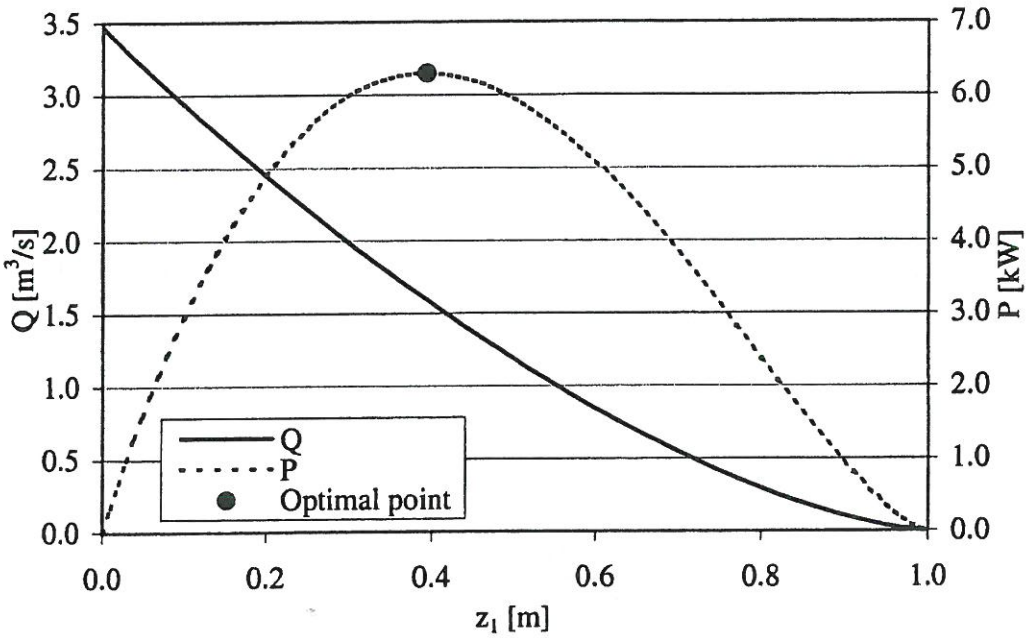

Figure A.2: Plot of overtopping discharge, Q, and obtained power, $P(z_1)$, as a function of the z-level of the string, z_1.

$$\begin{aligned}\frac{d}{dz_1}P(z_1) &= \frac{bL\gamma_w}{\pi T}\left(a\sqrt{1-(\frac{z_1}{a})^2} - \frac{z_1^2}{a\sqrt{1-(\frac{z_1}{a})^2}} - \left(2z_1\cos^{-1}(\frac{z_1}{a}) - \frac{z_1^2}{a\sqrt{1-(\frac{z_1}{a})^2}}\right)\right) \\ &= \frac{bL\gamma_w}{\pi T}\left(a\sqrt{1-(\frac{z_1}{a})^2} - 2z_1\cos^{-1}(\frac{z_1}{a})\right) = 0 \qquad \text{(A.4)}\end{aligned}$$

An attempt to solve equation (A.4) for z_1, in order to obtain z_1^{max}, leads to a recursive equation:

$$\sqrt{1-(\frac{z_1^{max}}{a})^2} = 2\frac{z_1^{max}}{a}\cos^{-1}(\frac{z_1^{max}}{a}) \qquad \text{(A.5)}$$

A numerical evaluation of equation (A.5) shows two possible solutions, namely $z_1^{max} = a$ and $z_1^{max} = 0.3942a$. Obviously, the first solution is trivial and of no interest, while the second is relevant to the solution of the problem.

Using this value of z_1^{max} the max. power that can be obtain, P^{max}, is determined by insertion into equation (A.3).

$$P^{max} = P(z_1^{max})$$

$$= \frac{bL\gamma_w}{\pi T}(0.3942a^2\sqrt{1-(\frac{0.3942a}{a})^2} - (0.3942a)^2\cos^{-1}(\frac{0.3942a}{a}))$$
$$= 0.1812\frac{a^2bL\gamma_w}{\pi T} \quad (A.6)$$

Finally, the ratio between P^{max} and the power that is moving through a vertical cross section of the water column, perpendicular to the wave direction with the width b, P_{wave}, can be calculated. This ratio is in the following referred to as the efficiency.

$$\text{Efficiency} = \frac{P^{max}}{P_{wave}}$$
$$= \frac{0.1812\frac{a^2bL\gamma_w}{\pi T}}{\frac{1}{16}\gamma_w(2a)^2\frac{L}{T}(1+\frac{2\frac{2\pi}{L}d}{\sinh(2\frac{2\pi}{L}d)})b}$$
$$= \frac{0.2307}{(1+\frac{2\frac{2\pi}{L}d}{\sinh(2\frac{2\pi}{L}d)})} \quad (A.7)$$

where d is the water depth.

Using (A.7) for shallow water shows that the efficiency in this case is $\approx$ 11.5 %, while it for deep water is $\approx$ 23.1 %.

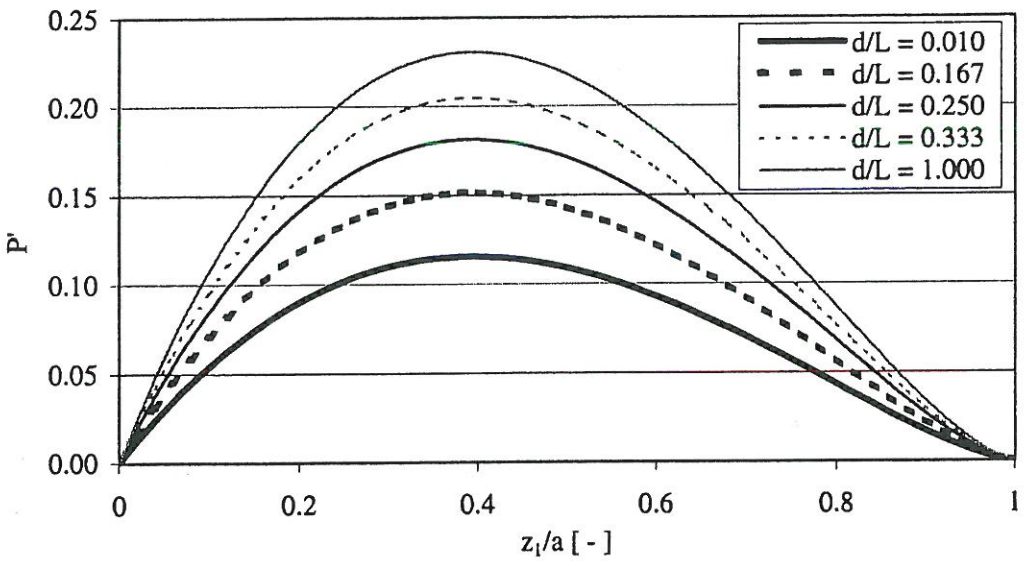

Figure A.3: Plot of non-dimensionalized obtained power, $P'(\frac{z_1}{a})$, as a function of the non-dimensionalized z-level of the string, $\frac{z_1}{a}$.

The variation of the non-dimensionalized mean power, P', defined as

$$\begin{aligned} P' &= \frac{P}{P_{wave}} \\ &= \frac{P}{\frac{1}{16}\gamma_w(2a)^2\frac{L}{T}(1+\frac{2\frac{2\pi}{L}d}{\sinh(2\frac{2\pi}{L}d)})b} \end{aligned} \tag{A.8}$$

is shown in figure A.3.

If, instead of capturing the water in the level of the string, each infinitesimal volume of water over $z = z_1$ is captured in the level it reaches, the mean power obtained is

$$\begin{aligned} P &= \frac{1}{T}\int_0^a \gamma_w bzc(t_2 - t_1)dz \\ &= \frac{\gamma_w bL}{T^2}\int_0^a z(\frac{T}{\pi}\cos^{-1}\frac{z}{a} - (-\frac{T}{\pi}\cos^{-1}\frac{z}{a}))dz \\ &= \frac{\gamma_w bL}{\pi T}\int_0^a z\cos^{-1}\frac{z}{a}dz \\ &= \frac{a^2\gamma_w bL}{8T}(1 - \frac{4z_1^2}{\pi a^4}\cos^{-1}(\frac{z_1}{a}) + \frac{2z_1}{\pi a^3}\sqrt{1-(\frac{z_1}{a})^2} - \frac{2}{\pi}\sin^{-1}(\frac{z_1}{a})) \end{aligned} \tag{A.9}$$

P obtain its maximum value for $z_1 = 0$ and, thus, the maximum obtainable power P^{max} for this case becomes

$$P^{max} = \frac{a^2\gamma_w bL}{8T} \tag{A.10}$$

The efficiency for this case then becomes

$$\begin{aligned} \text{Efficiency} &= \frac{P^{max}}{P_{wave}} \\ &= \frac{1}{2}\frac{1}{1+\frac{2\frac{2\pi}{L}d}{\sinh(2\frac{2\pi}{L}d)}} \end{aligned} \tag{A.11}$$

Thus, the efficiency in deep water becomes 50 % and for shallow water 25 %.

APPENDIX B

Results - average overtopping rates

In the following pages the results of the performed model tests are presented in terms of non-dimensional average overtopping rates Q (defined as $Q = \frac{q}{\sqrt{gH_{m0}^3}}$) as a function of dimensionless crest freeboard R (defined as R_c/H_{m0}, where H_{m0} is the incident significant wave height).

The dimensions given in this appendix are all in model scale.

B.1 Linear overtopping ramp

In this section results of tests performed with a linear ramp are presented. Three series of tests have been performed with a linear ramp geometry:

- Varying slope angle α.
- Varying crest freeboard R_c.
- Varying draught d_r.

The principle layout of the ramp is given in figure B.1.

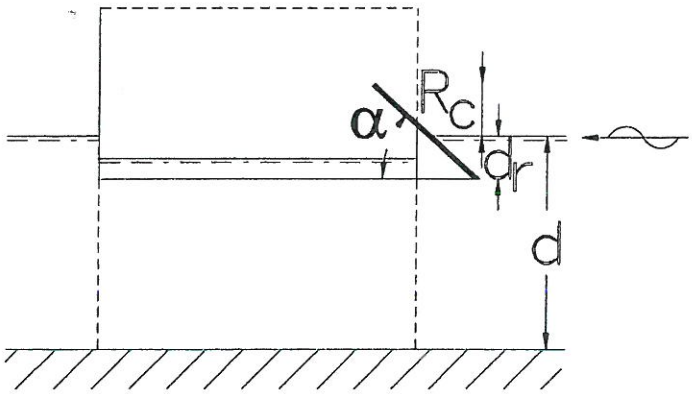

Figure B.1: Principle layout of linear overtopping ramp.

B.1.1 Varying slope angle

Test AA01
Slope angle: 20° Draught: 0.162 m Crest freeboard: 0.077 m

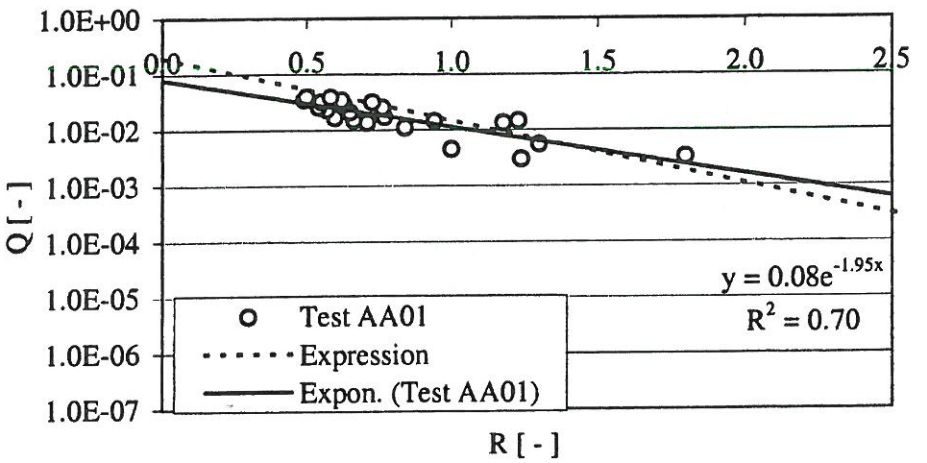

Figure B.2: Results of tests with test geometry AA01.

Test AA02
Slope angle: 30° Draught: 0.166 m Crest freeboard: 0.083 m

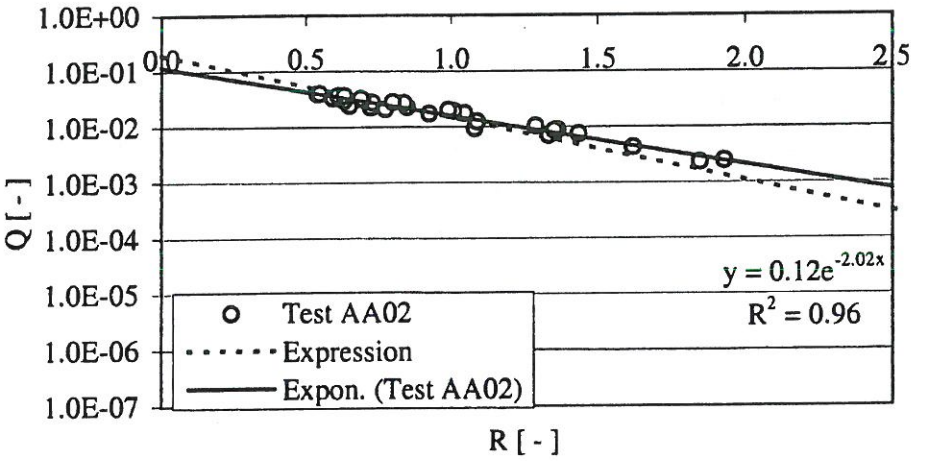

Figure B.3: Results of tests with test geometry AA02.

Test AA03
Slope angle: 40° Draught: 0.162 m Crest freeboard: 0.086 m

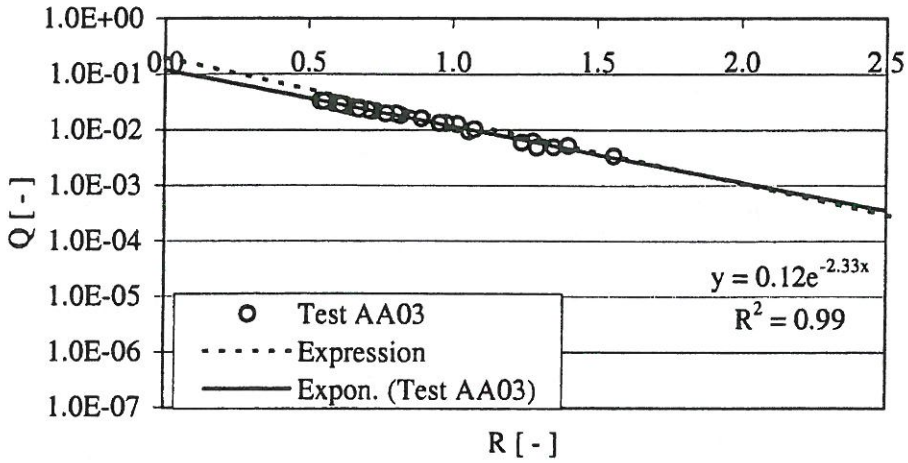

Figure B.4: Results of tests with test geometry AA03.

Test AA04
Slope angle: 50° Draught: 0.162 m Crest freeboard: 0.082 m

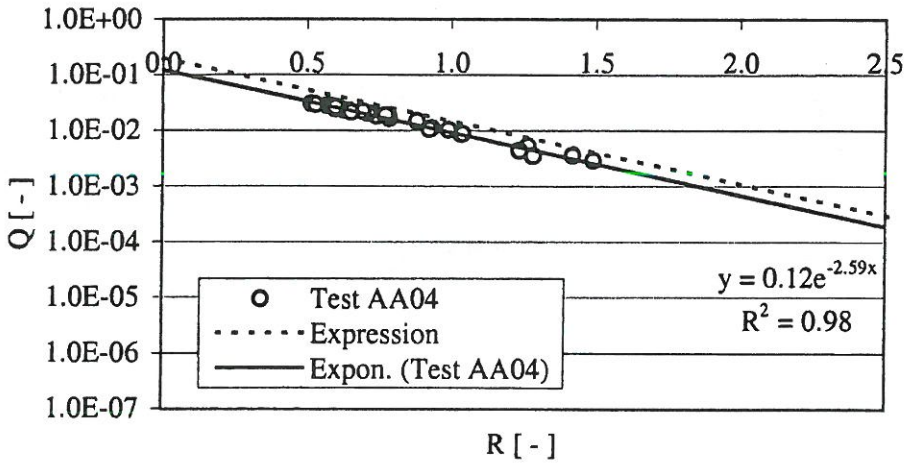

Figure B.5: Results of tests with test geometry AA04.

Test AA05
Slope angle: 60° Draught: 0.123 m Crest freeboard: 0.081 m

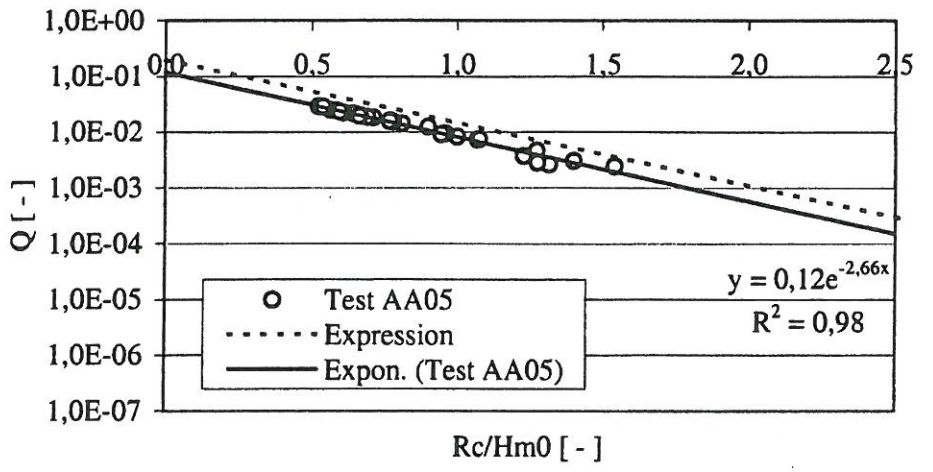

Figure B.6: Results of tests with test geometry AA05.

B.1.2 Varying crest freeboard

AB01
Slope angle: 40° Draught: 0.166 m Crest freeboard: 0.021 m

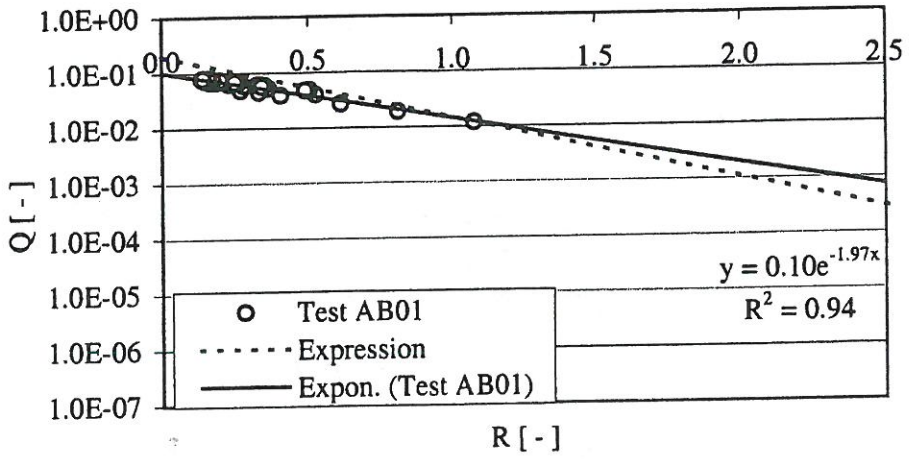

Figure B.7: Results of tests with test geometry AB01.

AB02
Slope angle: 40° Draught: 0.166 m Crest freeboard: 0.052 m

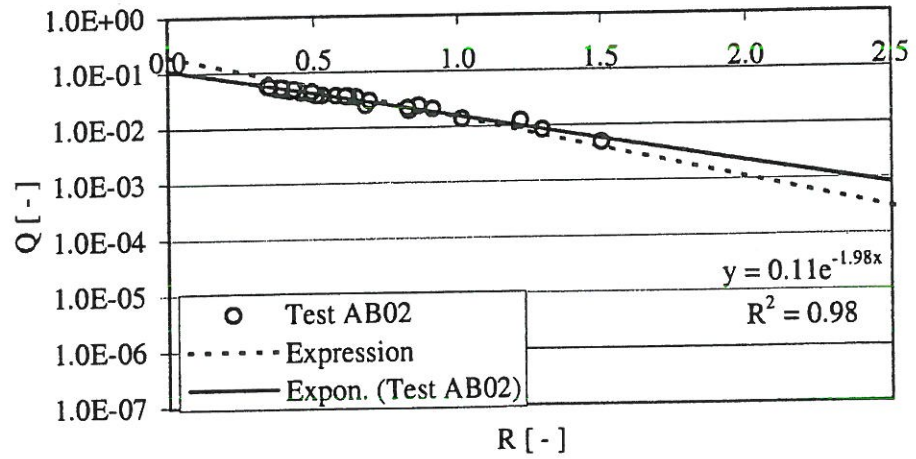

Figure B.8: Results of tests with test geometry AB02.

AB03

Slope angle: 40° Draught: 0.163 m Crest freeboard: 0.098 m

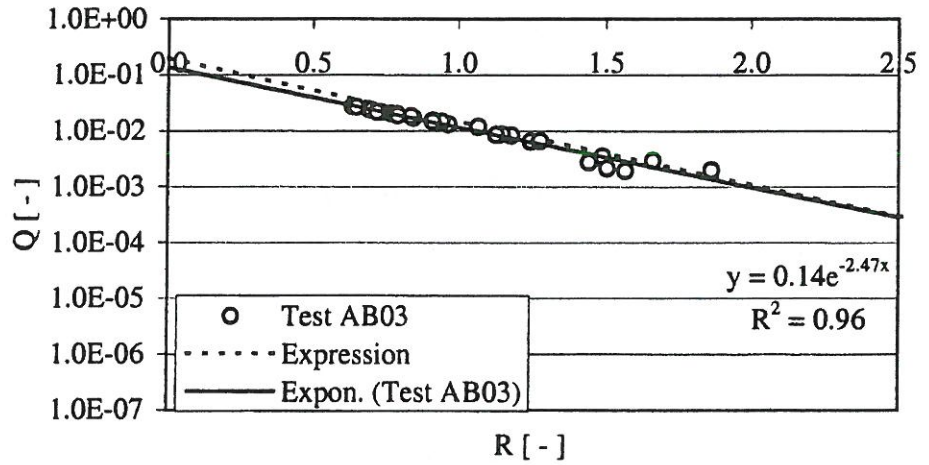

Figure B.9: Results of tests with test geometry AB03.

AB04

Slope angle: 40° Draught: 0.167 m Crest freeboard: 0.142 m

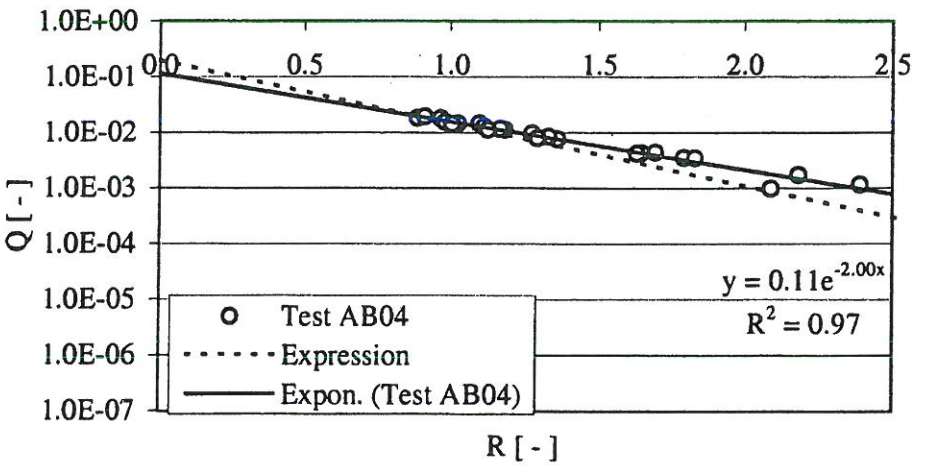

Figure B.10: Results of tests with test geometry AB04.

B.1.3 Varying draught

AC01
Slope angle: 40° Draught: 0.100 m Crest freeboard: 0.087 m

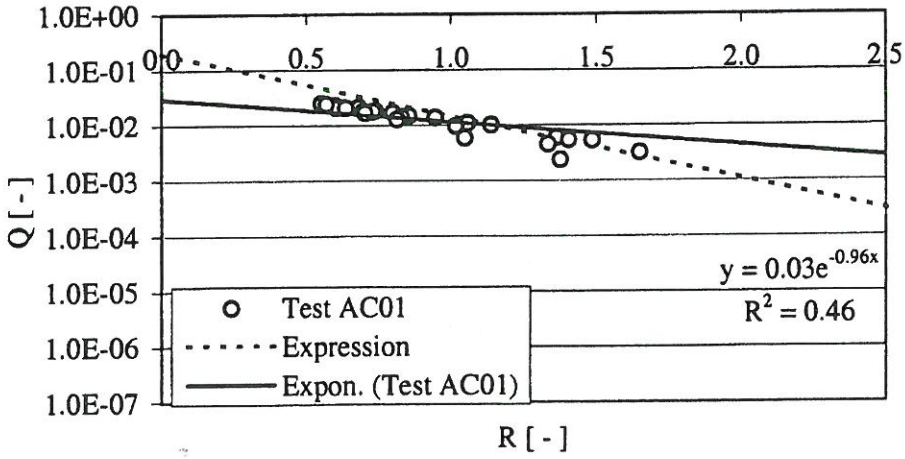

Figure B.11: Results of tests with test geometry AC01.

AC02
Slope angle: 40° Draught: 0.243 m Crest freeboard: 0.087 m

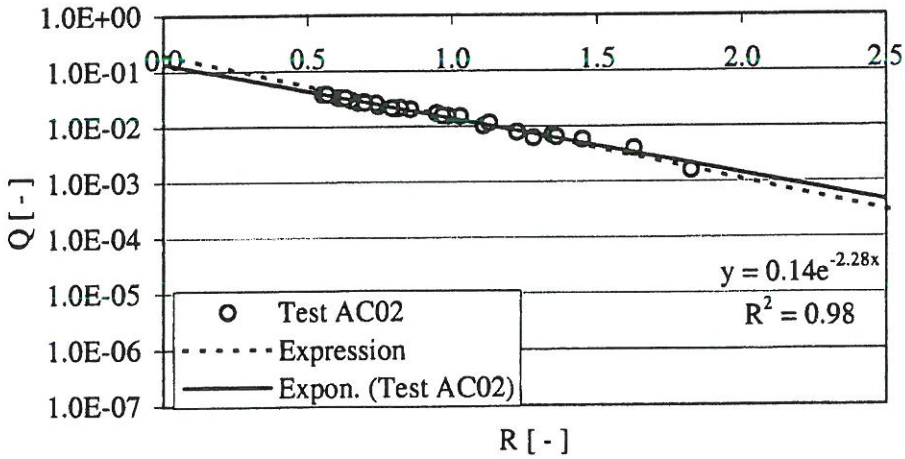

Figure B.12: Results of tests with test geometry AC02.

AC03
Slope angle: 40° Draught: 0.358 m Crest freeboard: 0.087 m

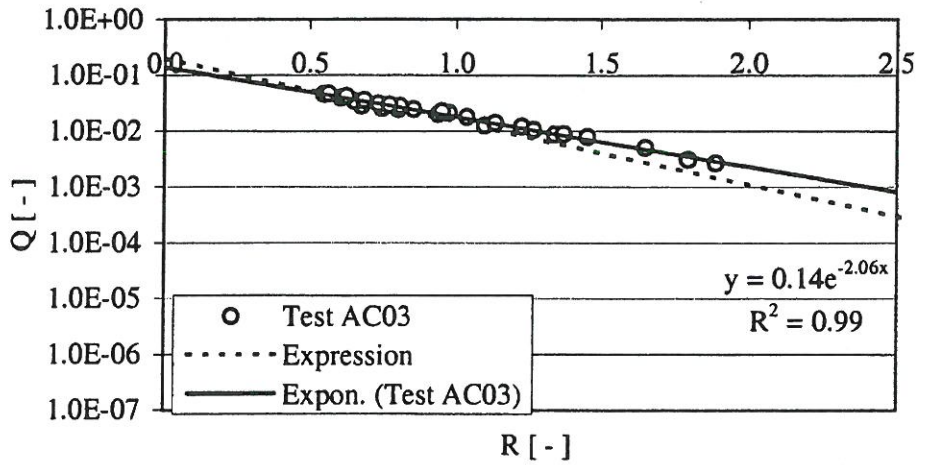

Figure B.13: Results of tests with test geometry AC03.

AC04
Slope angle: 40° Draught: 0.500 m Crest freeboard: 0.087 m

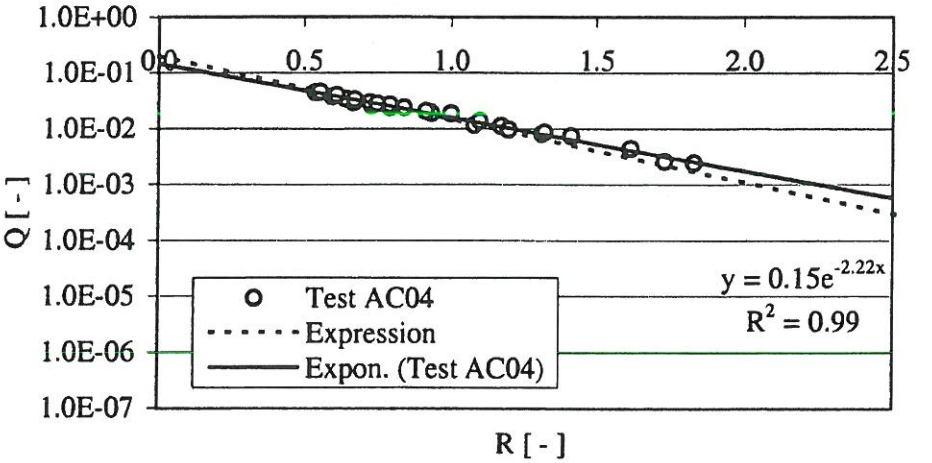

Figure B.14: Results of tests with test geometry AC04.

B.2 Modifications of the ramp profile

In this section results of tests performed with modifications of the ramp profile geometry are presented. At first results of a test series with a reference geometry (linear ramp, principle layout as given in figure B.1) are presented. These are used for evaluation of the tested modifications. The tested modifications are:

- Horizontal plate at ramp bottom.
- Convex top of ramp.
- Concave top of ramp.

B.2.1 Reference geometry

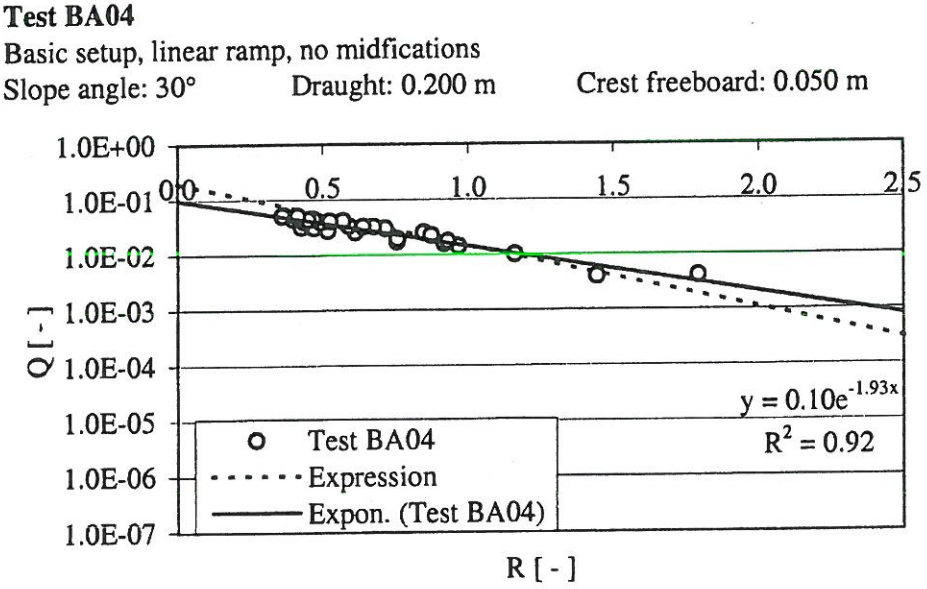

Figure B.15: Results of tests with test geometry BA04.

B.2.2 Horizontal plate at ramp bottom

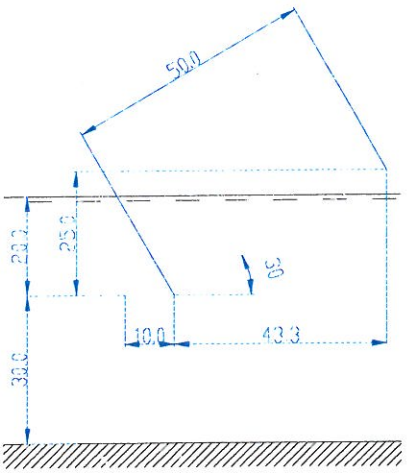

Figure B.16: The geometry of the ramp in the BA01 tests. Measures are in m.

Test BA01
Horizontal plate at ramp bottom: 0.100 m
Slope angle: 30° Draught: 0.200 m Crest freeboard: 0.050 m

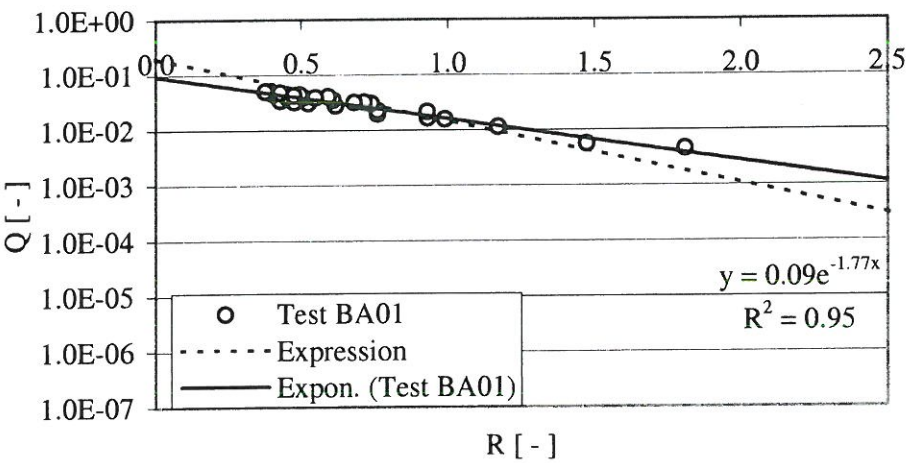

Figure B.17: Results of tests with test geometry BA01.

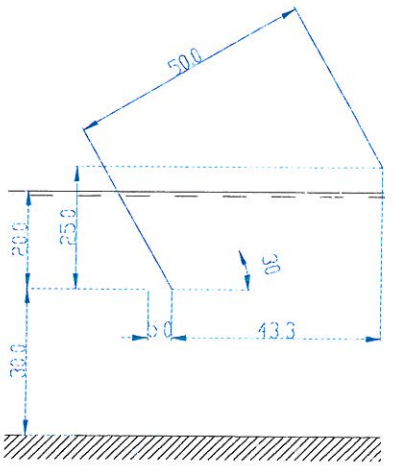

Figure B.18: The geometry of the ramp in the BA02 tests. Measures are in m.

Test BA02

Horizontal plate at ramp bottom: 0.050 m

Slope angle: 30° Draught: 0.200 m Crest freeboard: 0.050 m

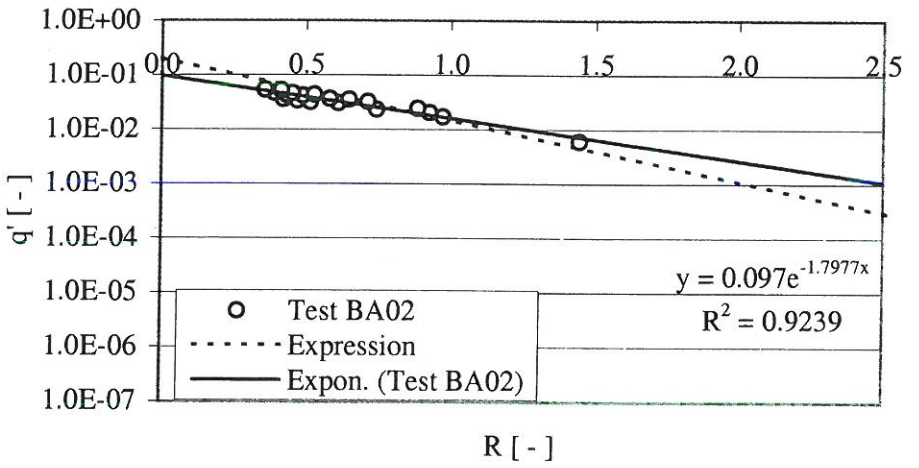

Figure B.19: Results of tests with test geometry BA02.

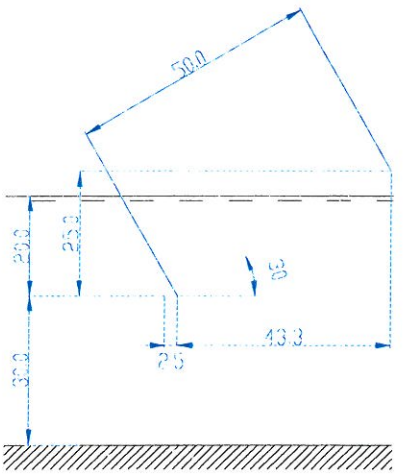

Figure B.20: The geometry of the ramp in the BA03 tests. Measures are in m.

Test BA03
Horizontal plate at ramp bottom: 0.025 m
Slope angle: 30° Draught: 0.200 m Crest freeboard: 0.050 m

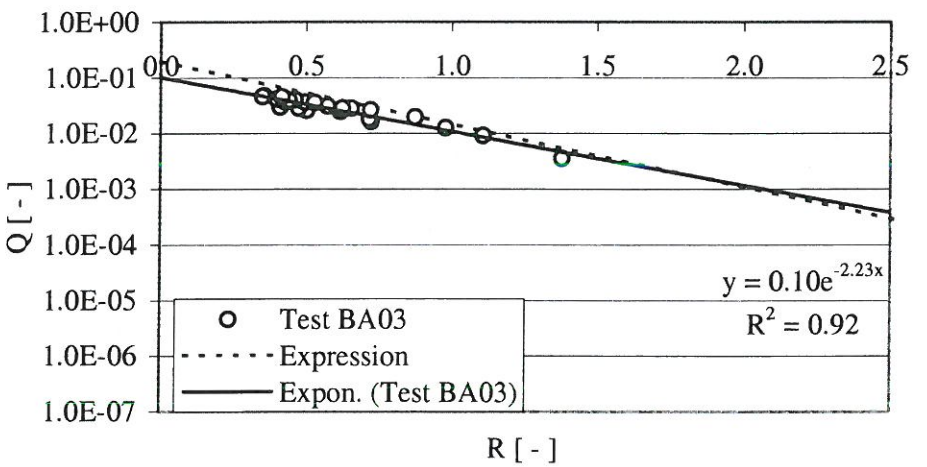

Figure B.21: Results of tests with test geometry BA03.

B.2.3 Convex top of ramp

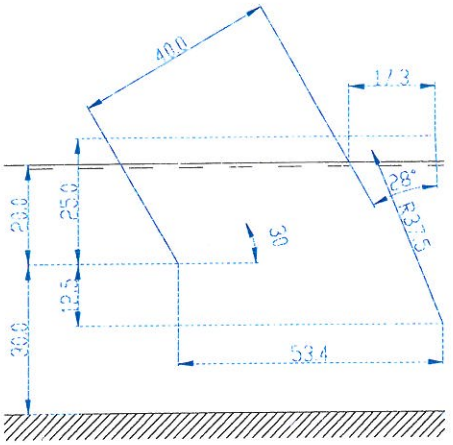

Figure B.22: The geometry of the ramp in the CA01 tests. Measures are in m.

Test CA01

Convex ramp | Curve radius: 0.375 m | Sector of circle: 28°

Slope angle: 30° | Draught: 0.200 m | Crest freeboard: 0.050 m

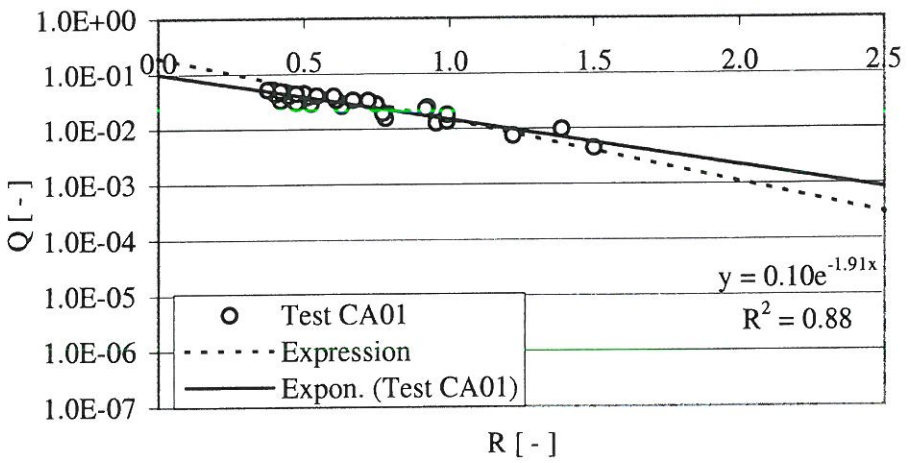

Figure B.23: Results of tests with test geometry CA01.

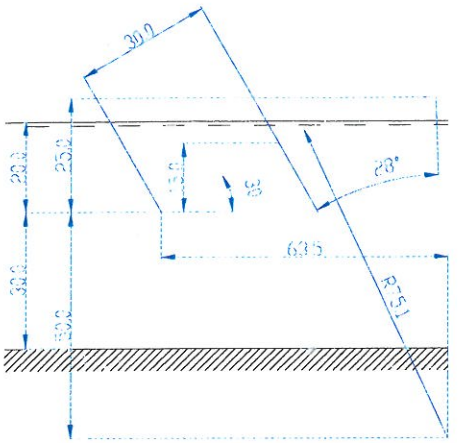

Figure B.24: The geometry of the ramp in the CA02 tests. Measures are in m.

Test CA02

Convex ramp	Curve radius: 0.751 m	Sector of circle: 28°
Slope angle: 30°	Draught: 0.200 m	Crest freeboard: 0.050 m

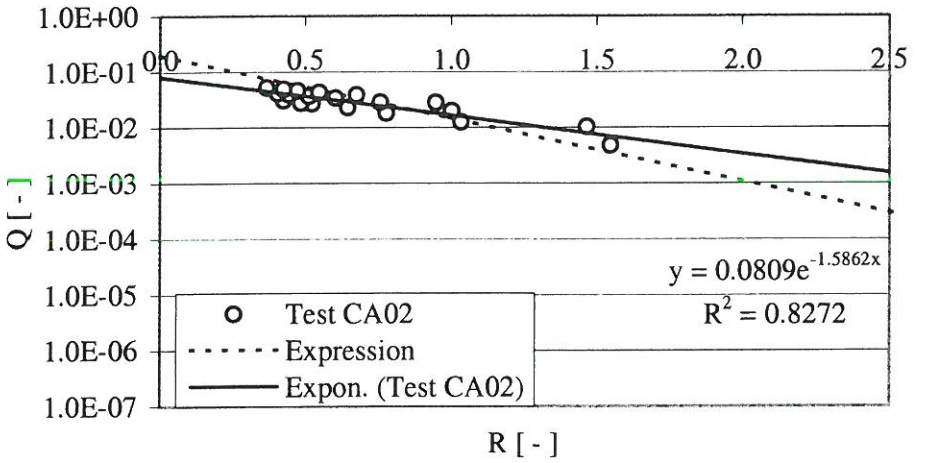

Figure B.25: Results of tests with test geometry CA02.

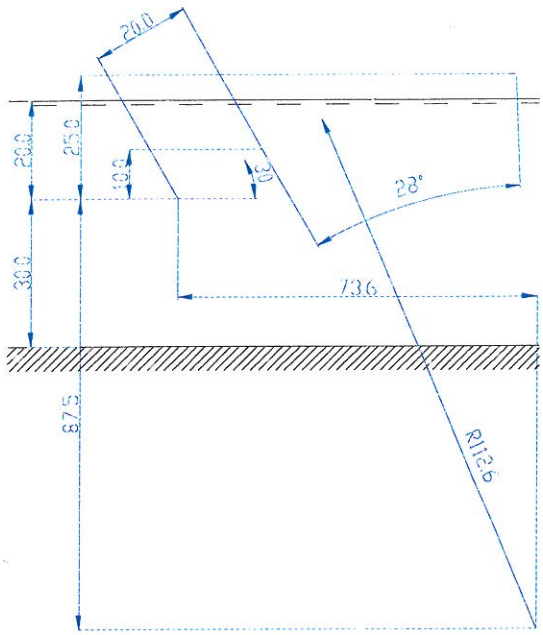

Figure B.26: The geometry of the ramp in the CA03 tests. Measures are in m.

Test CA03

Convex ramp	Curve radius: 1.126 m	Sector of circle: 28°
Slope angle: 30°	Draught: 0.200 m	Crest freeboard: 0.050 m

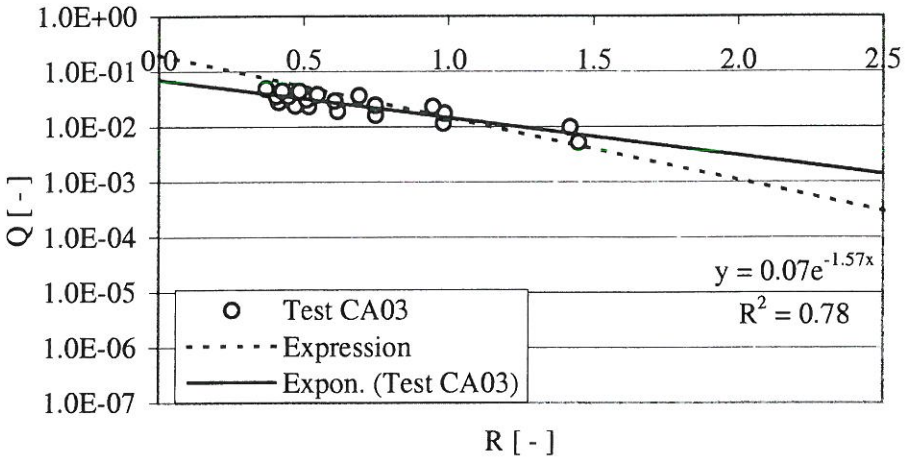

Figure B.27: Results of tests with test geometry CA03.

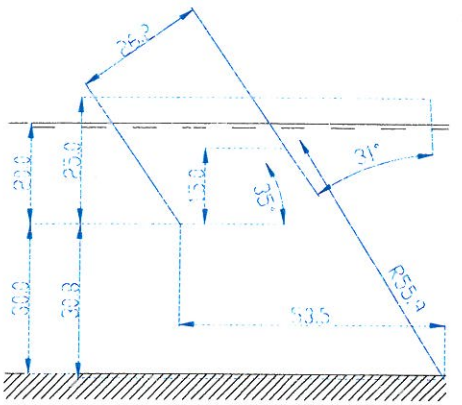

Figure B.28: The geometry of the ramp in the CB01 tests. Measures are in m.

Test CB01

Convex ramp	Curve radius: 0.559 m	Sector of circle: 31°
Slope angle: 35°	Draught: 0.200 m	Crest freeboard: 0.050 m

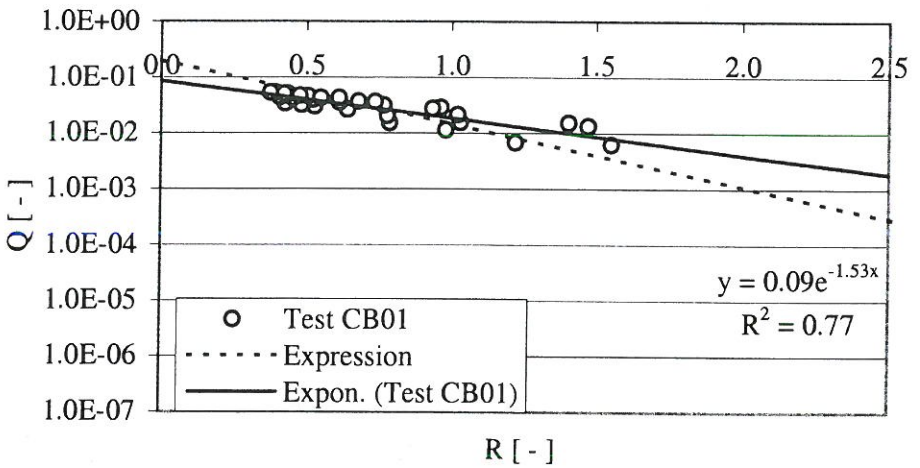

Figure B.29: Results of tests with test geometry CB01.

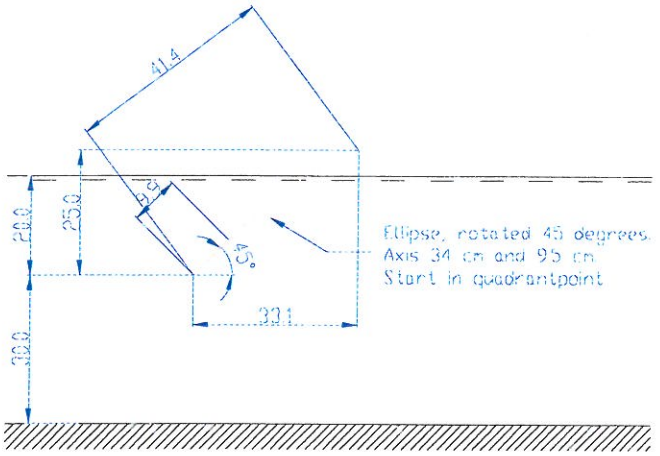

Figure B.30: The geometry of the ramp in the CC01 tests. Measures are in m.

Test CC01
Convex ramp, elliptic
Slope angle: 45° Draught: 0.200 m Crest freeboard: 0.050 m

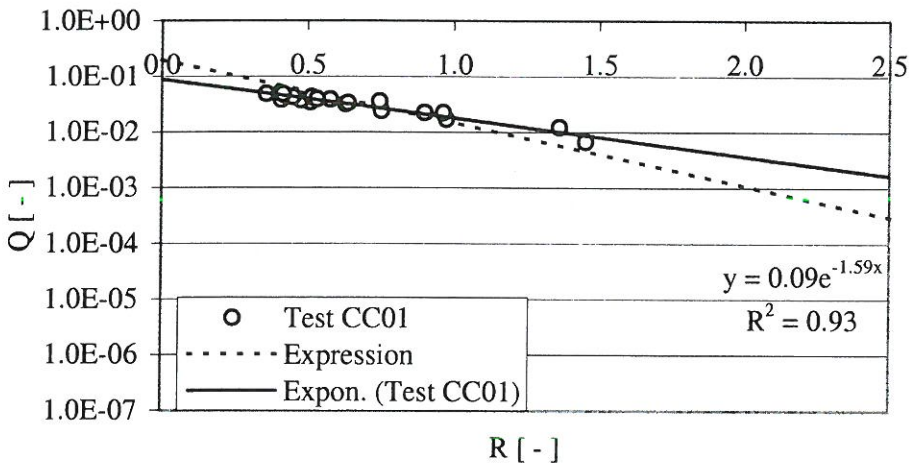

Figure B.31: Results of tests with test geometry CC01.

B.2.4 Concave top of ramp

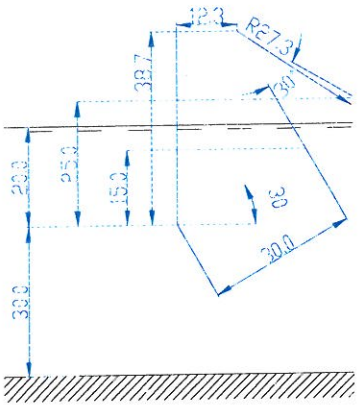

Figure B.32: The geometry of the ramp in the DA01 tests. Measures are in m.

Test DA01

Concave ramp | Curve radius: 0.273 m | Sector of circle: 30°

Slope angle: 30° | Draught: 0.200 m | Crest freeboard: 0.050 m

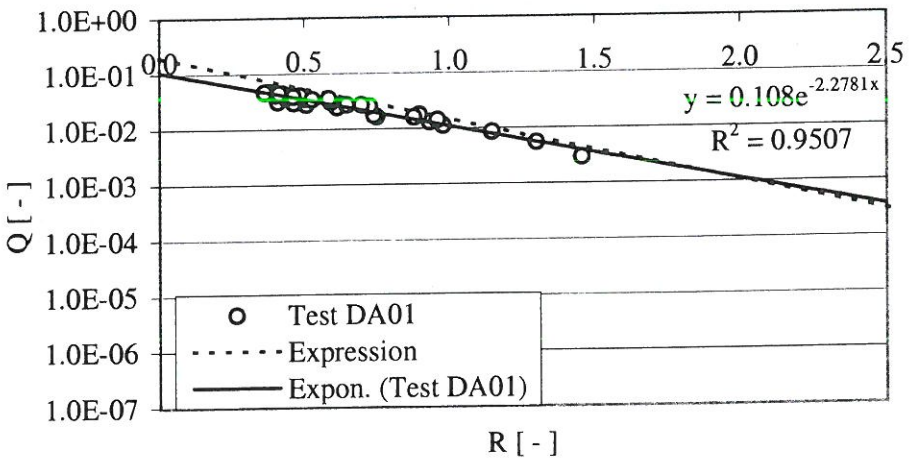

Figure B.33: Results of tests with test geometry DA01.

B.3 Modifications of the side walls of the ramp

In this section results of tests performed with modifications of the side walls of the ramp are presented. The tested modifications are:

- Linear converging guiding walls.
- Curved converging guiding walls.

B.3.1 Linear converging guiding walls

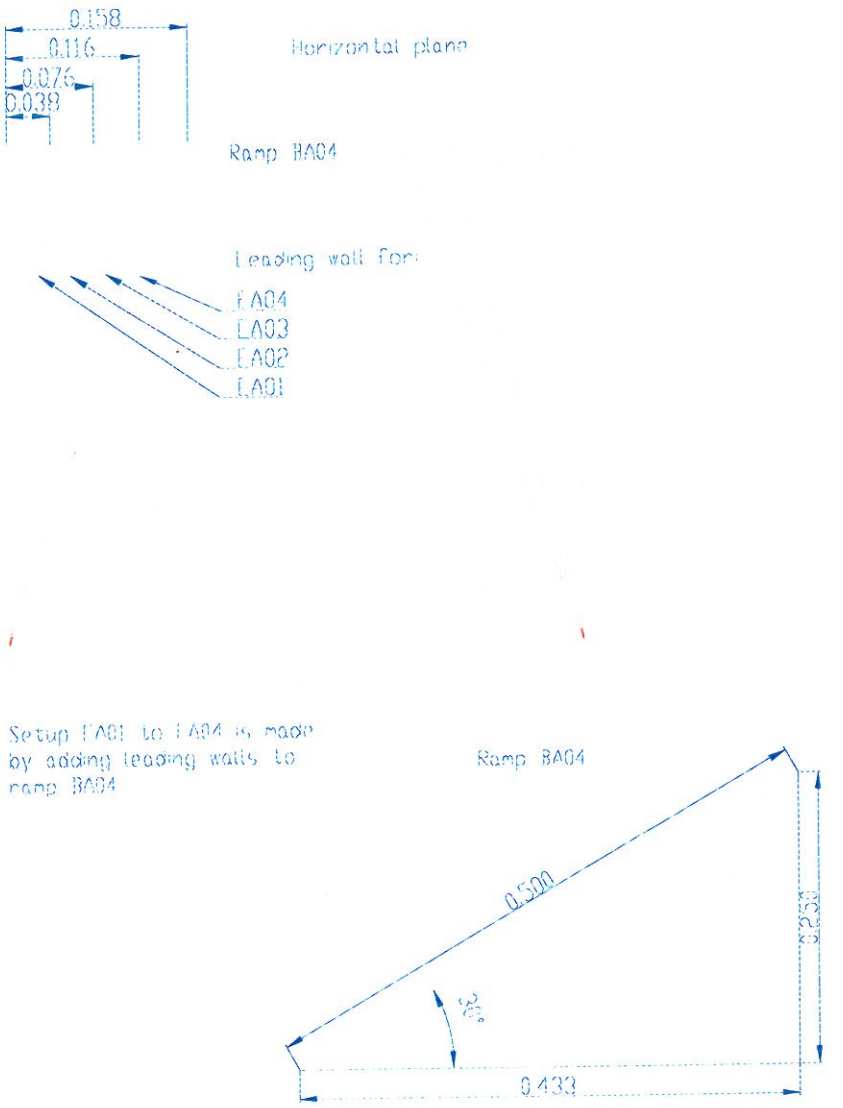

Figure B.34: The geometry of the ramp in the EA01 to EA04 tests. Measures are in m.

Test EA01
Linear converging guiding walls, opening ratio: 0.848
Slope angle: 30° Draught: 0.200 m Crest freeboard: 0.050 m

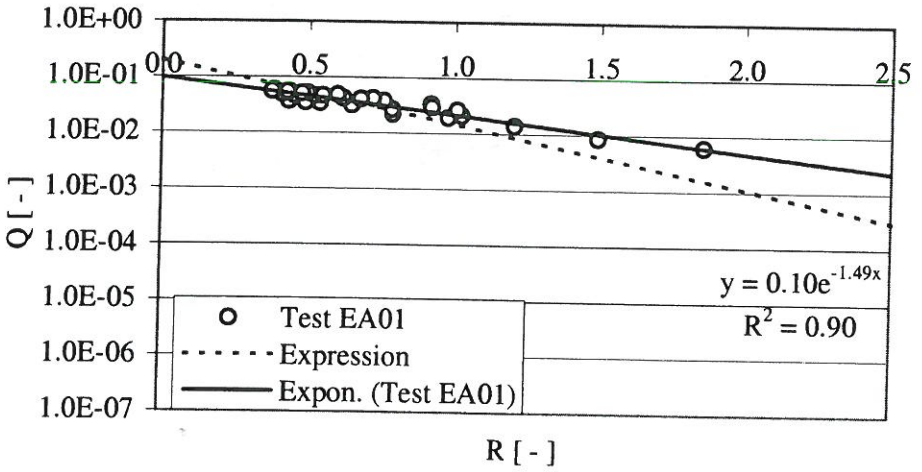

Figure B.35: Results of tests with test geometry EA01.

Test EA02
Linear converging guiding walls, opening ratio: 0.696
Slope angle: 30° Draught: 0.200 m Crest freeboard: 0.050 m

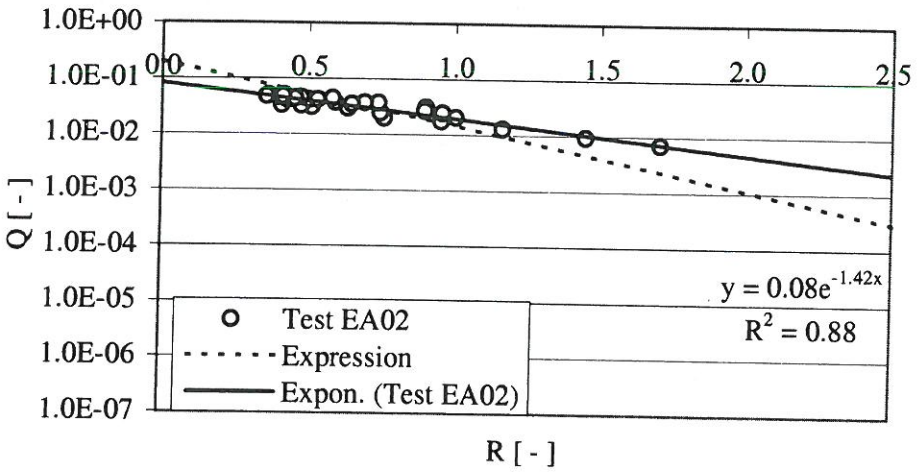

Figure B.36: Results of tests with test geometry EA02.

Test EA03
Linear converging guiding walls, opening ratio: 0.536
Slope angle: 30° Draught: 0.200 m Crest freeboard: 0.050 m

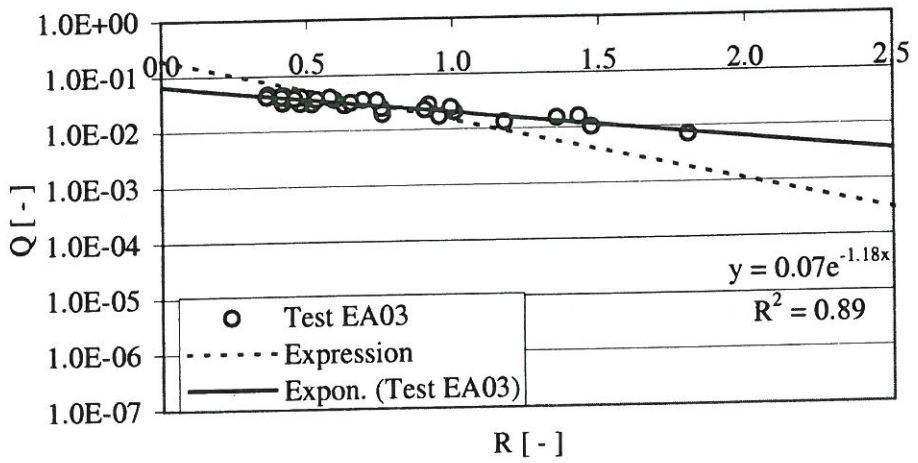

Figure B.37: Results of tests with test geometry EA03.

Test EA04
Linear converging guiding walls, opening ratio: 0.368
Slope angle: 30° Draught: 0.200 m Crest freeboard: 0.050 m

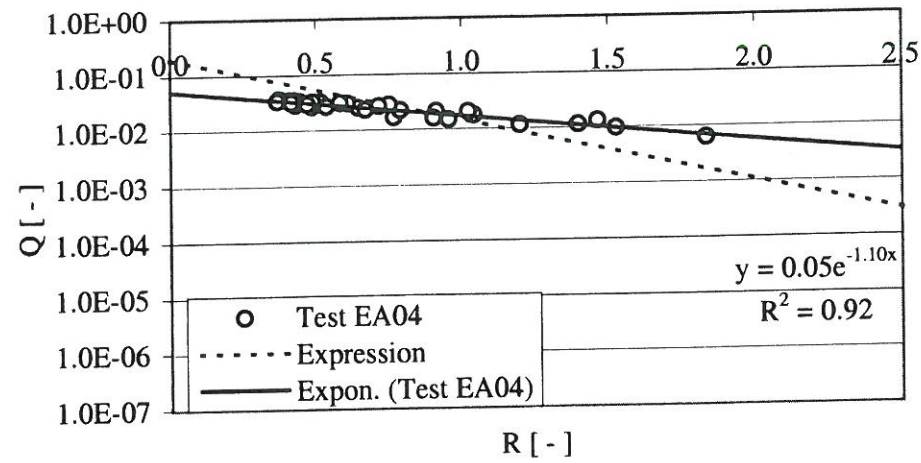

Figure B.38: Results of tests with test geometry EA04.

B.3.2 Curved converging guiding walls

Figure B.39: The shape the curved converging guiding walls (horizontal projection) for geometry FA02.

Test FA02
Curved converging guiding walls
Opening ratio: 0.696 Large radius in ellipse: 0.095 m
Slope angle: 30° Draught: 0.200 m Crest freeboard: 0.050 m

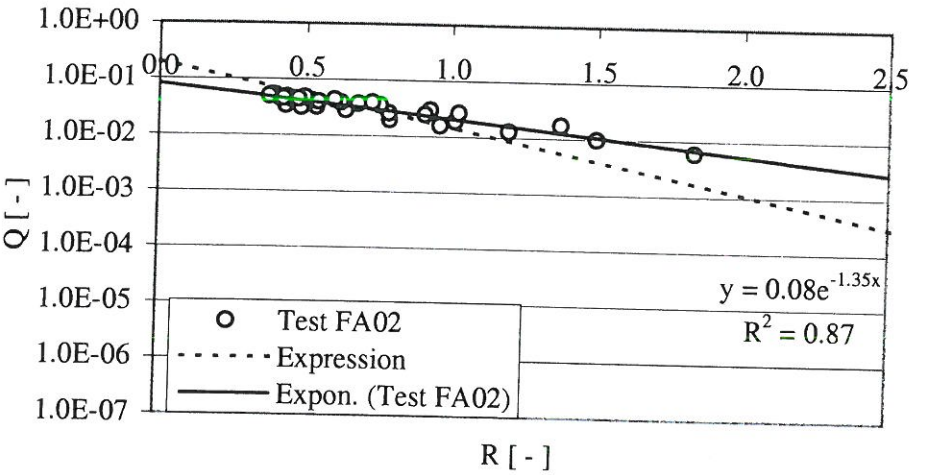

Figure B.40: Results of tests with test geometry FA02.